

5

STUDY OF ATMOSPHERIC DEGRADATION OF LASER BEAMS

Prepared for  
National Aeronautics and Space Administration  
Electronics Research Center  
575 Technology Square  
Cambridge, Massachusetts

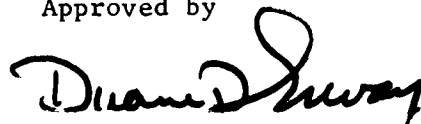
Contract NAS12-130

EOS Report 7097-Final

December 1967

Prepared by Staff  
Optical-Electronic Systems Division

Approved by



D. D. Erway, Associate Manager  
Optical-Electronic Systems Division



**ELECTRO-OPTICAL SYSTEMS, INC.**

A XEROX COMPANY

PRECEDING PAGE BLANK NOT FILMED.

# FOREWORD

This report was prepared by Electro-Optical Systems, Inc., under Contract NAS12-130.

The period covered by the report is from 1 June 1966 to 31 May 1967. Work was performed in the Applied Research Department of the Optical Electronic Systems Division by Dr. J. Boyden, L. Carrier, Dr. G. Clark, E. Harris, M. Katzman and C. D. Wilson. The contributions of H. Bohling, F. Brion, and T. Watson are herewith acknowledged.

The EOS report designation is 7097-Final. The experimental results reported herein are preliminary. Work is continuing and as more data becomes available, these will be reported in later reports and papers.

The NASA/ERC Project Monitor was Dr. Philip Hanst.



PRECEDING PAGE BLANK NOT FILMED.

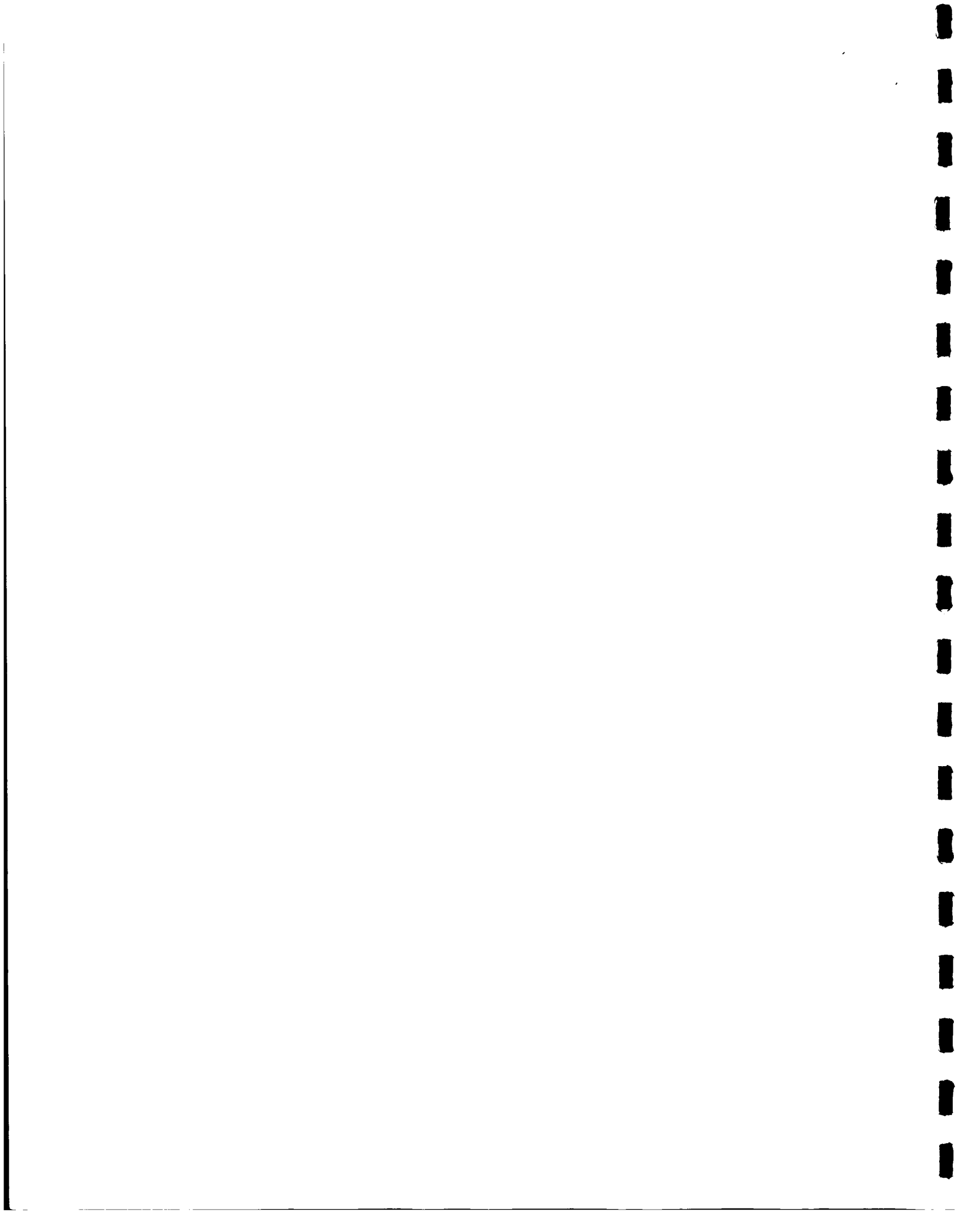
ABSTRACT

A summary of the current state of theoretical understanding of the interaction of optical radiation with the atmosphere is presented along with an extensive bibliography. Particular attention is given to scattering and attenuation due to particulate matter contained in the atmosphere, and also to amplitude and phase fluctuations induced by atmospheric turbulence.

An assembly of equipment to measure meteorological parameters, along with optical transmission parameters of the atmosphere, and with some preliminary measurements are presented. This included an optical link over a 5 km path in the lower atmosphere and having each end of the link instrumented for the collection of meteorological data.

Actual data collection, correlation of meteorological data with optical propagation data and comparison with theory remains yet to be done.





PRECEDING PAGE BLANK NOT FILMED.

## CONTENTS

1.	INTRODUCTION	1
2.	OPTICAL PROPAGATION THROUGH THE ATMOSPHERE	5
2.1	Optical Attenuation by Hazes and Major Clouds	5
2.2	Optical Properties of Random Atmospheres and Related Effects on Laser Propagation	20
2.2.1	Dependence of Refractive Index Fluctuations on Environmental Parameters	20
2.2.2	Optical Propagation in a Random Atmosphere	31
3.	EXPERIMENT DESCRIPTION AND DISCUSSION	47
3.1	General Description	47
3.2	Optical Experimental Apparatus	59
3.3	Meteorological Instrumentation	65
3.4	Data Recording Instrumentation	74
3.5	Experiment Discussion	75
4.	EXPERIMENTAL RESULTS	77
5.	CONCLUSIONS AND RECOMMENDATIONS	83
	REFERENCES	85
	APPENDIX A - BIBLIOGRAPHY ON ATMOSPHERIC EFFECTS ON OPTICAL COMMUNICATIONS	87
	APPENDIX B - APPLIED OPTICS PAPER	105

PRECEDING PAGE BLANK NOT FILMED.

ILLUSTRATIONS

1	Percentage Frequency of 6/10 to 10/10 Cloud Cover at Altitudes from Sea Level to 5,000 feet (Winter)	6
2	Percentage Frequency of 6/10 to 10/10 Cloud Cover at Altitudes from 5,000 to 10,000 feet (Winter)	7
3	Percentage Frequency of 6/10 to 10/10 Cloud Cover at Altitudes from 10,000 to 15,000 feet (Winter)	8
4	Percentage Frequency of 6/10 to 10/10 Cloud Cover at Altitudes from 15,000 to 20,000 feet (Winter)	9
5	Percentage Frequency of 6/10 to 10/10 Cloud Cover at Altitudes from 20,000 to 30,000 feet (Winter)	10
6	Percentage Frequency of 6/10 to 10/10 Cloud Cover at Altitudes from Sea Level to 5,000 feet (Summer)	11
7	Percentage Frequency of 6/10 to 10/10 Cloud Cover at Altitudes from 5,000 to 10,000 feet (Summer)	12
8	Percentage Frequency of 6/10 to 10/10 Cloud Cover at Altitudes from 10,000 to 15,000 feet (Summer)	13
9	Percentage Frequency of 6/10 to 10/10 Cloud Cover at Altitudes from 15,000 to 20,000 feet (Summer)	14
10	Three Size Distribution Functions Used in the Integration of the Mie Functions (after Deirmendjian)	16
11	Model Cloud Drop Spectra (after Cato, Carrier, von Essen, Ref. 2)	18
12	Typical Gross Temperature Differences (after Conway, et al., (Ref. 12))	26
13	Index of Refraction Structure "Constant" versus Altitude (after Hufnagel and Stanley, Ref. 17)	35
14	Topographic Map Showing Optical Path	48
15	Ground Profile and Optical Path Between EOS and Henninger Flats	49
16	Laser Transmitter Receiver Station	51
17	Laser Transmitter - Optical Receiver Bench Setup for Optical Propagation Experiments	54
18	Recording Instruments for Optical and Meteorological Signals During Laser Propagation Research	55

# ILLUSTRATIONS (contd)

19	Meteorological Sensor Mast	56
20	Meteorological Instrumentation Substation No. 1	57
21	Photograph of Remote Station taken from EOS Facility Through Telephoto Lens	58
22	10.6 $\mu$ Radiation Detector and Preamplifier Schematic	60
23	0.6328 $\mu$ Radiation Detector Wire Diagram	61
24	CO <sub>2</sub> Laser Reference Signal Detector	64
25	Temperature Sensor, Radiation and Wind Shield, and Bridge	67
26	Temperature Sensor Bridge Schematic	68
27	Hot-Wire Anemometer System (WCRC Type) Sensor, Bridge and Meter	69
28	Hot-Wire Wind Velocity System (WCRC) Schematic	70
29	Hot-Wire Anemometer System (Hastings-Raydist Type)	71
30	Electro-Humidity Sensors and Bridge	72
31	Humidity Sensor Electronics Schematic	73
32	Effects of Atmosphere on CO <sub>2</sub> Laser Intensity	78
33	Effects of Atmosphere on He-Ne Laser Intensity	81

## SECTION 1

### INTRODUCTION

Recently acquired close-up photographs of the surface of the moon clearly demonstrate, once again, the tremendous significance of photo-optical and electro-optical techniques for gathering, processing, and transferring large quantities of data with meaningful scientific and engineering impact. Graphical communications will assuredly play an ever increasing role in future space exploration. Furthermore, optical communications systems promise to carry a major portion of the information load. For example, a 20 cm x 20 cm photograph of Mars or Venus containing  $10^8$  bits of information has a transmission time requirement of about 1 day for an RF system, assuming a state-of-the-art data rate of 1000 bits/second; whereas the on-time requirement for a laser system is about 10 seconds, assuming a data rate of  $10^7$  bits/second (Ref. 1). The potential of the laser for deep-space communications seems implicitly clear.

However, it is well known that the channel capacity of any communications system depends not only upon the allowable bandwidth of the system, but also upon the signal power at the receiver as well as the receiver effective-noise power. It is also known that electromagnetic waves can become severely attenuated, reflected, deflected, and distorted during propagation through the atmosphere, such that high data rates or system simplicity must be compromised for lower error rates. Atmospheric degradation of optical signals can be especially severe, and the ultimate usefulness of laser communications depends upon the optical transmission and the noise generating processes of the atmosphere.

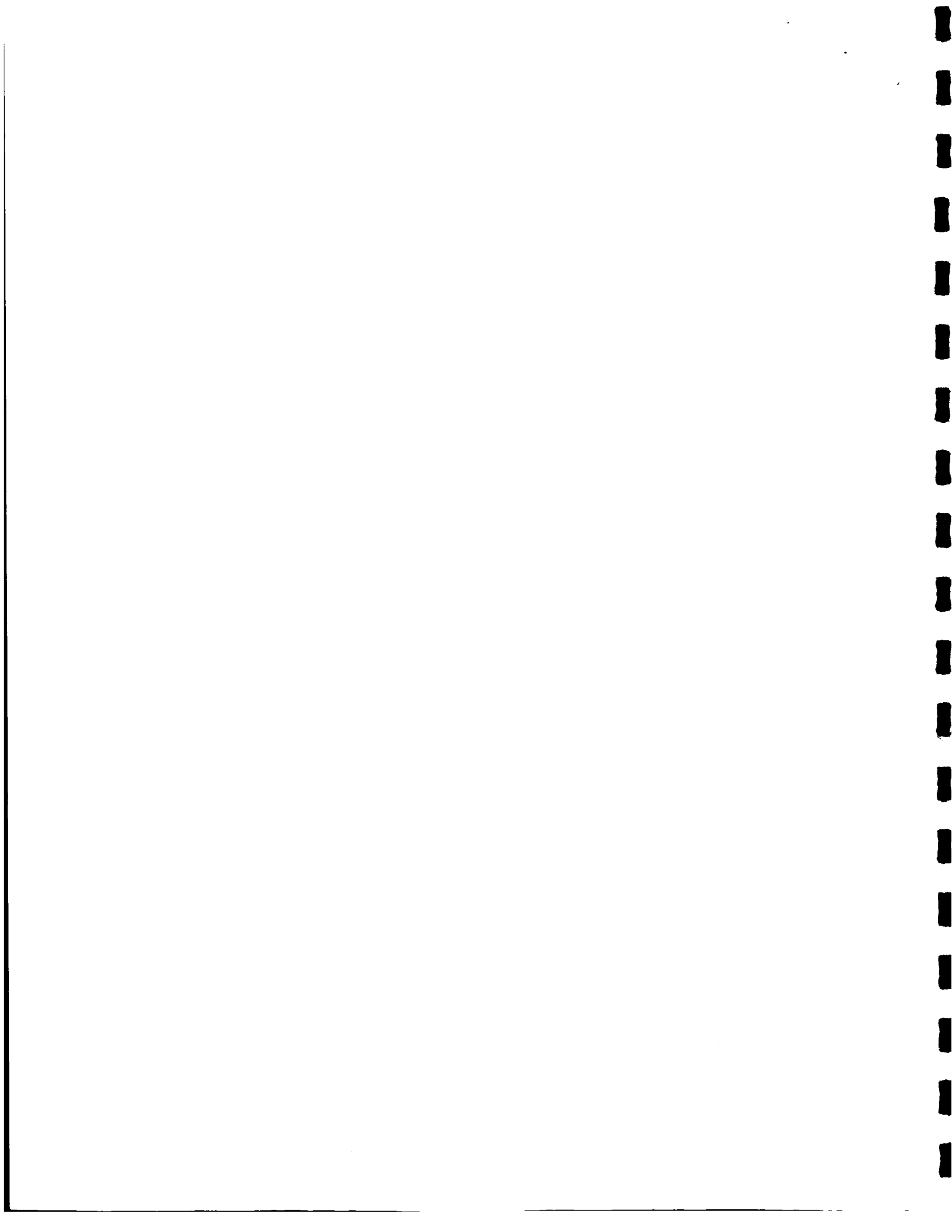
Several researchers have investigated the problem of atmospheric limitations to the propagation of stellar, laser, and nonlaser light. Appendix A contains a bibliography of much of this work, with particular emphasis on the latest laser propagation investigations. Models, theories, and functional relationships have been developed in order to describe or predict the magnitude of the effects of the atmosphere on optical beam properties, based upon certain simplifying assumptions and upon limited experimental data. There presently exist limited experimental data with which to verify existing theories, to apply existing data to dissimilar atmospheric conditions, or to reliably optimize system designs or techniques.

The objective of this study is to more fully investigate the effects of the atmosphere on transmitted laser beams and to identify the limitations that these atmospheric effects will impose on the design and capabilities of future optical communications systems. The two laser beam characteristics of particular interest are the intensity and degree of coherence subsequent to propagation through the atmosphere.

Section 2 contains a brief discussion of the physical properties of the atmosphere and the related deterministic and stochastic optical properties, based upon meteorological and environmental conditions. The randomness of the atmosphere results in signal intensity and coherence degradation and in a noisy communication channel. The predicted significance of these degradations is also discussed.

Experiments, apparatus, and facilities, described in Section 3, were designed and developed during the present investigation to measure the laser beam degradation and to relate these effects to the meteorological conditions along the optical path.

A He-Ne laser and a CO<sub>2</sub> laser were transmitted simultaneously over a six-mile round-trip optical path and were subsequently detected and recorded. Experimental results, discussed in Section 4, do not allow an adequate comparison between data and theory.





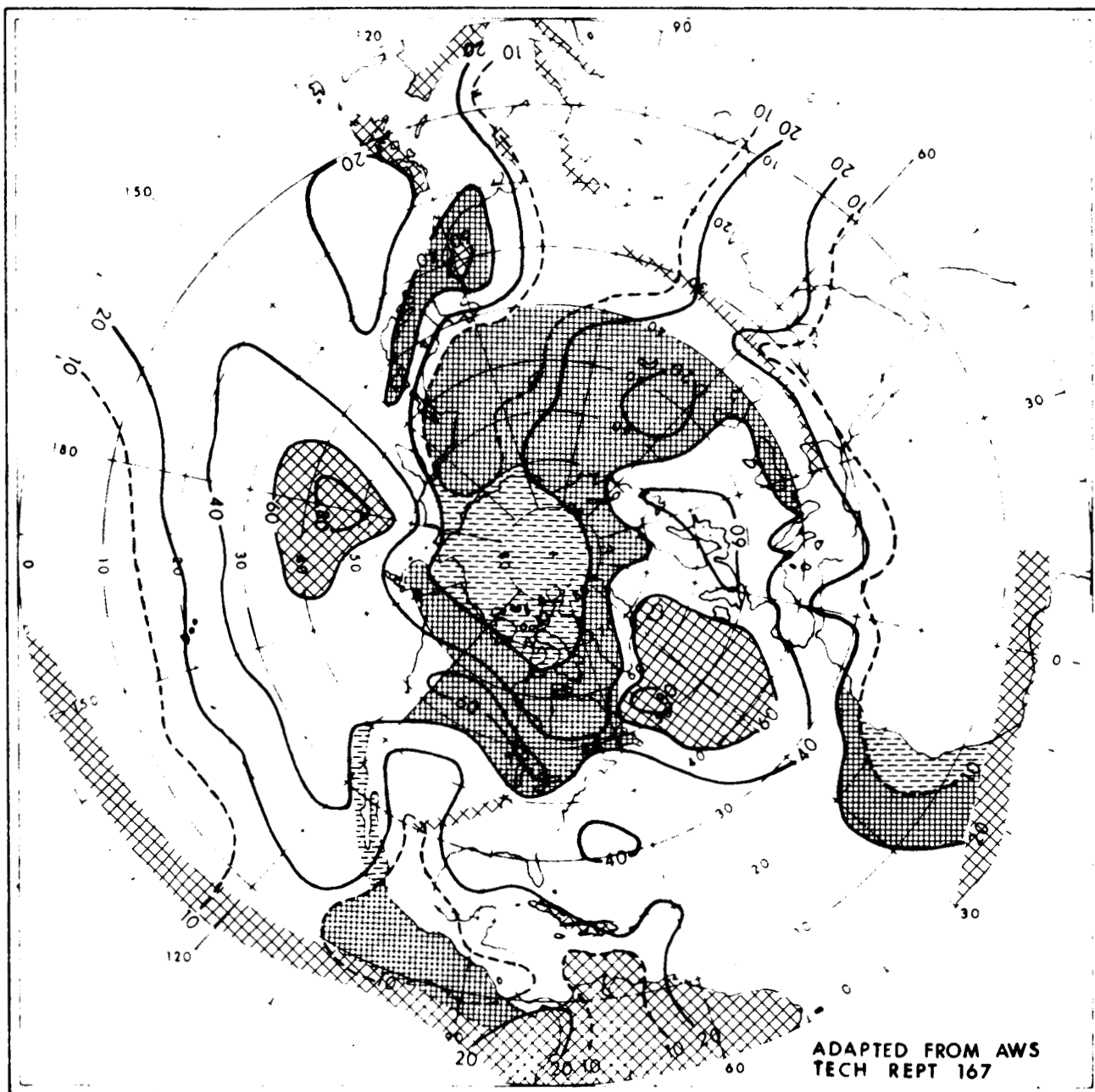
## SECTION 2

### OPTICAL PROPAGATION THROUGH THE ATMOSPHERE

Very few portions of the earth remain unobscured from hazes and clouds for extended periods of time so that optical communications over certain paths through the earth's atmosphere can become marginal or even impractical. Furthermore, even some "clear air" atmospheric conditions are not particularly conducive to reliable and efficient optical communications, owing to "poor seeing" conditions. These factors are well known, in general; however, the optical properties of major clouds and the relationship between "poor seeing" and meteorological conditions have not been amply treated in the literature. In this section, we shall present results of a theoretical analysis of the optical properties of the major clouds, and shall describe how the optical properties of the random atmosphere depend upon the physical properties of the atmosphere.

#### 2.1 OPTICAL ATTENUATION BY HAZES AND MAJOR CLOUDS

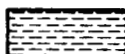
The percentage frequencies of cloud cover (6/10 to 10/10) over the northern hemisphere are shown in Figs. 1 through 9 for various cloud types, incremental altitudes, and seasons (Ref. 2). The probability of having a clear line of sight through the clouds depends upon the relative dimensions of the cloud structure in the vertical and horizontal directions. Kauth and Penquite (Ref. 3) and Lund (Ref. 4) describe methods for determining the probability functions; these are not discussed here. However, from common experience, we know that there is a reasonably high probability that a cloud will intercept and partially obstruct an optical beam in transit through the atmosphere, depending more or less on the communication terminal locations. The main question then is: "What are the attenuating properties of these obstructions?"



STRATUS

STRATOCUMULUS

CUMULONIMBUS



ALTOCUMULUS



ALTOSTRATUS



CUMULUS CONGESTUS

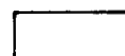
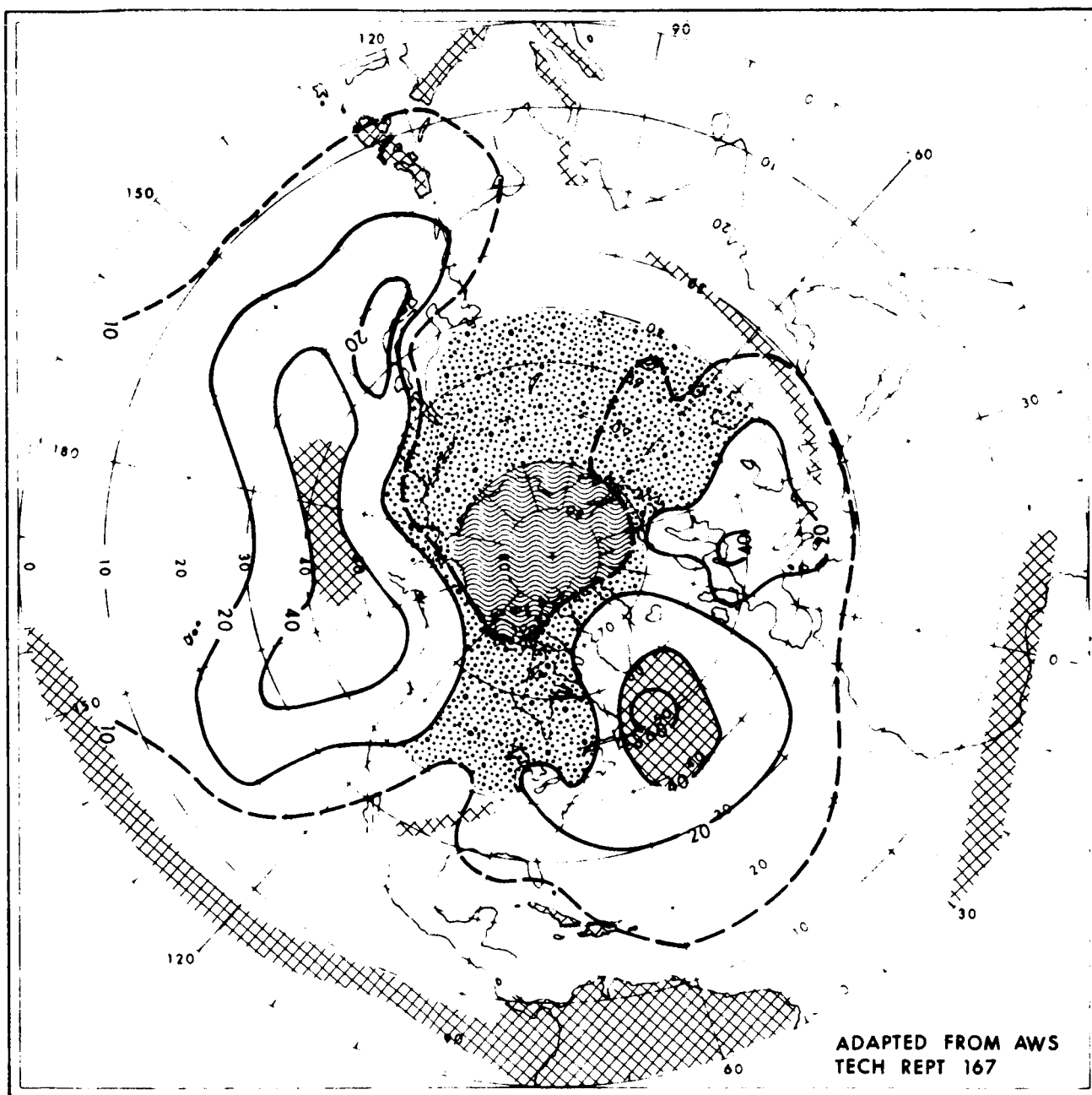


Figure 1. Percentage Frequency of 6/10 to 10/10 Cloud Cover at Altitudes from Sea Level to 5,000 feet (Winter)



STRATUS

STRATOCUMULUS

CUMULONIMBUS



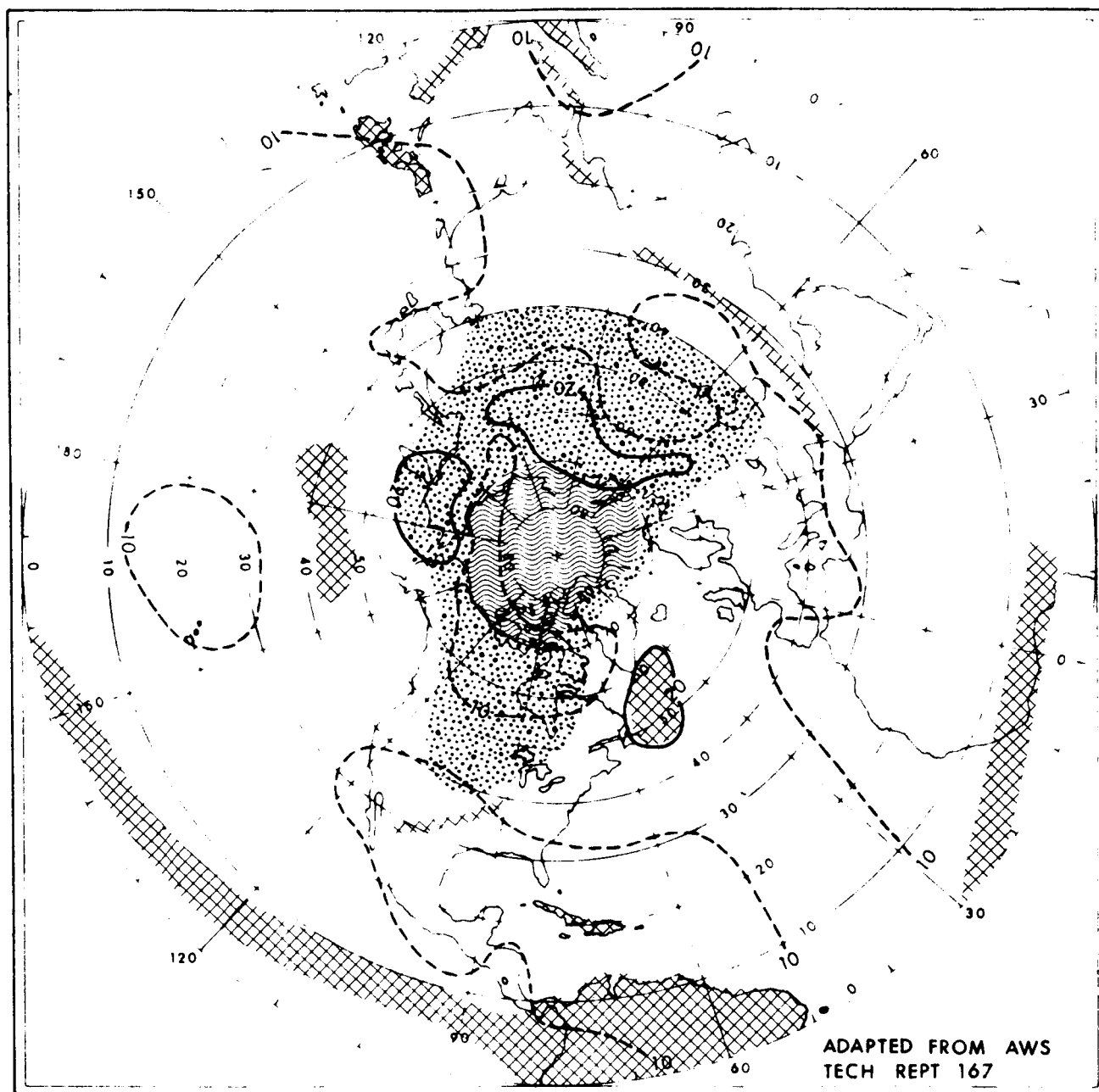
ALTOCUMULUS

ALTOSTRATUS

CUMULUS CONGESTUS



Figure 2. Percentage Frequency of 6/10 to 10/10 Cloud Cover at Altitudes from 5,000 to 10,000 feet (Winter)



STRATUS

STRATOCUMULUS

CUMULONIMBUS



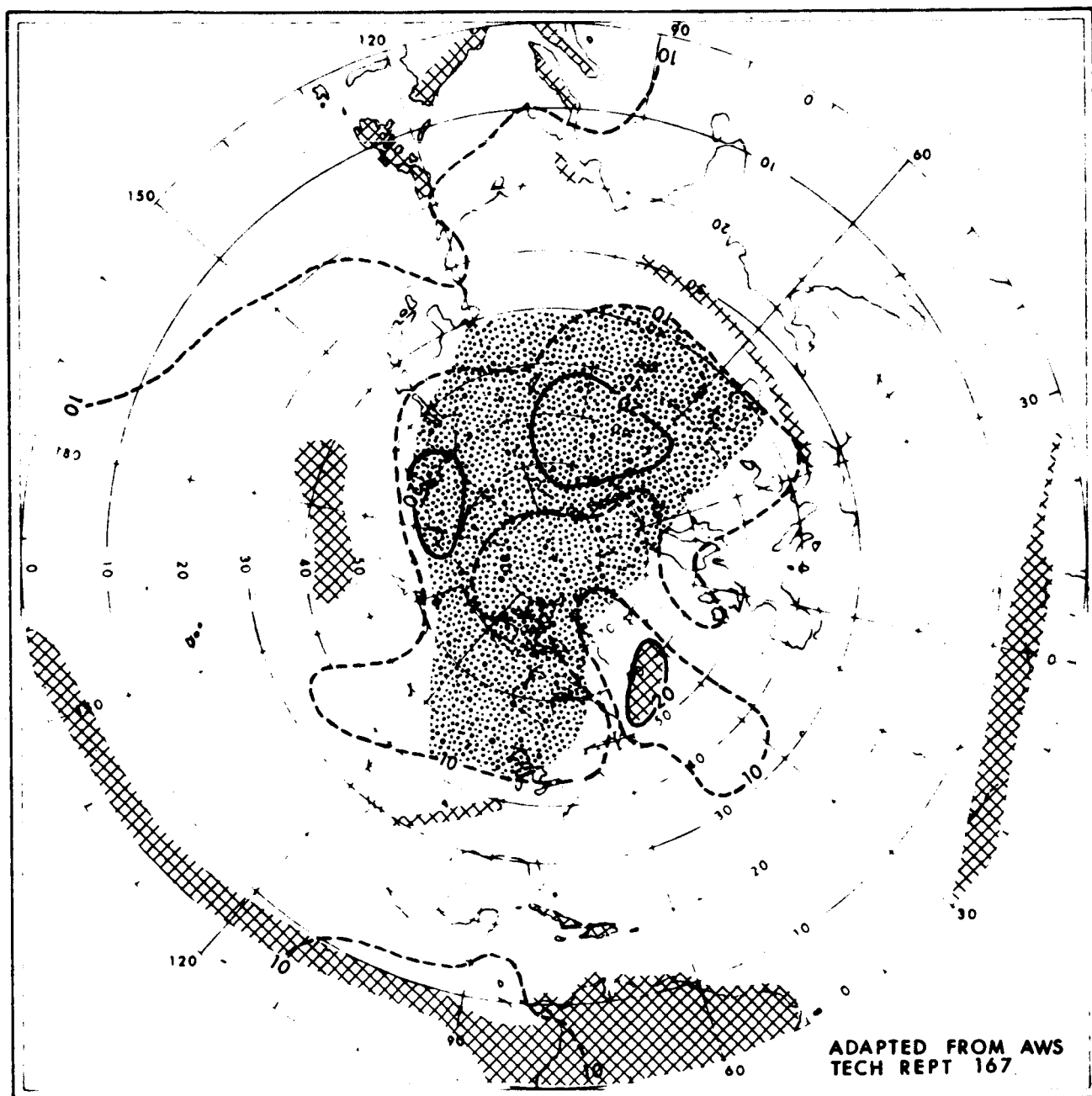
ALTOCUMULUS

ALTOSTRATUS

CUMULUS CONGESTUS



Figure 3. Percentage Frequency of 6/10 to 10/10 Cloud Cover at Altitudes from 10,000 to 15,000 feet (Winter)



STRATUS

STRATOCUMULUS

CUMULONIMBUS



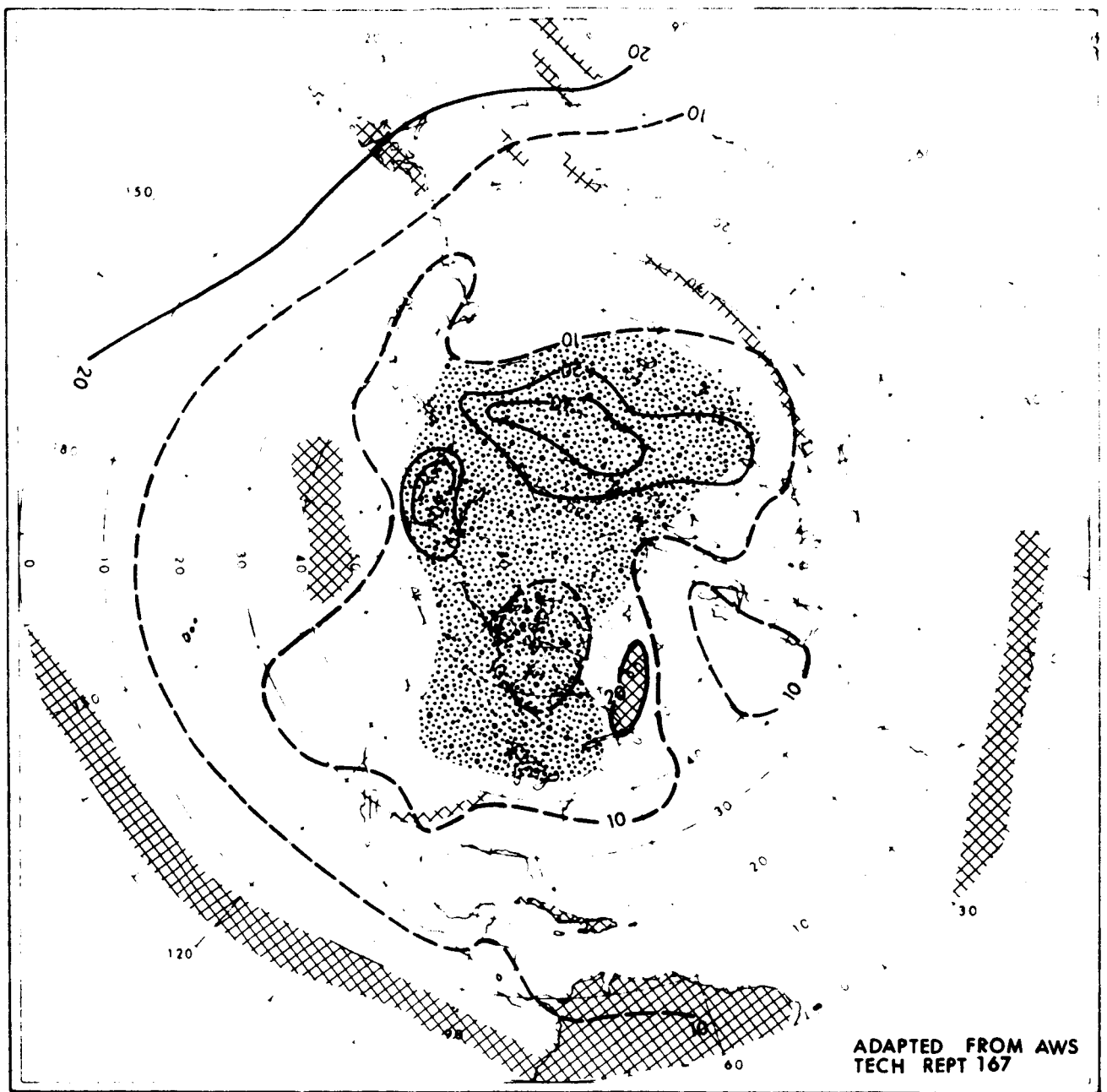
ALTOCUMULUS

ALTOSTRATUS

CUMULUS CONGESTUS



Figure 4. Percentage Frequency of 6/10 to 10/10 Cloud Cover at Altitudes from 15,000 to 20,000 feet (Winter)



STRATUS



ALTOCUMULUS



STRATOCUMULUS



ALTOSTRATUS



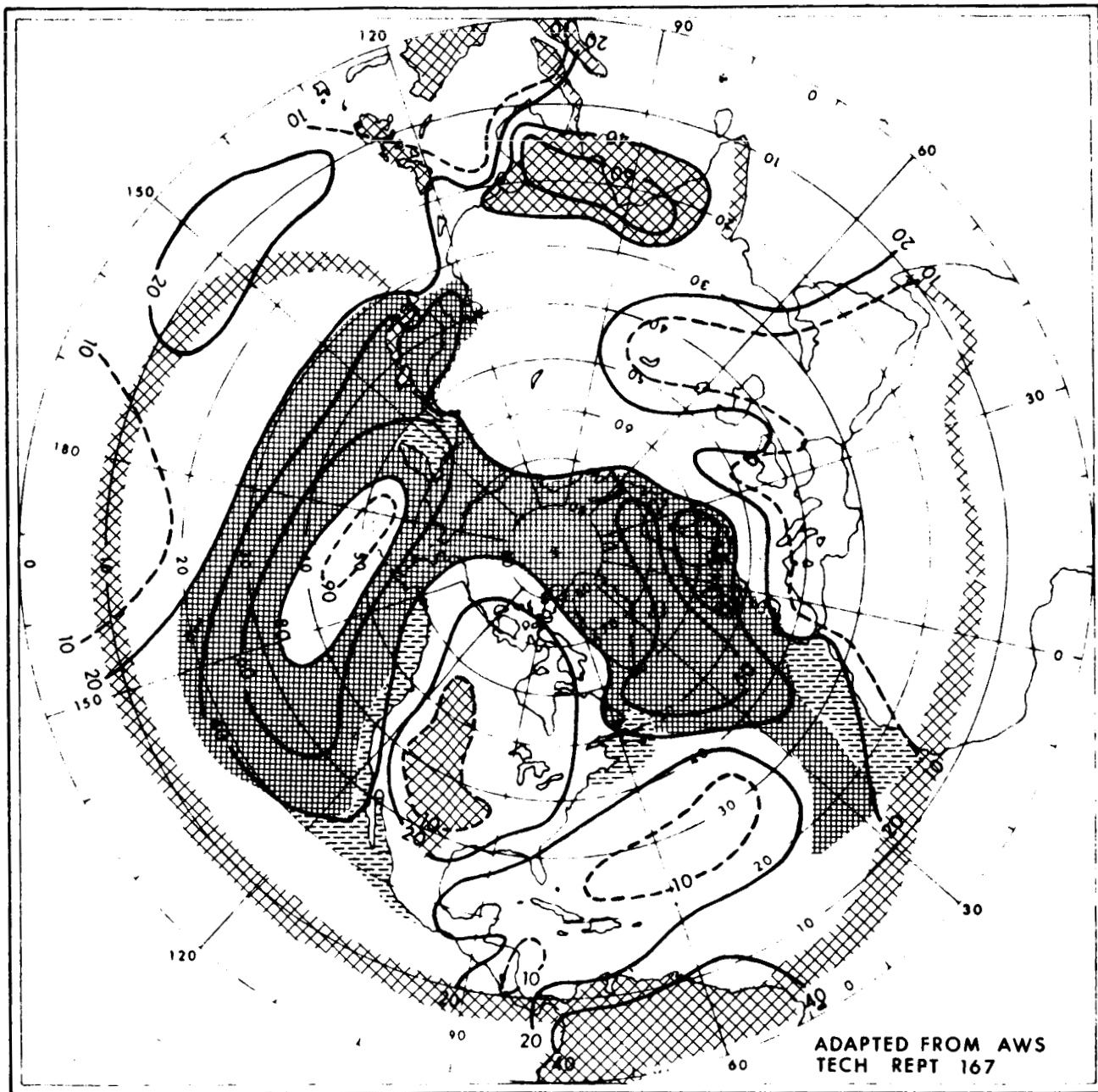
CUMULONIMBUS



CUMULUS CONGESTUS



Figure 5. Percentage Frequency of 6/10 to 10/10 Cloud Cover at Altitudes from 20,000 to 30,000 feet (Winter)



STRATUS

STRATOCUMULUS

CUMULONIMBUS



ALTOCUMULUS



ALTOSTRATUS



CUMULUS CONGESTUS

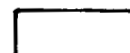
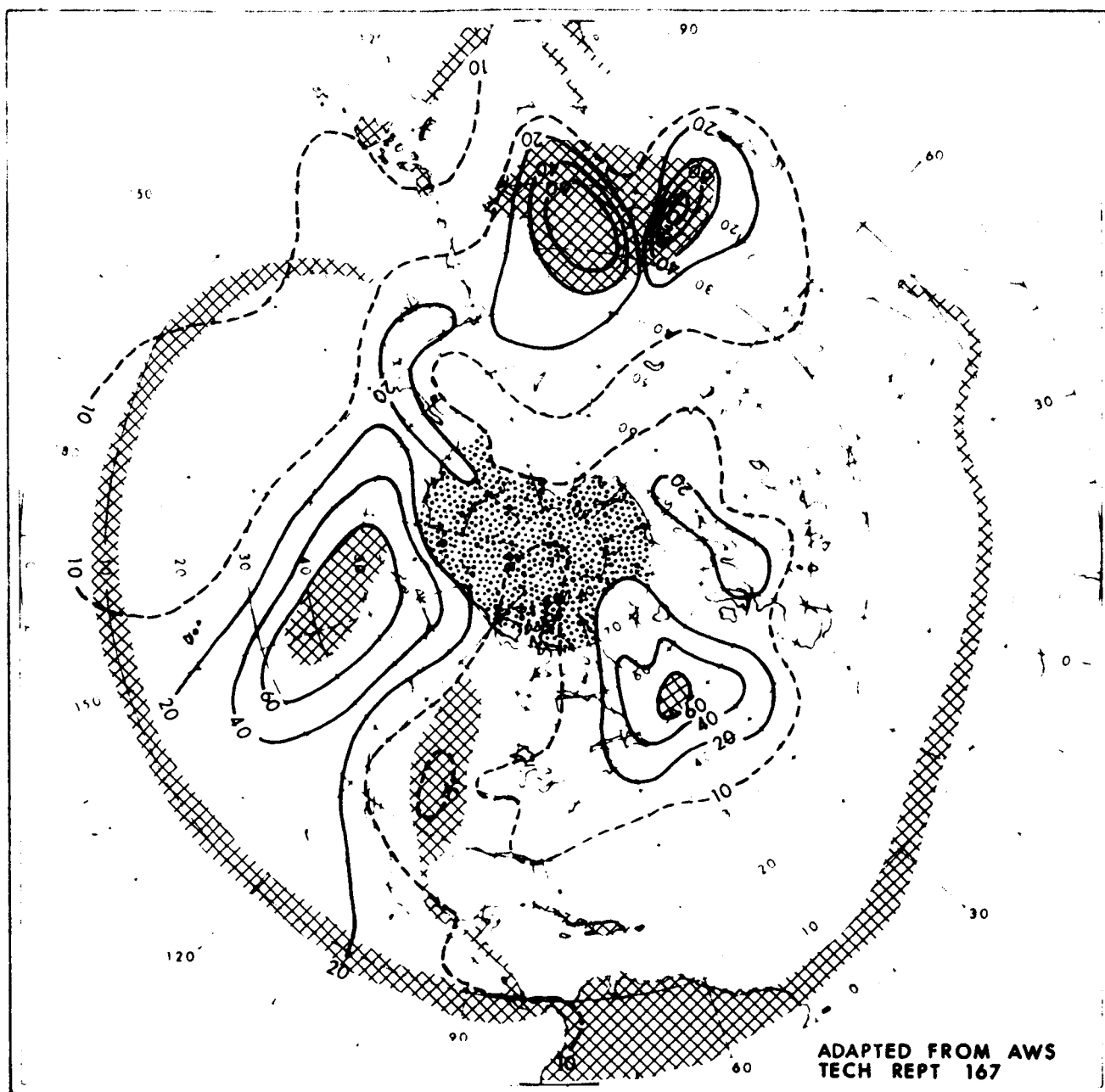


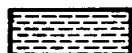
Figure 6. Percentage Frequency of 6/10 to 10/10 Cloud Cover at Altitudes from Sea Level to 5,000 feet (Summer)



STRATUS

STRATOCUMULUS

CUMULONIMBUS



ALTOCUMULUS

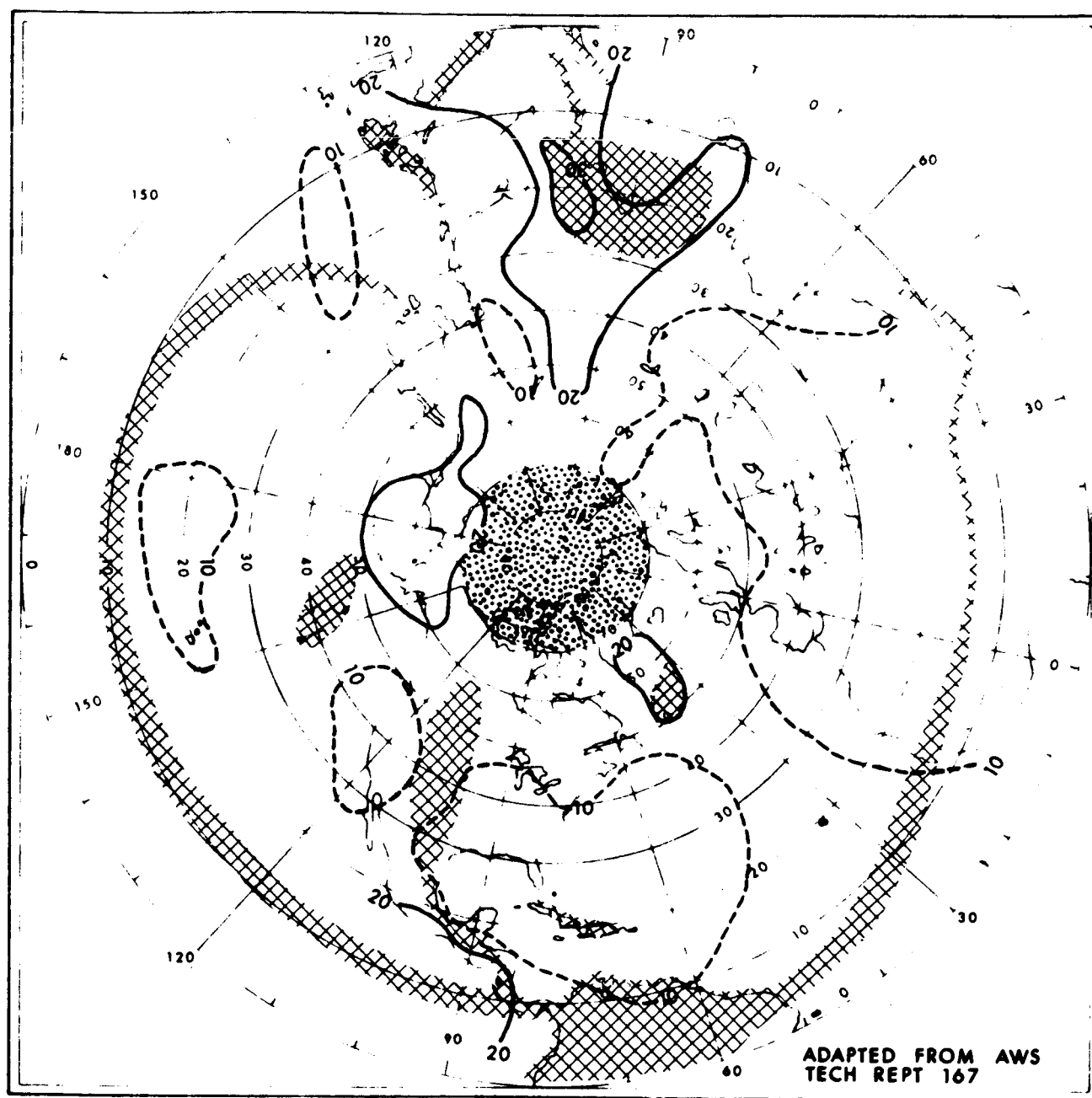
ALTOSTRATUS

CUMULUS CONGESTUS



Figure 7. Percentage Frequency of 6/10 to 10/10 Cloud Cover at Altitudes from 5,000 to 10,000 feet (Summer)





STRATUS

STRATOCUMULUS

CUMULONIMBUS



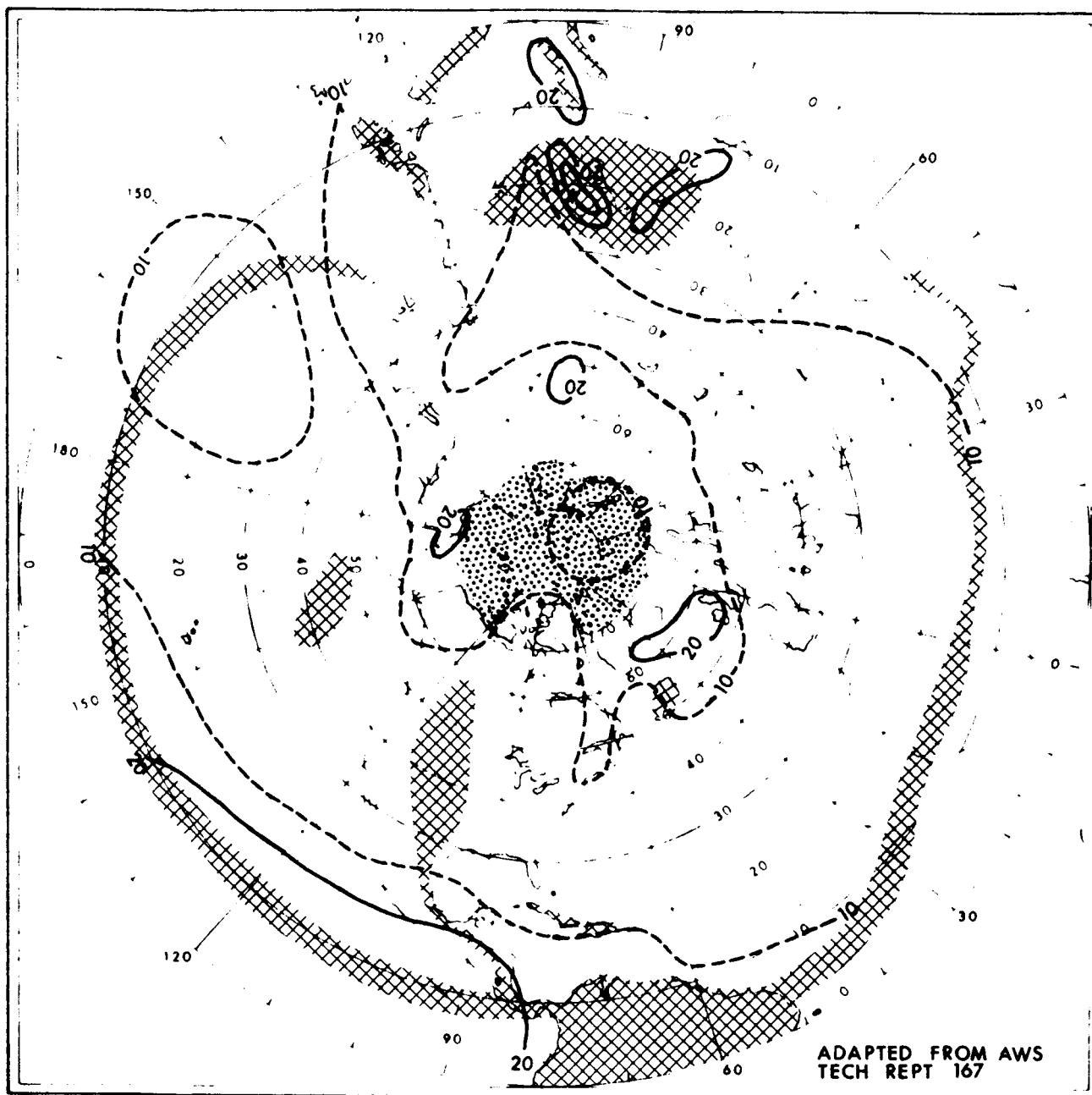
ALTOCUMULUS

ALTOSTRATUS

CUMULUS CONGESTUS



Figure 8. Percentage Frequency of 6/10 to 10/10 Cloud Cover at Altitudes from 10,000 to 15,000 feet (Summer)



STRATUS

STRATOCUMULUS

CUMULONIMBUS



ALTOCUMULUS



ALTOSTRATUS



CUMULUS CONGESTUS



Figure 9. Percentage Frequency of 6/10 to 10/10 Cloud Cover at Altitudes from 15,000 to 20,000 feet (Summer)

The optical properties of hazes and clouds can be computed using the exact Mie theory of electromagnetic wave scattering providing the size, number, and distribution and the index of refraction of the scatterers are known. The Mie theory is discussed lucidly and amply by van de Hulst (Ref. 5). Typical size distributions of hazes and cumulus clouds are described by Deirmendjian (Ref. 6) and their attenuating effects on visible and infrared radiation are calculated. Figure 10 shows the size distributions of both continental and maritime hazes and of a cumulus cloud with a total concentration of  $100 \text{ cm}^{-3}$ . Table I summarizes the spectral attenuation properties of these distributions; it is noted that for the case of scattering by hazes, or small particles, infrared radiation surpasses visible light for transmission through the haze. On the other hand, clouds are comprised of larger droplets, and it is noted that their related optical extinction properties are relatively insensitive to wavelength.

The cloud particle-size distribution of Fig. 10 is not an all-encompassing cloud model; hence, the values of optical attenuation by clouds in Table I are not completely descriptive of the optical properties of the atmosphere. Cato, Carrier, and von Essen (Ref. 2) conducted an extensive survey of the literature in order to establish representative cloud models for the eight major clouds (comprised of water drops); the conclusion of the study is that the cloud droplet spectra depicted in Fig. 11 represent typical cloud models. The optical properties of these cloud models were computed, based upon the Mie theory, and during the present program the computations were extended to include the optical effects of clouds on 4 and 10 micron radiation; the calculations, results, and conclusions of this analysis are discussed in Appendix B, a paper which has been accepted for publication in the July issue of Applied Optics. The optical scattering coefficients associated with the cloud models are summarized in Table II. It is significant to note that optical extinction, due to the scattering processes, shows little

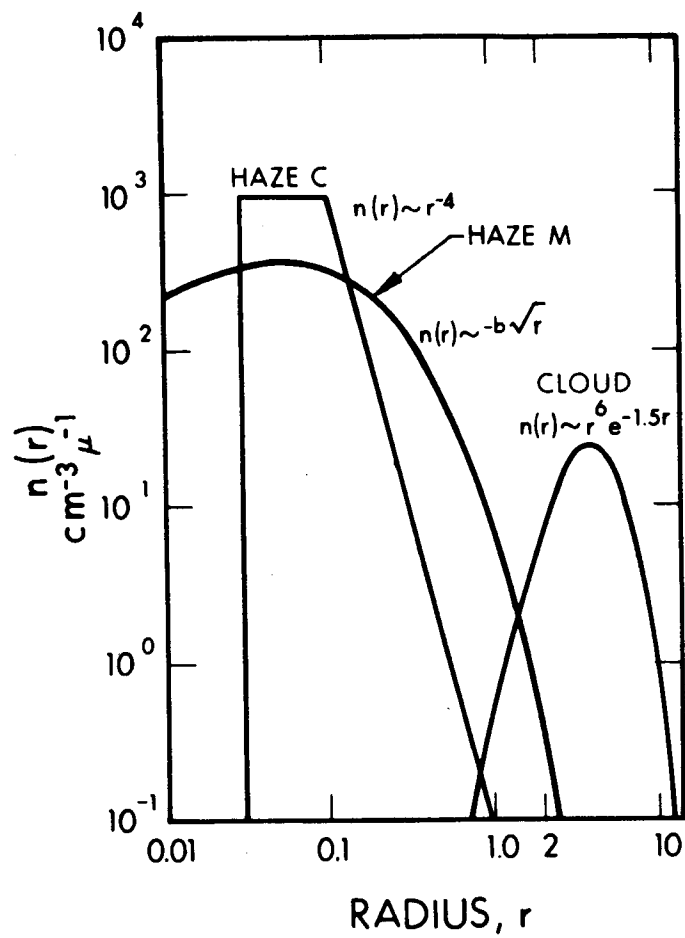


Figure 10. Three Size Distribution Functions Used in the Integration of the Mie Functions (after Deirmendjian)

TABLE I  
ATTENUATION OF OPTICAL RADIATION  
BY HAZES AND CUMULUS CLOUD

(After Deirmendjian, Ref. 6)

Wavelength ( $\mu$ )	Continental Haze $b_{\text{ext}} \text{ (m}^{-1}\text{)}$	Maritime Haze $b_{\text{ext}} \text{ (m}^{-1}\text{)}$	Cumulus Cloud $b_{\text{ext}} \text{ (m}^{-1}\text{)}$
0.45	$1.21 \times 10^{-4}$	$1.06 \times 10^{-4}$	$1.63 \times 10^{-2}$
0.70	$7.59 \times 10^{-5}$	$1.06 \times 10^{-4}$	$1.67 \times 10^{-2}$
1.61	$3.12 \times 10^{-5}$	$6.91 \times 10^{-5}$	$1.76 \times 10^{-2}$
2.25	$1.94 \times 10^{-5}$	$4.24 \times 10^{-5}$	$1.82 \times 10^{-2}$
3.07	$2.89 \times 10^{-5}$	$6.02 \times 10^{-5}$	$1.86 \times 10^{-2}$
3.90	$1.28 \times 10^{-5}$	$2.36 \times 10^{-5}$	$2.06 \times 10^{-2}$
5.30	$7.50 \times 10^{-6}$	$1.12 \times 10^{-5}$	$2.40 \times 10^{-2}$
6.05	$1.29 \times 10^{-5}$	$1.89 \times 10^{-5}$	$1.99 \times 10^{-2}$
8.15	$5.00 \times 10^{-6}$	$6.20 \times 10^{-6}$	$1.88 \times 10^{-2}$
10.0	$3.20 \times 10^{-6}$	$4.5 \times 10^{-6}$	$1.12 \times 10^{-2}$
11.5	$6.40 \times 10^{-6}$	$9.70 \times 10^{-6}$	$1.01 \times 10^{-2}$
16.6	$8.20 \times 10^{-6}$	$1.34 \times 10^{-5}$	$1.70 \times 10^{-2}$

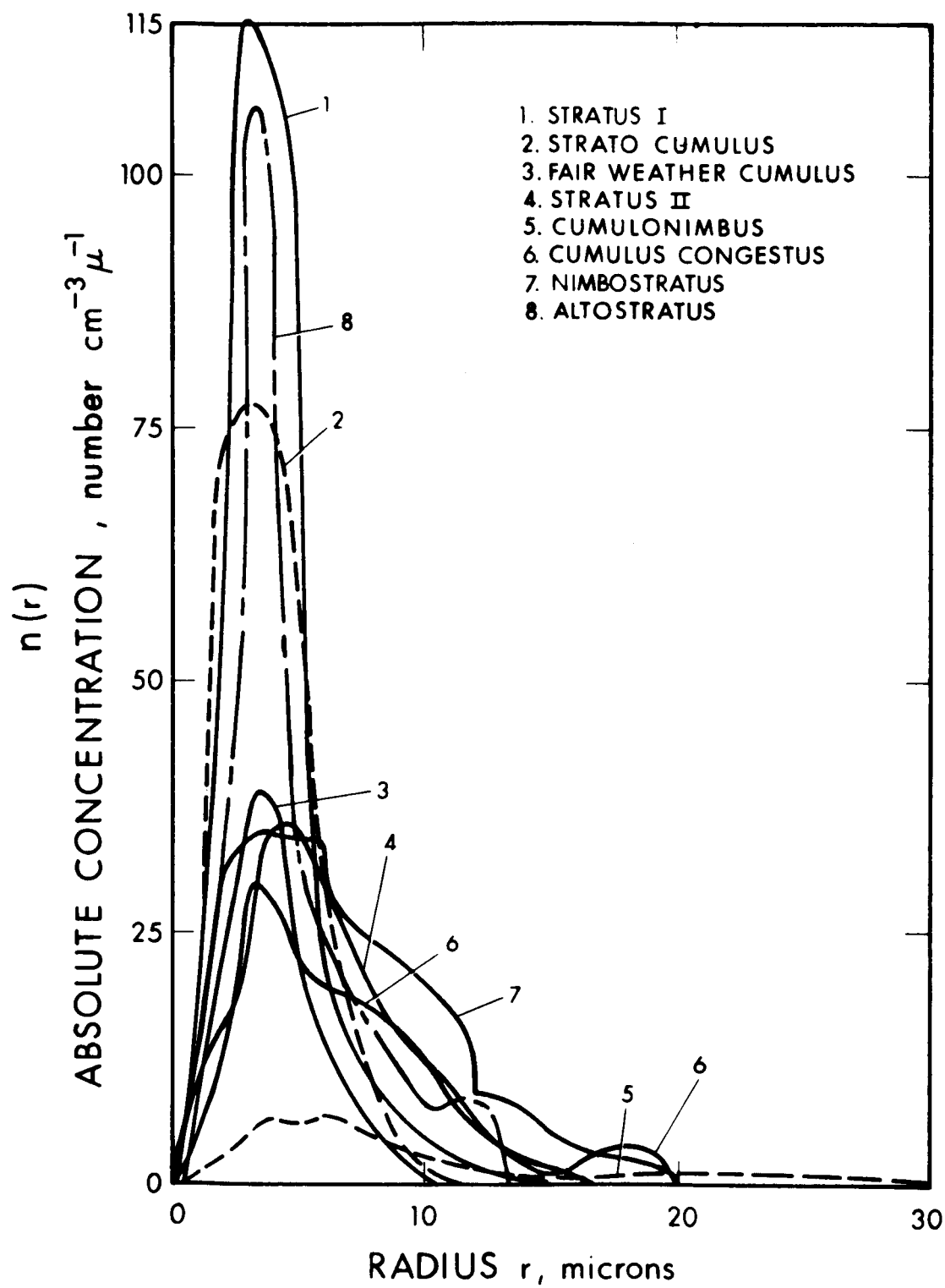


Figure 11. Model Cloud Drop Spectra (after Cato, Carrier, von Essen, Ref. 2)

TABLE II  
OPTICAL SCATTERING COEFFICIENTS OF THE MAJOR CLOUD TYPES

Optical Scattering Coefficient $b$ ( $m^{-1}$ )					
Wavelength					
Cloud Type	0.488 $\mu$	0.694 $\mu$	1.06 $\mu$	4.0 $\mu$	10.6 $\mu$
Nimbostratus	$1.28 \times 10^{-1}$	$1.30 \times 10^{-1}$	$1.32 \times 10^{-1}$	$1.47 \times 10^{-1}$	$1.36 \times 10^{-1}$
Altostratus	$1.08 \times 10^{-1}$	$1.09 \times 10^{-1}$	$1.12 \times 10^{-1}$	$1.30 \times 10^{-1}$	$8.39 \times 10^{-2}$
Stratus II	$1.00 \times 10^{-1}$	$1.01 \times 10^{-1}$	$1.03 \times 10^{-1}$	$1.14 \times 10^{-1}$	$1.04 \times 10^{-1}$
Cumulus Congestus	$6.92 \times 10^{-2}$	$6.98 \times 10^{-2}$	$7.13 \times 10^{-2}$	$8.10 \times 10^{-2}$	$6.76 \times 10^{-2}$
Stratus I	$6.69 \times 10^{-2}$	$6.79 \times 10^{-2}$	$6.97 \times 10^{-2}$	$9.01 \times 10^{-2}$	$4.28 \times 10^{-2}$
Cumulonimbus	$4.35 \times 10^{-2}$	$4.38 \times 10^{-2}$	$4.44 \times 10^{-2}$	$4.82 \times 10^{-2}$	$5.09 \times 10^{-2}$
Stratocumulus	$4.53 \times 10^{-2}$	$4.60 \times 10^{-2}$	$4.71 \times 10^{-2}$	$5.96 \times 10^{-2}$	$2.48 \times 10^{-2}$
Fair-Wx Cumulus	$2.10 \times 10^{-2}$	$2.13 \times 10^{-2}$	$2.19 \times 10^{-2}$	$2.76 \times 10^{-2}$	$1.17 \times 10^{-2}$

dependence upon wavelength, in agreement with Deirmendjian's calculations; however, optical extinction can be appreciably higher than that predicted by Deirmendjian for his cumulus cloud model.

Another significance of the predicted values of optical scattering coefficients for clouds other than that of optical extinction is that multiple scattering effects can become appreciable; as a consequence an optical signal becomes smeared in time and intensity, with a commensurate degradation of an optical system's communication efficiency. The problem is treated in part by Dell-Imagine (Ref. 7).

## 2.2 OPTICAL PROPERTIES OF RANDOM ATMOSPHERES AND RELATED EFFECTS ON LASER PROPAGATION

In the previous section we discussed the propagation of optical radiation through cloudy atmospheres and showed that the use of long wavelength transmitters offers the possibility of improved optical communications system performance. In this section we discuss the advantages of long wavelengths in propagating through a random atmosphere. First, we describe the optical properties of a random atmosphere and their dependence upon meteorological conditions. Then, we discuss the effects of random atmospheres upon the characteristic properties of optical beams.

### 2.2.1 DEPENDENCE OF REFRACTIVE INDEX FLUCTUATIONS ON ENVIRONMENTAL PARAMETERS

The refractive index of the atmosphere is both regular and random, denoted by

$$n = \bar{n} + \mu \quad (1)$$

where the bar designates the time average and  $\mu$  indicates the instantaneous value of the fluctuation of the parameter. The value for refractive index for any medium depends upon both the wavelength of the propagating wave and the density of the medium. Various ways of expressing refractive index can be found in the literature. We will follow Portman (Ref. 8) and Munick (Ref. 9).

For air at pressures on the order of 1 atmosphere

$$n = 1 + Kp \quad (2)$$



where K is a constant and p is density. It has been shown that the index of refraction of air can be rewritten in terms of temperature, pressure, and water vapor pressure as

$$n = 1 + \frac{(p - e)A_1 + e\epsilon A_2}{RT} \quad (3)$$

where T = temperature ( $^{\circ}\text{K}$ )  
 p = atmospheric pressure (mb)  
 e = water vapor pressure (mb)  
 $\epsilon$  = ratio of molecular weights of water vapor and dry air = 0.622  
 R = gas constant for dry air =  $2.876 \times 10^6 \text{ cm}^2 \text{ sec}^{-2} \text{ deg}^{-1}$   
 $A_1 = 2.28$   
 $A_2 = 3.25$

Equation 3 is written more simply as:

$$n = 1 + \frac{Ap}{T} - \frac{Be}{T} \quad (4)$$

where

$$A = \frac{A_1}{R} = 79 \times 10^{-6} \text{ } ^{\circ}\text{K mb}^{-1} \quad (\lambda = 5893\text{\AA})$$

$$B = \left( \frac{\epsilon A_2 - A_1}{R} \right) = 11 \times 10^{-6} \text{ } ^{\circ}\text{K mb}^{-1} \quad (\lambda = 5893\text{\AA})$$

It should be noted that A and B are wavelength-dependent and that the index of refraction is more generally described by

$$n-1 = \frac{A'p}{T} + \frac{Cp}{T\lambda^2} - \frac{Be}{T} \quad (5)$$

where  $A' = 77.6 \times 10^{-6} \text{ }^{\circ}\text{K mb}^{-1}$  for  $(\lambda < 20 \text{ microns})$   
 $C = 0.584 \times 10^{-6} \text{ }^{\circ}\text{K } \mu^2 \text{ mb}^{-1}$

Values of refractive modules (i.e.,  $N = (n - 1)(10^6)$ ) are given in the Handbook of Geophysics (Ref. 10) for wavelengths from 0.2 micron to 20 microns, for negligible water vapor.

It is now useful to determine the relative effects and significance of temperature, pressure and vapor pressure on the index of refraction of air. The meteorological parameters  $T$ ,  $p$ , and  $e$  are time varying so they can be written:

$$T = \bar{T} + \Delta T \quad (6)$$

$$p = \bar{p} + \Delta p \quad (7)$$

$$e = \bar{e} + \Delta e \quad (8)$$

Water vapor pressure is related to relative humidity,  $f$ , as

$$e = \frac{e_s f}{100}$$

where  $e_s$  = saturation vapor pressure at the same temperature so that

$$e = \frac{e_s}{100} (\bar{f} + \Delta f) \quad (9)$$

Since the relative fluctuations  $\Delta T$ ,  $\Delta p$ , and  $\Delta f$  are small compared to the average values, then, following Munick, Eq. 4 can be rewritten as

$$\bar{n} - 1 = \frac{\Delta \bar{p}}{\bar{T}} - \frac{\bar{p} \Delta \bar{e}}{\bar{T}} \quad (10)$$

Further, the fluctuation in refractive index is found by subtracting Eq. 10 from Eq. 4 and rearranging:

$$\mu = A \left( \frac{\bar{p}}{\bar{T}} \right) \left[ \frac{\Delta p}{\bar{p}} - \frac{\Delta T}{\bar{T}} - \left( \frac{\bar{B_e}}{\bar{A_p}} \right) \left( \frac{\Delta e}{\bar{e}} - \frac{\Delta T}{\bar{T}} \right) \right] \quad (11)$$

or in terms of relative humidity

$$\Delta n = A \left( \frac{\bar{p}}{\bar{T}} \right) \left[ \frac{\Delta p}{\bar{p}} - \frac{\Delta T}{\bar{T}} - \left( \frac{\bar{B_e} \bar{f}}{100 \bar{A_p}} \right) \left( \frac{\Delta f}{\bar{f}} - \frac{\Delta T}{\bar{T}} \right) \right] \quad (12)$$

Fluctuations in the meteorological parameters can be expressed in terms of standard deviations ( $\sigma$ ), and, according to Munick, the relative changes in each of these parameters are typically

$$\sigma_p / \bar{p} < 10^{-5}$$

$$\sigma_T / \bar{T} < 10^{-2}$$

$$\sigma_e / \bar{e} < 4 \times 10^{-2}$$

This latter variation is multiplied by the factor  $\bar{B_e} / \bar{A_p}$ , and, in most cases for visible light, the net effect of water vapor variations is negligible.\*

Fluctuations in refractive index, therefore, from Eq. 11, can be related to meteorological measurements of average pressure, average temperature, and temperature fluctuations approximately as

---

\* Carlon (Ref. 11) indicates, however, that for high relative humidities (greater than about 70%) and for 10-micron radiation, water vapor variations can become dominant in producing fluctuations in refractive index.

$$\Delta n = A_{\lambda} \frac{\bar{p} \Delta T}{T^2} \quad (13)$$

From Eq. 13 it is apparent that large index gradients are produced during conditions of high pressure (clear weather at sea level) and of low temperatures. Also, it can be shown that a one-degree temperature deviation produces an index of refraction deviation of about  $10^{-6}$ .

The generating mechanisms of large fluctuations of refractive index in the atmosphere due to turbulence are related to the time of day and season, meteorological conditions, topography, surface conditions, and altitude. For a detailed description of atmospheric physical processes and environmental relationships to temperature, pressure, wind velocity, turbulence, etc., the reader is referred to Sutton (Ref. 13). Turbulent flow is generally made manifest by temperature and velocity fields.

The first 100 meters of the atmosphere is characterized by a marked diurnal variation of temperature gradients, with vertical gradients being orders of magnitude greater than horizontal gradients. The rate of decrease of temperature with altitude is called the temperature lapse rate,  $\Gamma$ . One of the fundamental constants of meteorology is the dry adiabatic lapse rate,  $\Gamma_d$ , which is equal to about  $-1^{\circ}\text{C}$  per 100 meters. If the air is inhomogeneously mixed due to unstable air, wind, turbulence, or other factors, parcels of air at one temperature are moved to regions at another temperature, thereby creating random temperature fluctuations. When the parcels change height,  $\Delta z$ , this temperature differential of the displaced air with its surroundings is given by

$$\frac{\Delta T}{\Delta z} = (\Gamma - \Gamma_d) \quad (14)$$

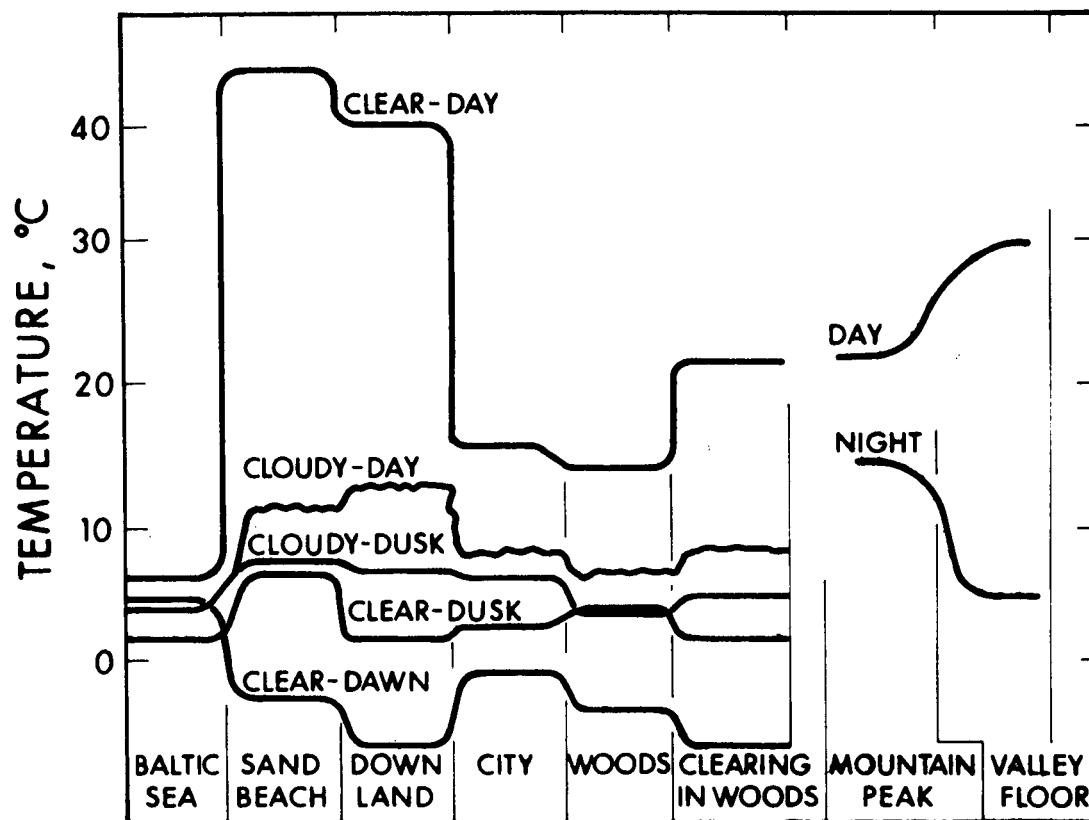
When the lapse rate equals the adiabatic lapse rate it is apparent that temperature fluctuations will not occur.

The magnitude of local temperature lapse rate depends upon the time of day, weather conditions, locality, surface conditions, season, height above surface, etc. Figure 12 depicts typical gross temperature differences at the earth's surface. Values of  $\Gamma$  reach quantities as high as several thousand times the adiabatic lapse rate at distances within a few centimeters of the ground.

During clear weather,  $\Gamma$  is often characterized by super adiabatic lapse rates during daylight hours, increasing rapidly during the early part of morning and reaching a maximum value at local noon; after remaining steady for some hours after noon, the quantity  $(\Gamma - \Gamma_d)$  decreases and becomes zero about sunset. Pronounced inversion rates can occur at night during clear weather. For windy and overcast conditions, the temperature lapse rate and average temperature remain very steady with no large high frequency fluctuations. The quantity  $(\Gamma - \Gamma_d)$  is also altitude dependent; furthermore, the time for which  $(\Gamma - \Gamma_d)$  reaches a maximum value depends on altitude.

Surface conditions are also relevant in determining lapse rate by establishing heat transfer rates. Some of the germane factors are soil density, soil state, specific heat, conductivity, surface cover, surrounding terrain, surface roughness, and wind.

Surface roughness and wind speed go together to produce vertical motion of the atmosphere due to wind shear; the effect of wind shear tends to decrease the temperature gradient through a mixing action. The net effect of wind is to create turbulence, hence refractive index inhomogeneities; the magnitude of the wind effect depends on the mean wind velocity and the temperature lapse rate, and can be related by two turbulence parameters, i.e., Reynolds number,  $Re$ , and Richardson number,  $Ri$ .



### TYPICAL GROSS TEMPERATURE DIFFERENCES

Figure 12. Typical Gross Temperature Differences (after Conway, et al., (Ref. 12))

The average wind speed increases with height above the ground as the wind forces overcome the drag of the earth's surface. Sutton (Ref. 13) gives a general expression for the wind velocity gradient as:

$$\beta = \frac{\partial \bar{v}}{\partial z} = \frac{v^*}{k} z^{-\gamma} \quad (15)$$

where  $v^*$  = friction velocity, independent of height  
 $k$  = von Karman's constant  $\sim 0.4$   
 $\gamma > 1$  for superadiabatic temperature lapse rates  
 $\gamma = 1$  for adiabatic lapse rates  
 $\gamma < 1$  for inversions

In the case of adiabatic lapse rates, Eq. 15 is written as the logarithmic law

$$\bar{v}(z) = \frac{v^*}{k} \log \left( \frac{z}{z_0} \right) \quad (16)$$

where  $z_0$  = surface roughness height, independent of height

Equation 16 is valid for heights up to 30-50 m; for large  $z$ , values of  $\bar{v}$  change slowly.

The friction velocity  $v^*$  is a characteristic parameter of turbulence, which can be determined from wind profile measurements using Eq. 16.

$$v^* = \frac{k (\bar{v}_1 - \bar{v}_2)}{\log z_1 - \log z_2} \quad (17)$$

In general, the velocity gradient exhibits a diurnal variation, being small in daytime and large at night. The significance of the velocity gradient is that it determines the rate at which refractive index

inhomogeneities are being transported horizontally; in addition, if the velocity gradient increases beyond a certain value then the simple mean flow of the air makes a transition to turbulent flow, hence vertical mixing of the atmosphere.

The motion of air produces a shearing stress per unit area,  $\tau$ , that is related to the velocity gradient by

$$\tau = \nu \rho \frac{\partial v}{\partial z} \quad (18)$$

where  $\nu$  = kinematic viscosity  
 $\rho$  = density of moving medium

Equation 18 is rewritten for wind shear as

$$\frac{\tau}{\rho} = \nu \frac{\partial v}{\partial z} \quad (19)$$

Finally, wind shear is related to friction velocity by

$$v^* = \frac{\sqrt{\tau}}{\rho} \quad (20)$$

When the dynamic pressure of the wind (i.e.,  $\rho \bar{v}^2$ ) exceeds the viscous forces at the ground, the flow of the wind makes a transition to turbulent flow. The parameter, Reynolds number,  $Re$ , relates the relative importance of viscous and inertial forces and is defined as:

$$Re = \frac{\rho \bar{v}'^2}{\mu \bar{v}' / \ell_e} = \frac{\bar{v}' \ell_e}{\nu} \quad (21)$$



where  $v'$  = fluctuation in velocity

$\ell_e$  = average size of energy-containing eddies

$\mu$  = medium dynamic viscosity  $\approx \nu \rho$

When  $Re$  exceeds a critical value (of about 2000), then laminar flow becomes unstable and turbulent eddies are produced. The sizes of the eddies vary from an outer scale length,  $L_o$ , which is characteristic of the size of the fluctuation containing most of the energy of the turbulence, to an inner scale length,  $\ell_o$ , which is a characteristic size of the very small eddies that are responsible for the ultimate dissipation of energy into heat by the action of viscosity.

The energy dissipated as heat per unit mass of fluid per unit time,  $\epsilon$ , (Ref. 14) is of the order

$$\epsilon \sim \frac{\nu v'^2}{\ell^2}$$

where  $v'$  = velocity fluctuation of the eddy

$v^3/\ell$  = the energy per unit mass received per unit time by the eddies

Then solving for  $v$  and rearranging in terms of  $\ell$ , we have the size of the eddy for the case of the smallest size given:

$$\ell_o \sim \sqrt[4]{\frac{\nu^3}{\epsilon}} \quad (22)$$

Typical sizes of  $\ell_o$  range from a few millimeters to a maximum of a few centimeters in the lowest 10 km of the atmosphere. Now making use of the relationship  $\epsilon \sim v^3/\ell$  and Eq. 21, we have the size of the smallest eddy in terms of Reynolds number and the turbulence scale length as

$$l_o \sim \frac{L_o}{(Re)^{3/4}} \quad (23)$$

The outer scale lengths vary from a few meters at the ground to hundreds or thousands of meters at the top of the tropopause.

The transition to turbulent flow can be determined directly from measurements at two different levels of average wind velocity, average temperature, and temperature lapse rate using another turbulent flow parameter called Richardson number. This parameter is defined (Ref. 15) as

$$Ri = \frac{g \partial T / \partial z}{\bar{T} \beta^2} = \frac{g (\Gamma - \Gamma_d)}{\bar{T} \beta^2} \quad (24)$$

where  $\beta$  = wind velocity gradient  
 $g$  = acceleration due to gravity

Unstable temperature lapse rates give negative Richardson numbers and generally correspond to turbulent atmospheric conditions.

In summary, optical propagation effects due to fluctuations of the refractive index of the local atmosphere correlate with the following meteorological parameters:

- a. Mean temperature
- b. Mean pressure
- c. Mean relative humidity
- d. Fluctuations in vertical temperature gradient (lapse rate)
- e. Mean wind velocity and direction
- f. Fluctuations in wind velocity gradient
- g. Reynolds number
- h. Richardson number

Other environment-defining conditions such as time of day or night, season topography, altitude, cloud cover, solar irradiance, surface conditions, etc., should also be noted for each experimental measurement.

So far we have discussed the gross features of turbulence and the related production of variations in refractive index. However, to relate these refractive index fluctuations to effects on optical propagation, we shall review the optical properties in terms of statistical properties of the atmosphere.

#### 2.2.2 OPTICAL PROPAGATION IN A RANDOM ATMOSPHERE

There are many articles on the subject of optical propagation in a random medium; among the recent and significant discussions are those of Tatarski (Ref. 14), Chernov (Ref. 16), Hufnagel and Stanley (Ref. 17), Beckmann (Ref. 18), and Hodara (Ref. 19). Only some key points will be discussed here for the purpose of describing the significant quantitative relationships of optical propagation effects, and of comparing the theory with the experimental results.

In the following paragraphs, we will discuss the random turbulent medium under conditions when temperature is the most influential factor in producing random variations in the refractive index of atmosphere.

##### Statistical Description of a Random Atmosphere

The optical properties of the atmosphere are determined from local conditions of the refractive index which are generally random functions of both time and space, i.e.,  $n(s, y, z, t)$ . For a particular position, the refractive index can be described sufficiently by the mean value  $\bar{n}$  and its correlation function:

$$B_n(\bar{r}_1, \bar{r}_2, t) = \langle [n(\bar{r}_1, t) - \overline{n(\bar{r}_1, t)}][n(\bar{r}_2, t) - \overline{n(\bar{r}_2, t)}] \rangle \quad (25)$$

where  $\langle \rangle$  indicates statistical average

$\mu$  = the fluctuation in refractive index

Assuming ergodicity, Eq. 25 becomes

$$B_n(\bar{r}_1, \bar{r}_2, t) = \overline{[n(\bar{r}_1, t) - \overline{n(\bar{r}_1, t)}][n(\bar{r}_2, t) - \overline{n(\bar{r}_2, t)}]} \quad (26)$$

where the bar indicates time average.

As pointed out by Tatarski (Ref. 20),  $\overline{n(r, t)}$  varies with time so that the stationary condition cannot be invoked in the statistical analysis. Instead, the structure function  $D_n(\bar{r}_1, \bar{r}_2, \tau)$  is introduced together with the assumption of random functions with stationary increments; considering only the spatial dependence of index of refraction,  $n_r(\bar{r}_1, \bar{r}_2) = n(\bar{r}_1) - n(\bar{r}_2)$ , then

$$D_n(\bar{r}_1, \bar{r}_2) \equiv \overline{[n(\bar{r}_1) - n(\bar{r}_2)]^2} \quad (27)$$

If it is assumed that the medium is homogeneous, then the correlation between two points depends only upon the distance between the points and not location (i.e.,  $D_n(\bar{r}_1, \bar{r}_2) = D_n(\bar{r})$ ). Furthermore, if it is assumed that the atmosphere is locally isotropic, then the correlation is independent of direction; hence,  $D_n(\bar{r}) = D_n(r)$ . Although the atmosphere is generally anisotropic, we will for simplicity assume local isotropy.

Recalling from Eq. 1 that  $n(r)$  is comprised of an average term and a fluctuation from the average,  $\mu$ , and  $\overline{n(r)} \sim 1$ , then Eq. 27 can be rewritten

$$D_n(r) = 2[\sigma_n^2 - B_n(r)] \quad (28)$$

where

$$\begin{aligned} \sigma_n^2 &= \overline{(\mu)^2} = B_n(0) \\ B_n(r) &= \overline{[\mu(r_1) \mu(r_2)]} \end{aligned} \quad (29)$$

and

$$r = |r_2 - r_1|$$

Since we assume that the fluctuations are produced by temperature fluctuations, it can be seen from Eqs. 10 and 11 that

$$\mu = \frac{\Delta p}{T} \left( - \frac{\Delta T}{T} \right) \approx \frac{(\bar{n} - 1) \Delta T}{T} \quad (30)$$

Consequently, one can evaluate the correlation function  $B_n(r)$  directly from Eq. 29 or from Eq. 28:

$$B_n(r) = \overline{(\mu)^2} - \frac{1}{2} D_n(r) \quad (31)$$

where

$$\overline{(\mu)^2} \approx \left( \frac{\bar{n}-1}{T} \right)^2 \overline{\Delta T(r)^2} \quad (32)$$

from Eq. 30;  $D_n(r)$  comes from measurements of  $n(r_1) \sim 1 + A p_2 / T_2$  and evaluations of Eq. 27.

Tatarski (Ref. 21) shows on the basis of Kolmogoroff's law for isotropic turbulence that the structure function is of the form:

$$D_n(r) = \begin{cases} C_n^2 r^{2/3} & \text{for } l_o \ll r \ll L_o \\ C_n^2 l_o^{2/3} \left(\frac{r}{l_o}\right)^2 & r \ll l_o \end{cases} \quad (33)$$

where  $C_n \equiv$  structure constant related to  $\epsilon$ ,  $\beta$ , and temperature lapse rate by (Ref. 17)

$$C_n^2 = \alpha^2 \epsilon^{2/3} \gamma^2 / \beta^2$$

$$\alpha = \text{constant}$$

$$\gamma = (\Gamma - \Gamma_d)$$

Rewriting Eq. 32 and substituting the expressions for  $\overline{(\mu)^2}$  and  $\beta_n(r)$  into Eq. 28 gives

$$C_n^2 = \frac{2[\overline{(\mu)^2} - \mu(r_1) \mu(r_2)]}{r^{2/3}} \quad (34)$$

$$C_n^2 = \frac{2\left[\left(1 + \frac{Ap}{\bar{T}}\right)^2 \left(\frac{\Delta T(r_1 r_2)}{\bar{T}}\right)^2 - \frac{Ap_1 \Delta T(r_1)}{\bar{T}_1^2} \frac{Ap_2 \Delta T(r_2)}{\bar{T}_2^2}\right]}{r^{2/3}} \quad (35)$$

Equation 35 shows the important relationship between the meteorological parameters and the turbulence parameter, the atmospheric structure constant. This turbulence parameter plays an important role in predicting optical beam degradation by the atmosphere. Figure 13 shows how  $C_n$  varies with altitude above the ground.

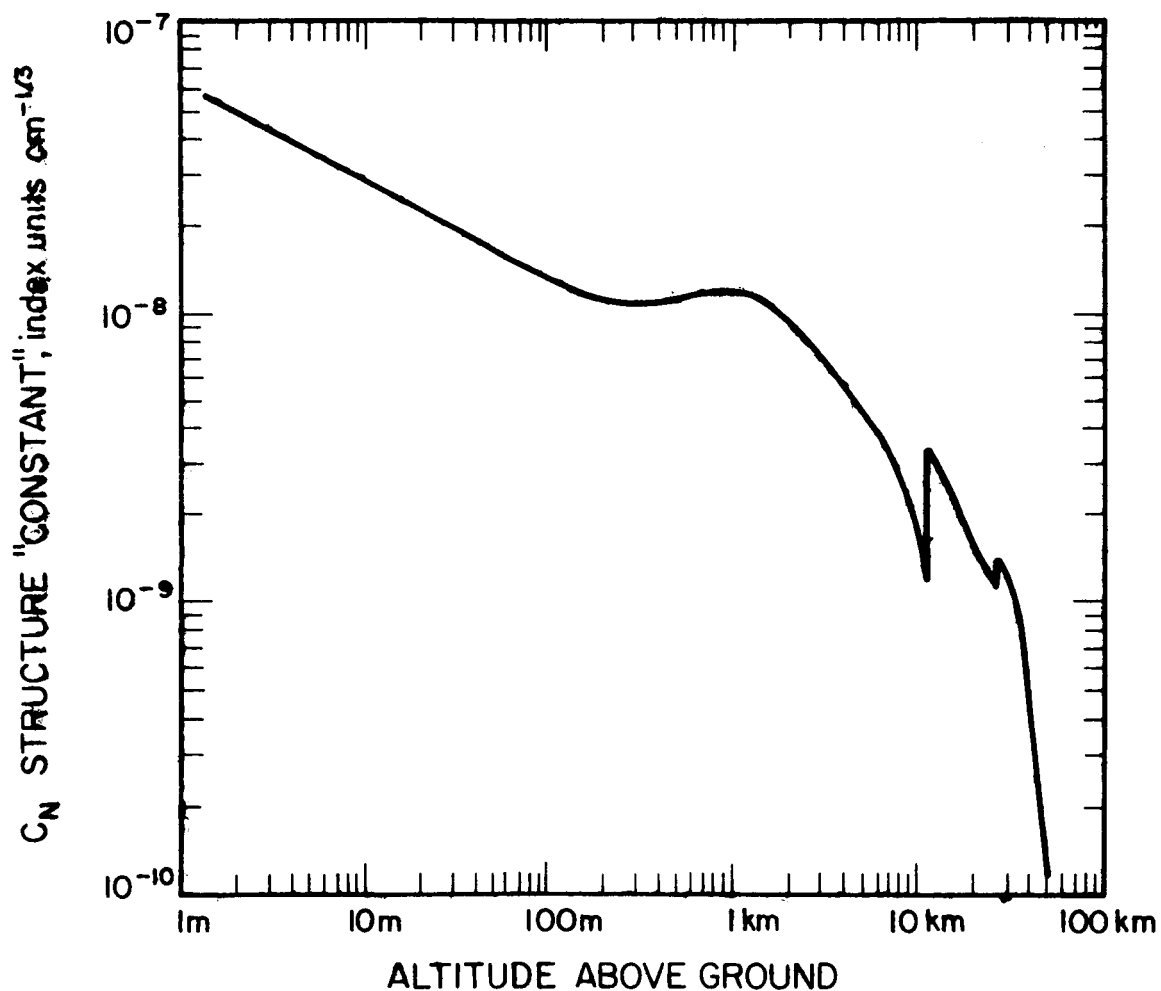


Figure 13. Index of Refraction Structure "Constant" versus Altitude (after Hufnagel and Stanley, Ref. 17)

Another important parameter is the outer scale of turbulence,  $L_o$ , or the correlation distance. As the separation distance  $r$  increases, the structure function  $D_n(r)$  changes from a function of  $r^2$  to a function of  $r^{2/3}$ ; this point establishes the inner scale of turbulence distance,  $l_o$ . As  $r$  increases further,  $D_n(r)$  no longer follows the  $r^{2/3}$  law beyond a separation distance\* called the outer scale of turbulence,  $L_o$ . Over a uniform optical path, a light beam traverses  $L/L_o$  such intervals; the total optical beam degradation depends upon both the number of turbulence zones and the strength of the zones, characterized by  $\mu^2$ .

The mean square fluctuation in the phase between two points on a wavefront, after the wavefront has propagated over a path length  $L$ , according to Tatarski, is given by

$$\sigma \phi^2(r) = D_n(r) = 2.91(2\pi/\lambda)^2 r^{5/3} \int_0^L C_n^2(z) dz \quad (36)$$

Assuming a horizontal path with  $C_n$  constant, then Eq. 36 becomes

$$D_n(r) = 2.91(2\pi/\lambda)^2 r^{5/3} L C_n^2 \quad (37)$$

Another derived expression for the structure function is given by (Ref. 22):

$$D_n(r) = 6.88(r/r_o)^{5/3} \quad (38)$$

where  $r_o$  = maximum effective aperture for coherent detection. Combining Eqs. 37 and 38, the maximum effective receiver aperture is

---

\*The inner and outer scales of turbulence are also related to the Reynolds number, using Eq. 23.



$$r_o = 1.2 \times 10^{-8} \left( \frac{\lambda^2}{c_n^2 L} \right)^{3/5} \quad (39)$$

where wavelength,  $\lambda$ , is in microns and path length  $L$  is in meters.

From the form of Eq. 39, the advantages of long wavelengths for coherent optical receivers is readily apparent.

Other atmospheric effects on optical beam properties and propagation are now discussed.

#### Intensity Fluctuations

Tatarski derived expressions that relate the dependence of the magnitude of scintillation on distance and on meteorological conditions, the form of the correlation function of the fluctuation of light intensity, and the shape of the normalized spectral density curve.

Tatarski (Ref. 23) derived the expression for amplitude fluctuation from the wave equation using Rytov's approximation. For the case  $\sqrt{\lambda L} \gg l_o$ , the mean square value of the amplitude fluctuation is given by

$$\overline{\chi^2} = \overline{(\log A/A_o)^2} = 0.31 c_n^2 k^{7/6} L^{11/6} \quad (40)$$

where  $K = 2\pi/\lambda$ . In terms of intensity this can be written

$$\sigma^2 = \overline{(\log I/I_o)^2} = 4\overline{\chi^2} = \log \left( 1 + \frac{\sigma_1^2}{(\overline{I})^2} \right) \quad (41)$$

where  $\sigma_1^2 = (\overline{I} - \overline{I})^2$  and  $\sigma^2 = 1.23 C_n^2 k^{7/6} L^{11/6}$ . Tatarski's experimental data verified the log normal distribution law for fluctuations of light intensity. Further, it was shown that  $\sigma^2 \propto L^{11/6}$ , according to theory.

The normalized frequency spectrum of the amplitude fluctuations, defined by

$$U(f) = \frac{fW(f)}{\int_0^\infty W(f) df} \quad (42)$$

where  $W(f)$  = spectral density of fluctuation at frequency  $f$ , was confirmed to be a function only of the argument  $f\sqrt{\lambda L}/v_n$ . The quantity  $f_m$  corresponds to the maximum of the curve  $U(f)$  and is equal to one-half the sum of the frequency for which  $U(f) = 1/2 [U(f)]_{\max}$ . The empirical quantity  $f_m\sqrt{\lambda L}/v_n \equiv m$  is approximately constant such that

$$f_m = 0.32 \frac{v_n}{\sqrt{\lambda L}} \quad (43)$$

and agreed closely with the form calculated on the basis of frozen-in turbulence ( $f_m = 0.55 v_n/\sqrt{\lambda L}$ ). Equation 43 states that as wind velocity increases, the curves of  $U(f)$  are shifted in the high-frequency direction. Other authors derived expressions for optical effects based upon the approximations of geometrical optics. For example, Beckmann, starting with the Divergence Theorem, derives the expression for fluctuation of logarithmic intensity for isotropic turbulence as

$$\left\langle \log \frac{I}{I_0} \right\rangle = 4 \left\langle \left( \log \frac{A}{A_0} \right)^2 \right\rangle = \frac{32 \sqrt{\pi} \langle \mu^2 \rangle L^3}{3L_0^3} \quad (44)$$

where  $L_o$  = correlation distance (Beckmann's R)  
 $L$  = optical path length  
 $\langle \mu^2 \rangle$  = mean square deviation of refractive index

For the case of intensity distributed log-normally and for the correlation function given by

$$B(\overline{r}) = \langle \mu^2 \rangle e^{-r^2/L_o^2} \quad (45)$$

then the fluctuation in intensity is given by

$$\langle I \rangle = I_o \exp\left(-\frac{16\sqrt{\pi} \langle \mu^2 \rangle L^3}{3L_o^3}\right) \quad (46)$$

Both the expression for logarithmic intensity fluctuation given by Eq. 44 and Eq. 41, are for small receivers. Signal averaging across large receivers will decrease the magnitude of intensity fluctuation. Beckmann further derives an expression to show that in order to have negligible noise distortion of an AM signal, the modulation depth,  $m$ , of the transmitted signal must satisfy the condition

$$m^2 \gg 2 \left[ \exp\left(\frac{8L^3}{3L_o^3} \sqrt{\pi} \langle \mu^2 \rangle\right) - 1 \right] \quad (47)$$

According to Beckmann the spectral density of the fluctuations is

$$\Phi(\Omega) = \frac{16\pi\sqrt{2}}{3} \langle \mu^2 \rangle \frac{L_o^3}{L^3} \exp(-\Omega L_o^3/4v_c^2) \quad (48)$$

where  $\Omega$  = angular frequency of noise modulation  
 $v_c$  = crosswind velocity

It is found that 99 percent of the noise spectrum lies below the frequency

$$\Omega_m = \frac{3.64 v_c}{L_o} \quad (49)$$

The maximum scintillation frequency detected at the receiver, however, is related to both the transmitter and receiver apertures,  $d$  and  $D$ , respectively (Ref. 24). When  $d \ll (\lambda L)^{1/2}$ , the maximum scintillation frequency is about  $v_c/(\lambda L)^{1/2}$ ; on the other hand, if  $d \gg (\lambda L)^{1/2}$ , the scintillation frequency will extend to approximately  $v_c/d$ .

Refractive index inhomogeneities in the vicinity of the transmitter produce random beam steering or spot dancing, with subsequent fluctuations in intensity at the receiver. In the case where the inhomogeneities are nearer the receiver, fluctuations in angle of arrival are produced as well as possible coherence degradation.

#### Angle of Arrival Fluctuations

The mean square of the total angular deviation of the beam propagating through isotropic turbulence is given by (Ref. 18)

$$\langle \epsilon^2 \rangle = \frac{4L \langle \mu^2 \rangle \sqrt{\pi}}{L_o} \quad (50)$$

The effect of angular deviations can be to deflect the incoming beam to different points on a detector, to produce spatial phase fluctuations across the beam diameter, or to produce lateral (temporal) phase distortions along the direction of propagation of the beam; which effect occurs depends on the relative size of the beam diameter to the size of inhomogeneities and on the diameter of the collecting optics.

### Spot Dancing

When the wavefront of the propagated beam is randomly deflected such that the phase varies linearly across the receiving aperture, the result is a random spot displacement of the focused beam at the plane of the detector. For isotropic turbulence, Beckmann shows the mean square fluctuation of spot position to be

$$\langle \rho^2 \rangle = \frac{2L^3 \langle \mu \rangle \sqrt{\pi}}{L_0} \quad (51)$$

For the case of detectors with very small active areas, the spot dancing could be severe enough to produce amplitude modulation of the signal.

### Transverse Phase - Spatial Coherence Degradation

On the other hand, if the phase across the receiver aperture varies randomly, the spatial coherence of the beam is degraded; or for the case where the incident wavefront is larger than the inhomogeneities and a large receiver aperture is used, then a blurred image is produced.

The correlation of the phase fluctuations in the plane of the receiver is, following Beckmann, for isotropic turbulence

$$\langle \psi_1 \psi_2 \rangle = \langle \mu^2 \rangle k^2 L \int_0^\infty C_n(x, y, z) dx \quad (52)$$

where  $C_n$  is assumed to be Rayleigh-distributed. Hence

$$\langle \psi_1 \psi_2 \rangle = \langle \mu^2 \rangle k^2 L L_0 \sqrt{\pi} \exp(-\rho^2/L_0^2) \quad (53)$$

To keep distortion due to spatial coherence degradation negligible, the condition  $\langle [\psi(\rho) - \psi(o)]^2 \rangle \ll \pi^2$  must be satisfied for the case of optical heterodyning; on the other hand, for direct detection, the condition

$$0.9 \leq \gamma_{12} = \frac{\overline{\Delta\psi_1 \Delta\psi_2}}{\Delta\psi^2} \leq 1 \quad (54)$$

must be satisfied.

In the first case, Beckmann shows that for a modulation frequency of the carrier wave ( $\Omega = cK$ ), the maximum aperture dimension is

$$(D_R)_{\max} = \sqrt{-\log \left( 1 - \frac{(\Delta\psi)^2}{2\langle \mu^2 \rangle K^2 L_{L_0} \sqrt{\pi}} \right)} \quad (55)$$

or for a given aperture the maximum modulation frequency (with phase  $\psi$ ) is

$$\Omega_{\max}^2 = \frac{c_n^2 (\Delta\psi)^2}{2\langle \mu^2 \rangle L_{L_0} \sqrt{\pi} [1 - \exp(-\rho^2/L_0^2)]} \quad (56)$$

When  $\rho \gg L_0$ , the allowable modulation bandwidth is given by

$$\Omega = \frac{c_n \Delta\psi}{\sqrt{2\langle \mu^2 \rangle L_{L_0} \sqrt{\pi}}} \quad (57)$$

The second criterion relaxes the conditions on receiver aperture size limits. This type of phase distortion is relatively unaffected by wind. The effects can partially be overcome by optimum selection of modulating frequency and receiver aperture.

### Temporal Coherence Degradation

Atmospheric conditions that produce fluctuating differences in transit times are the causes of temporal coherence degradation or phase or frequency random modulation.

Following Hodara (Ref. 19), the phase of the wavefront at any point  $z$  along the path is

$$\phi = \omega_0 t - k_0 z n$$

In the case of variations in index of refraction along the path,  $\phi$  fluctuates as

$$\psi = \phi - \omega_0 t$$

Over a coherence interval the change in phase is

$$\Delta\psi = k_0 L_0 \Delta n$$

Since over the total path there are  $L/L_0$  coherence intervals

$$\langle \Delta\psi^2 \rangle = k_0^2 L L_0 \langle \mu^2 \rangle \quad (58)$$

Since frequency modulation comes from  $d\psi/dt$ , Hodara shows that the mean square fluctuation in frequency is given by

$$\langle \Delta f^2 \rangle = \frac{L L_0}{\lambda_0^2} \frac{\langle \mu^2 \rangle}{T_0^2} \quad (59)$$

where  $T_0$  is a characteristic period arising from fluctuations in either temperature or from crosswinds, in the latter case,  $T_0 = L_0/v_c$ .

Beckmann shows that the frequency modulations produced by upwind or downwind components are negligible compared with the crosswind effects. Estimates of the standard deviation of frequency modulation are reported to be as high as 1 hertz for temperature fluctuations, with 100 kHz to 10 kHz more likely; these latter values are also Hodara's estimates for wind effects.

#### Additional Effects

There are two additional atmospheric effects that need mentioning. These are beam cross section fluctuations and polarization fluctuations. Summarizing from Hodara, the relative fluctuation in beam cross section is given by

$$\frac{\Delta S}{S_o} = \langle \mu^2 \rangle \left( \frac{L}{L_o} \right)^3 + 2 \sqrt{\langle \mu^2 \rangle} \left( \frac{L}{L_o} \right)^3 \quad (60)$$

The polarization,  $\phi$ , of the initial beam is defined by the argument of

$$\tan \phi = \frac{E_{Ty}}{E_{Tx}} \quad (61)$$

where  $E_{Ty}$  and  $E_{Tx}$  are polarized E-field components. After propagation to the receiver the polarization may be modified to

$$\tan(\phi + \Delta\phi) = \frac{E_{Ry}}{E_{Rx}} \quad (62)$$

The change in polarization through one coherent turbulence element is

$$\Delta\phi = \tan^{-1} \frac{E_{Ry}}{E_{Rx}} - \tan^{-1} \frac{E_{Ty}}{E_{Tx}} \quad (63)$$



which for the entire path length becomes

$$\Delta\phi \sim \frac{\mu L_{oz}^2 L}{2 L_{oT}^2 L_{oz}} \sin 2\phi \quad (64)$$

where  $L_{oz}$  and  $L_{oT}$  are coherence lengths along and transverse to the path, respectively. Finally, for the case of  $\phi = 45^\circ$ , the fluctuation in polarization is given by

$$\langle \Delta\phi^2 \rangle = \frac{\langle \mu^2 \rangle}{4} \left( \frac{L_{oz}^2}{L_{oT}^2} \right)^2 \frac{L}{L_{oz}} \quad (65)$$

In the foregoing sections, we have summarized some derived expressions for relating optical beam degradations produced by the atmosphere. These derivations, of course, are based upon certain assumptions and atmospheric models and require additional experimental verification. The first quarterly report\* of this study contained a discussion of past experimental investigations of optical propagation and proposed plans for additional experiments to determine the atmospheric effects on laser beams propagating through the lower atmosphere. Table III summarizes several possible experiments and indicates their relative importance in optical communications. Details of the experiments and experimental apparatus are given in the following section.

---

\*"Study of Atmospheric Degradation of Laser Beams," Report 7097-Q-1, Electro-Optical Systems, Inc., Pasadena, California, September 1966.

TABLE III  
SUMMARY OF SUGGESTED OPTICAL EXPERIMENTS

Experiment Category	Measurement	Measured Parameters	Derived Parameters	Experiment Variables	Significance
Coherence Degradation	1. Transverse correlation of wavefronts	Spatial coherence function	Spatial coherence length	Wavelength Receiver diameter Transmitter aperture	Optimum aperture sizes for coherent detection
	2. Correlation between wavefronts	Temporal coherence function	Temporal coherence length	Same as 1	Processing times for adaptive techniques
	3. Carrier frequency broadening	Power spectrum of heterodyned received signal	Phase distortion	Same as 1	FM distortion
	4. Pulse shape	Rise time, fall time, and width	Pulse shape distortion	Same as 1 plus pulse duration	PCM system capacity limitations
Attenuation	Intensity along path	Intensity distance	Extinction coefficient	Wavelength distance	Signal loss
Attenuation Fluctuation	Intensity variations	Power spectrum of received signal	Percent modulation modulation frequency bandwidth	Wavelength receiver diameter, transmitter aperture	Probability of error for AM system
Polarization	Intensity of polarized components of light at transmitter & receiver	$I_V, I_H, I_R, I_L$	$\Delta\phi/\phi$ - Atmospheric depolarization	Wavelength polarization	PCM/PL system probability of error
Visual Range	Chart resolution	Image distortion	Angular deviation	Resolution target dimensions and configuration	Correlate optical effects with visual seeing conditions

## SECTION 3

### EXPERIMENT DESCRIPTION AND DISCUSSION

Of the experiments listed in Table III there are two that are of primary importance in this present study. These are measurements of intensity fluctuations and transverse or spatial coherence correlation distance along the beam wavefront. In the former case, it is important to characterize the noise-generating properties of the atmosphere, and secondly, to determine the atmospheric limitations to coherent optical receivers. Experiments and apparatus were developed for the purpose of investigating the effects of the lower atmosphere on 10.6 $\mu$  and 0.6328 $\mu$  laser beams. The longer wavelength was selected to verify the theoretical advantages of long wavelengths for coherent detection; the shorter wavelength was selected for comparison of optical effects, especially since much laser experimental data exists for the He-Ne laser. The experimental program and apparatus are discussed in this section.

#### 3.1 GENERAL DESCRIPTION

Two laser beams, one from a CO<sub>2</sub> laser and one from a He-Ne laser, were transmitted to an array of four corner cubes at a distance of 3 miles from the transmitter site. The corner reflectors folded the optical path back to two optical receivers.

Figure 14 is a map showing the optical path and general topography. Figure 15 depicts the ground profile between the EOS facility and the corner cubes at Henninger Flats. The lasers and receivers are located at the EOS facility together with a meteorological station. A remote meteorological station is located at the hill site; in addition, there

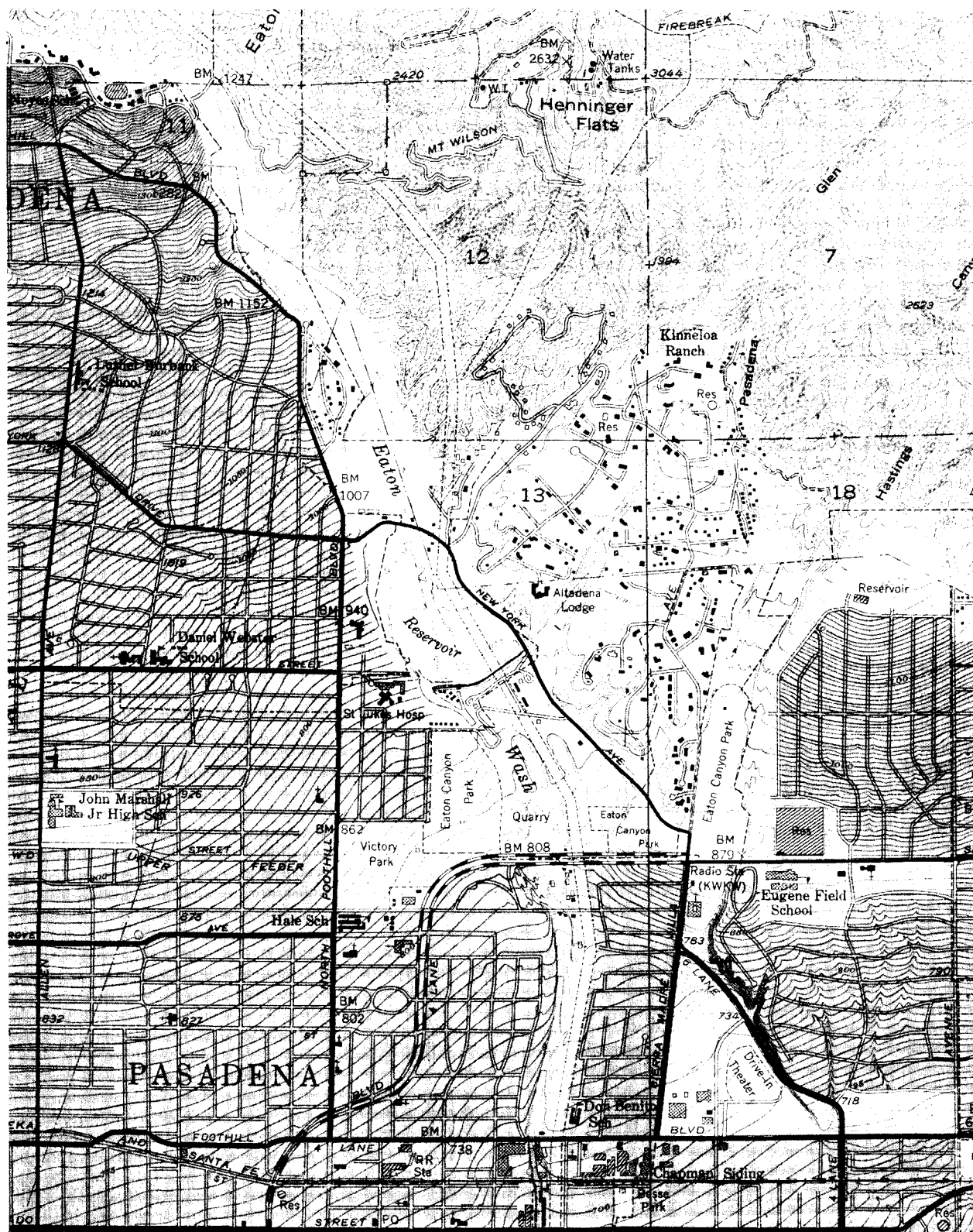


Figure 14. Topographic Map Showing Optical Path  
7097-Final

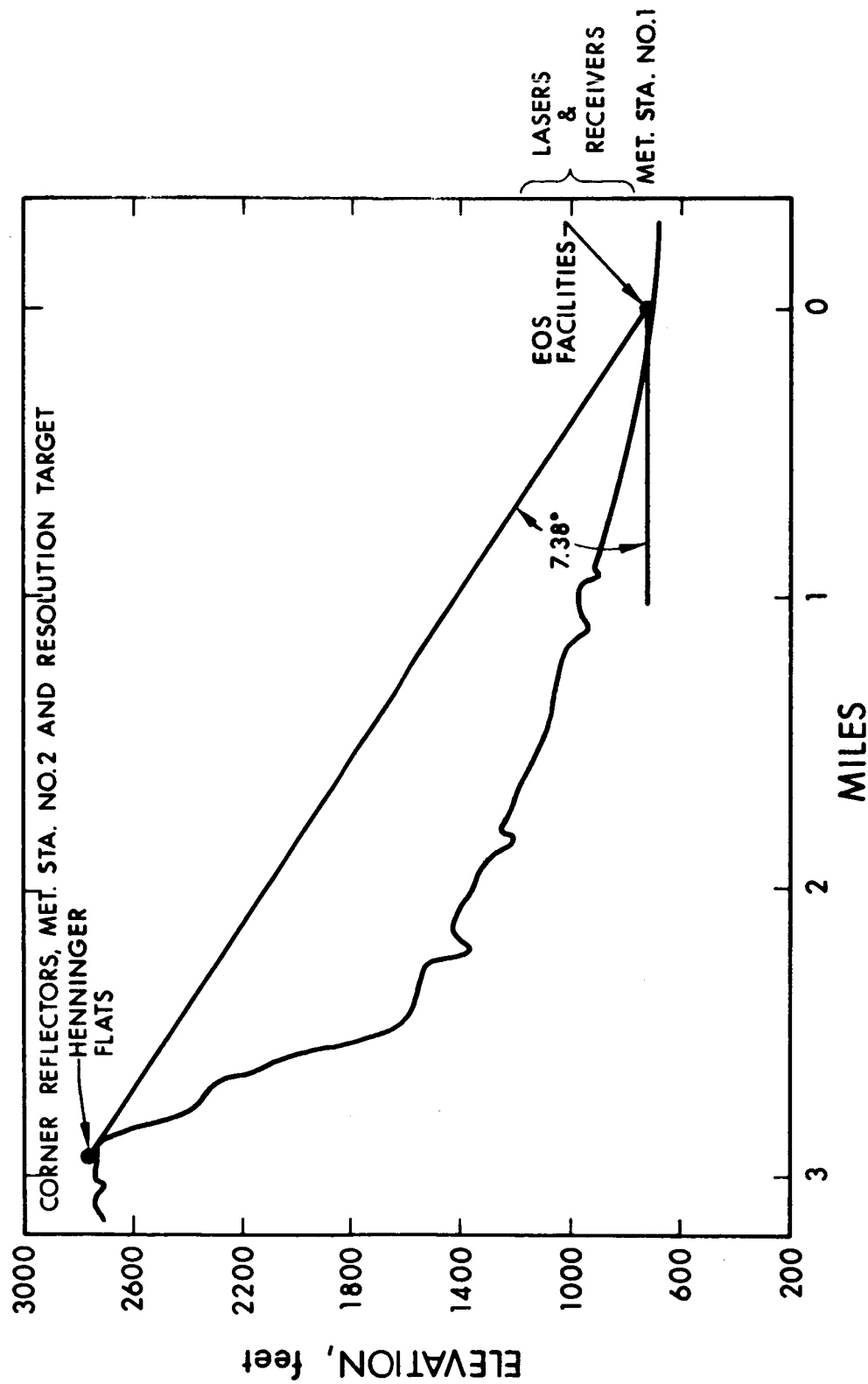


Figure 15. Ground Profile and Optical Path Between EOS and Henninger Flats

is a high-contrast optical resolution target for characterizing visibility and "seeing" conditions.

The reflected He-Ne laser beam is collected by a 6-inch telescope and the CO<sub>2</sub> laser beam by a 16-inch telescope; detectors respond to the laser beam intensity and intensity fluctuations and these signals are recorded, together with meteorological data, for later data processing and analysis. Figure 16 is an overall block diagram of the equipment at the EOS facility. Table IV describes the equipment indicated in Fig. 16.

Figure 17 is a photograph of the laser transmitter-receiver station. Recording instrumentation is shown in Fig. 18. The meteorological sensor mast is positioned outside the window, in the immediate vicinity of the transmitted and received beams; Fig. 19 shows the sensor mast and Fig. 20 shows the instrumentation substation. The mountain in the background is the location of the remote station. Figure 21 is a photograph of the remote station, which was taken through a telephoto lens; the resolution target is visible in front of the building; an enclosure containing four corner cube reflectors is situated at the peak of the roof; and a second meteorological sensor mast is also positioned in the foreground (not shown). This remote station uses auxiliary power from a storage battery and an ac-dc converter for operating a program timer and floodlights for resolution target illumination.

The experimental apparatus are described and discussed in more detail in the following subsections.

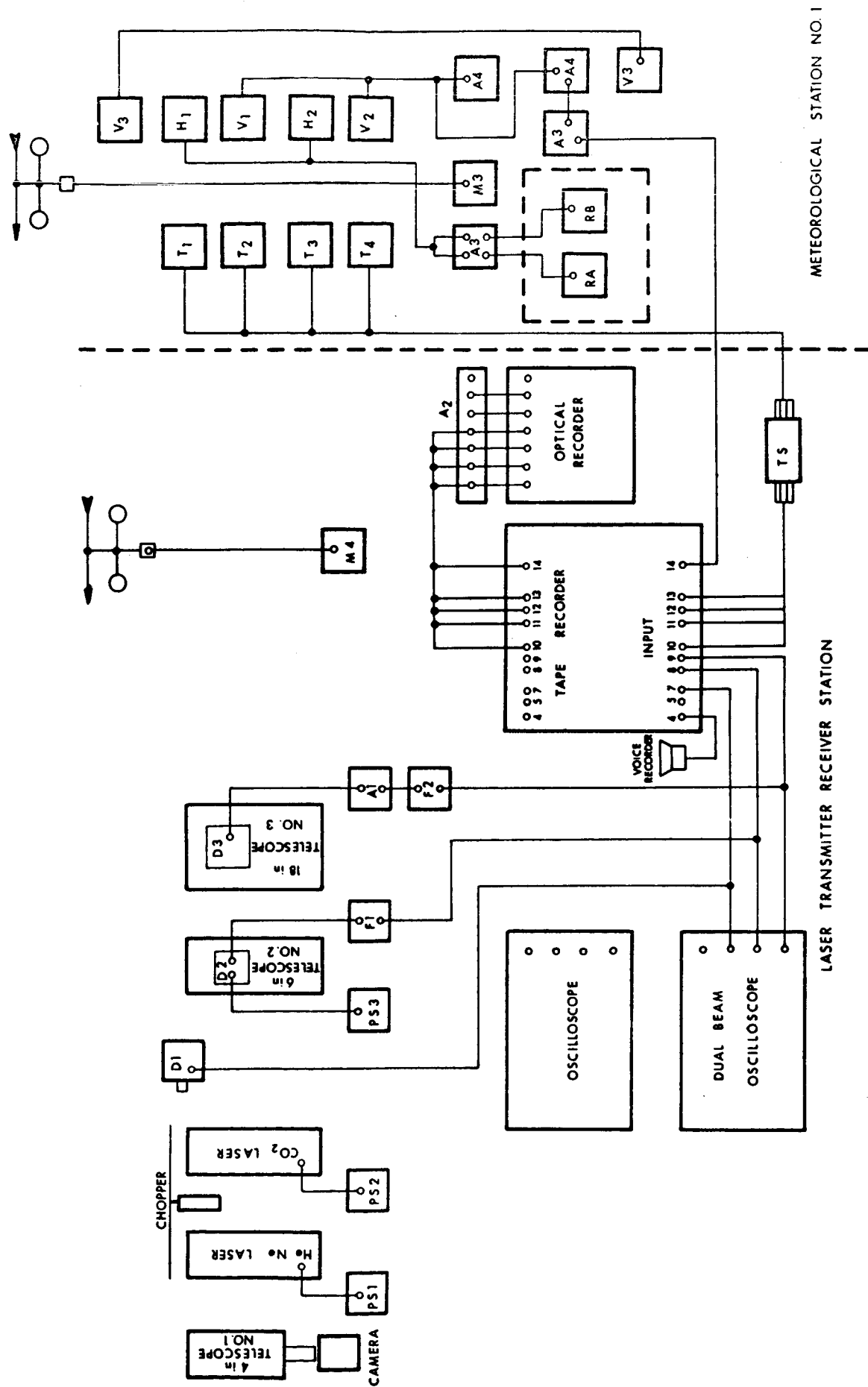


Figure 16. Laser Transmitter Receiver Station

TABLE IV  
ANNOTATED INDEX OF EXPERIMENTAL APPARATUS

A1	CO <sub>2</sub> laser detector amplifier. Tektronix Model 122 preamp
A2	Galvanometer amplifier - Honeywell Model T6GA
A3	Humidity sensor amplifier (EOS constructed)
A4, A5	Wind velocity amplifier and meter output. West Coast Mod. 910 Flowmeter
A6	Meter amplifiers - Bruel and Kjaer Mod. 2409
D1	Bolometer detector - Barnes Engineering Thermister type F-S25-S
D2	RCA 7265 multiplier phototube, S-20 response
D3	Infrared detector - Minneapolis-Honeywell Model DLK-13-B3
F1, F2	Wave analyzer, Hewlett Packard 302A
H1, H2	Humidity sensor - Physical Chemical Corporation Type PCRC-55
M1	Barometer, air guide
M2	Relative humidity - Stewart Hygrometer - wet and dry bulb
M3	Taylor wind scope
M4	Aerojet-General weather instrument
PS1	Spectra-Physics power supply for He-Ne laser
PS2	EOS power supply for CO <sub>2</sub> laser
PS3	Precision high voltage power supply for 7265 PM tube
RA, RB	Recorder, Brush Mark II
T1, T4	Temperature sensors MS1 T07-10-1000
TS	Temperature sensor bridge (4) (EOS constructed)
V1, V2	Wind velocity indicator, West Coast Mod. 910
V3	Taylor wind scope



TABLE IV  
ANNOTATED INDEX OF EXPERIMENTAL APPARATUS (contd)

Camera, Polaroid Scope  
Chopper, 500 and 1000 Hz  
Laser, He-Ne Spectra Physics Mod.  
Laser, CO<sub>2</sub> EOS, 75W  
Oscilloscope - Tektronix Dual Beam, Model 565  
Oscilloscope - Tektronix Dual Beam, Mod. 555A  
Optical recorder - Honeywell Viscorder, 12 channel  
Telescope No. 1, Celestron 4 in., 1500 mm FL, 25 mm eyepiece  
Telescope No. 2, Edmund Scientific 6 in., 48 in. FL, 25 mm eyepiece  
Telescope No. 3, Optical Craftsman 16 in., 90 in. FL  
Tape recorder, Precision Instruments, Model PI 200,  
14-channel

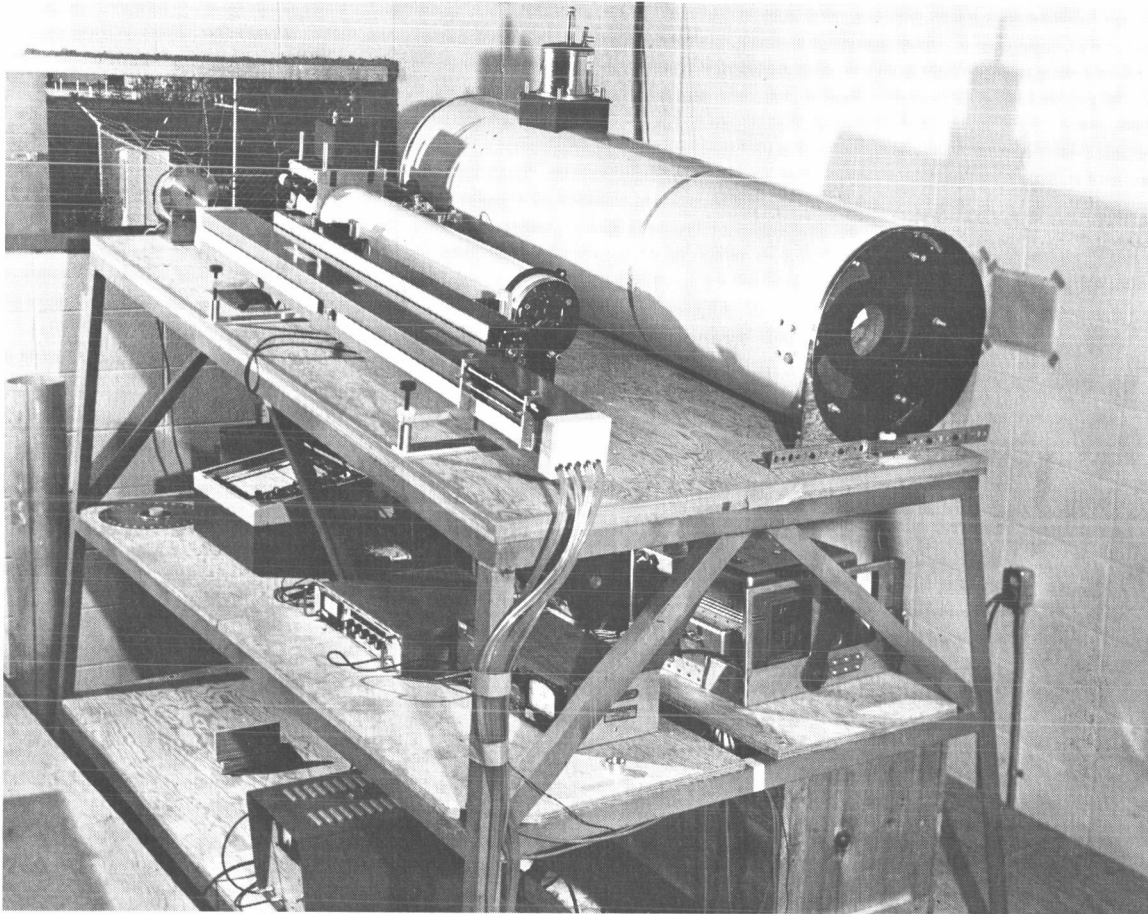


Figure 17. Laser Transmitter - Optical Receiver Bench Setup for Optical Propagation Experiments

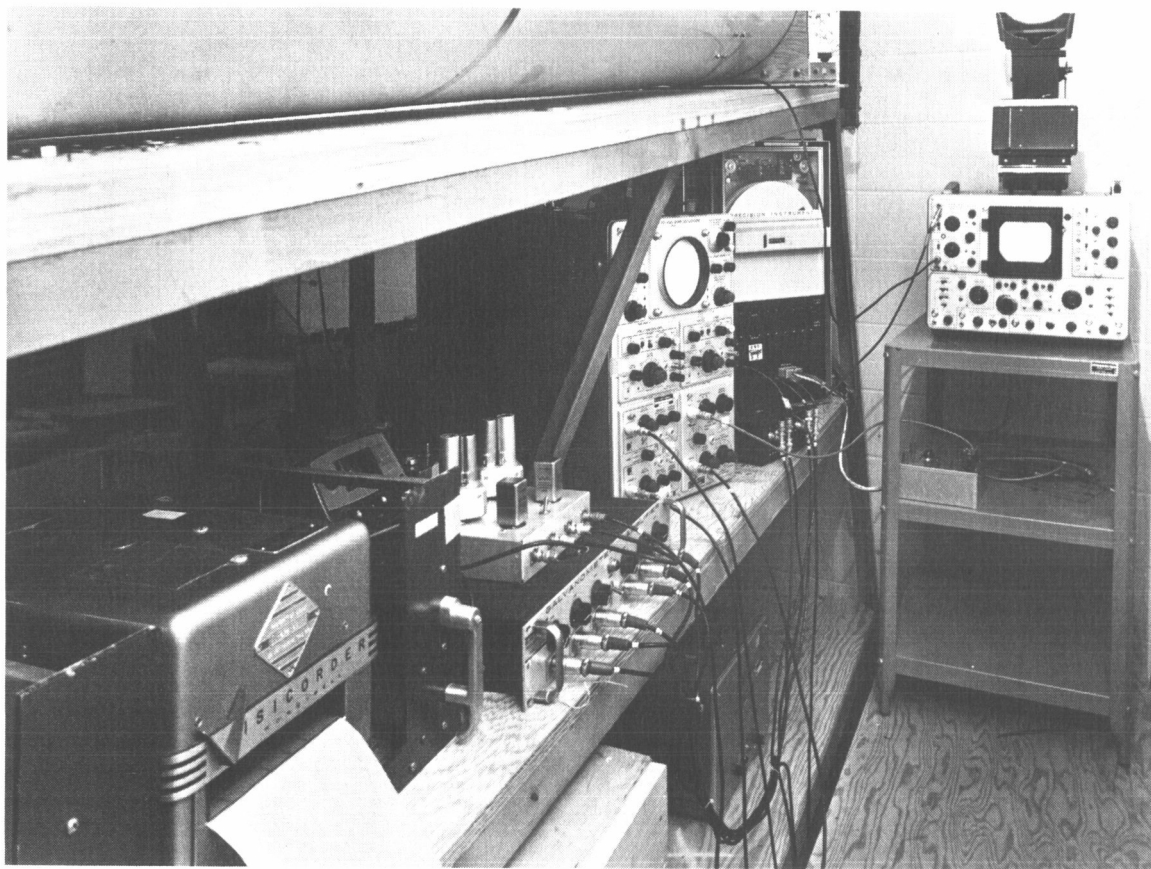


Figure 18. Recording Instruments for Optical and Meteorological Signals During Laser Propagation Research



Figure 19. Meteorological Sensor Mast



Figure 20. Meteorological Instrumentation Substation No. 1





Figure 21. Photograph of Remote Station taken from  
EOS Facility Through Telephoto Lens

### 3.2 OPTICAL EXPERIMENTAL APPARATUS

Both the CO<sub>2</sub> and He-Ne laser beams are transmitted simultaneously, with the CO<sub>2</sub> laser on the extreme left in Fig. 17, and the He-Ne alongside. The nominal cw power output of the CO<sub>2</sub> laser at 10.6μ is over 70 watts. The mode pattern was not studied in detail, but burn patterns indicate that the laser can be adjusted for single transverse mode operation. The CO<sub>2</sub> laser is dc excited so that output power fluctuations are reduced. The output power of the He-Ne laser is nominally 25 milliwatts at 0.6328μ.

The laser beams are chopped at 1000 Hz, transmitted to the corner cubes, and redirected back to the laser transmitters. Four corner cubes can be used, either individually or combined.

Reflected signals are collected by a 16-inch telescope, in the case of the 10.6μ radiation, and a 6-inch telescope, in the case of the 0.6328μ radiation. Figures 22 and 23 are schematic diagrams of the detection equipment for the 10.6μ and 0.6328μ radiation, respectively. The infrared detector requires cooling to liquid nitrogen temperatures. The preamplifier has a gain of about 120. Output signals from each detector are passed through wave analyzers, or filter-amplifiers tuned to 1000 Hz with 85-Hz bandwidths.

The received laser signal power is computed using the expression

$$P_S = \frac{P_o D_C^2 D_R^2 D_T^2 \eta_o T^2 A}{R^4 \lambda^4 (2.4)^4 K^2 K'} \quad (66)$$

where  $P_o$  = laser power output

$D_C$  = receiver aperture

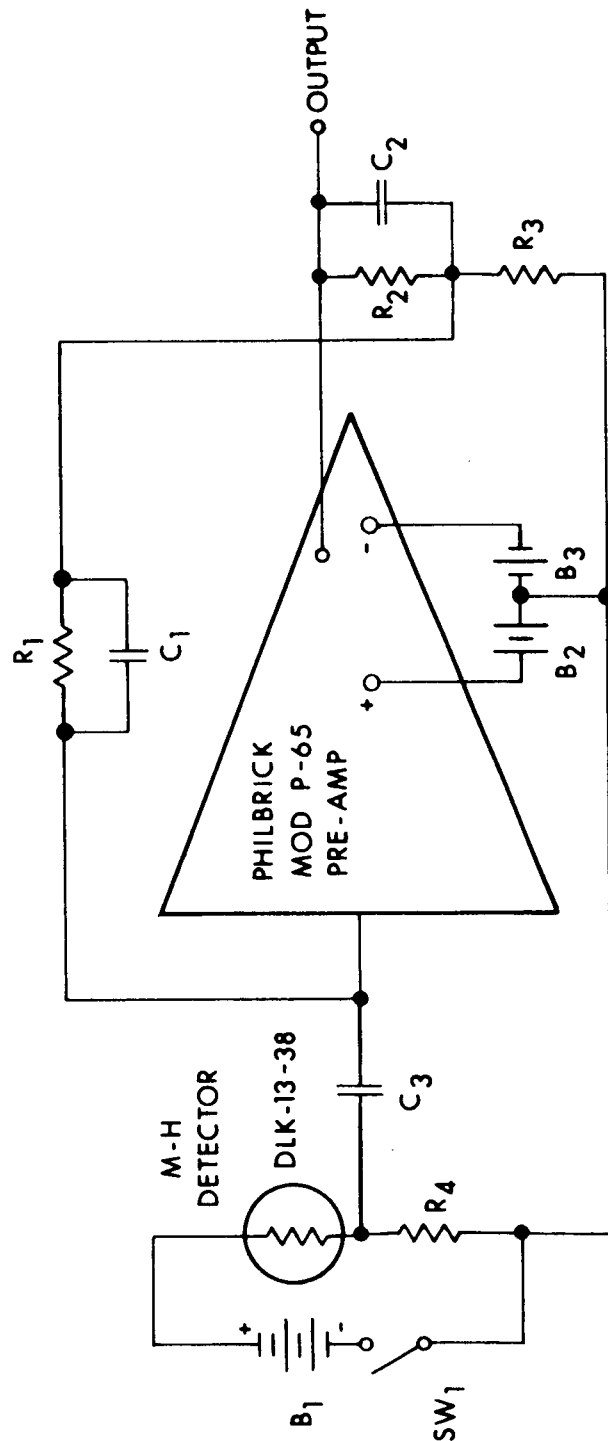


Figure 22. 10.6 $\mu$  Radiation Detector and Preamplifier Schematic



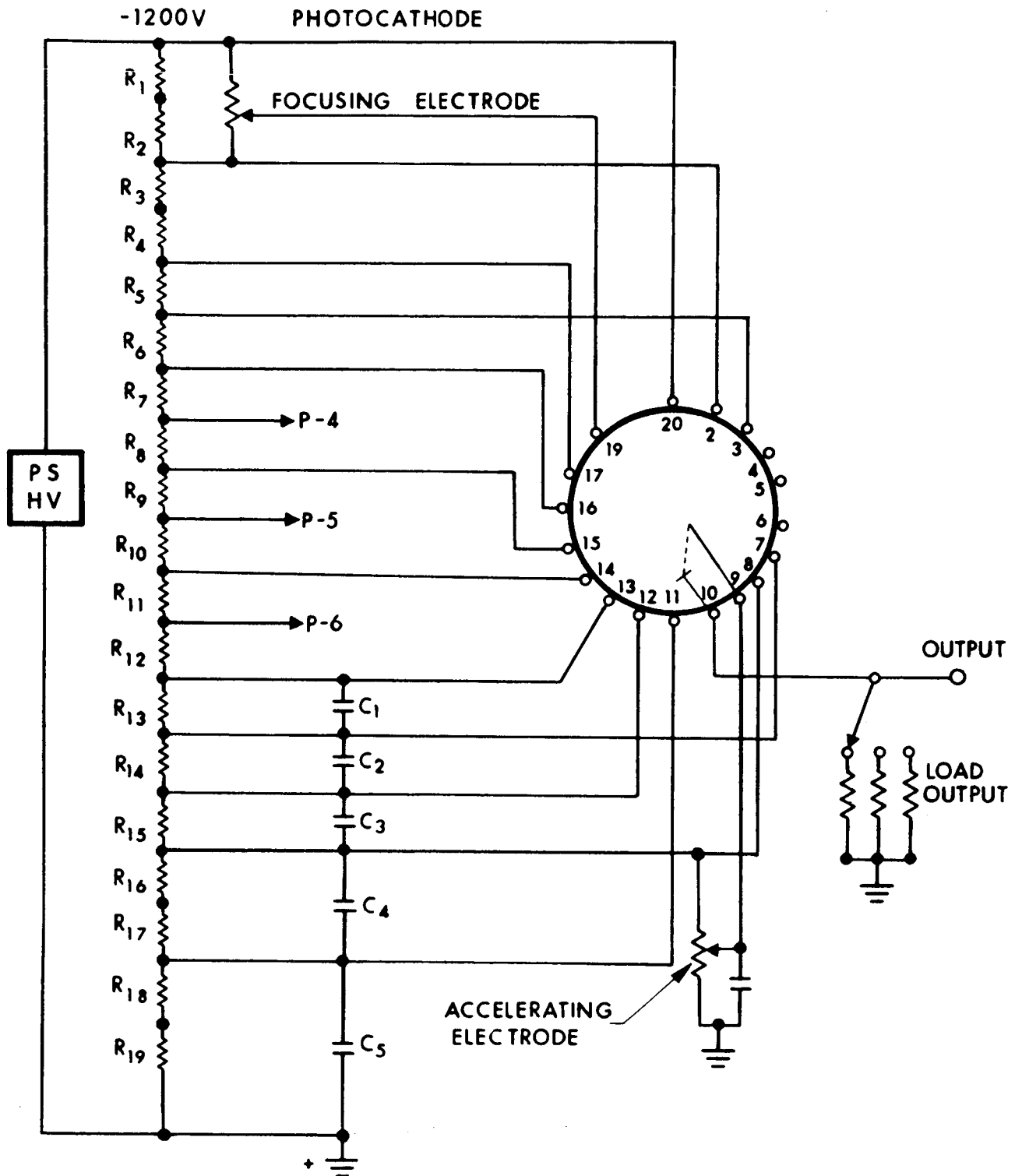


Figure 23. 0.6328 $\mu$  Radiation Detector Wire Diagram

$D_R$  = diameter of retroreflector  
 $D_T$  = diameter of transmitter beam  
 $R$  = range  
 $K$  = factor by which laser divergence exceeds diffraction limit  
 $K^1$  = retroreflector beam figure  
 $\eta_b$  = receiver optical efficiency  
 $T_A$  = atmospheric transmission

For the case of the infrared laser with the following parameters

$P_o$  = 50 watts  
 $D_C$  = ~ 50 cm  
 $D_R$  = 5 cm  
 $D_T$  = 1 cm  
 $R$  =  $5 \times 10^5$  cm  
 $\lambda$  =  $1.06 \times 10^{-3}$  cm  
 $K$  = 3  
 $K'$  = 1  
 $\eta_b$  = 1  
 $T_A$  ~ 1

we obtain

$P_S \sim 3$  microwatts

which is appreciably larger than the noise-equivalent-power of the detector.

The larger telescope is used to detect the infrared radiation so that variable-sized apertures can be positioned in front of the telescope with various center-to-center distances and spatial coherence measurements obtained. A chopper (360 rpm) alternately opens both apertures, closes one, opens both, closes the other, and then opens both apertures again. If the optical field at one aperture is  $A_1 \cos \omega t$  and  $A_2 \cos(\omega t + \varphi)$  for the other, the detector signals are proportional to

$$S_1 = kA_1^2 \quad (67)$$

$$S_2 = kA_2^2 \quad (68)$$

$$S_{1+2} = k \left( A_1^2 + A_2^2 + \frac{A_1 A_2}{2} \cos \varphi \right) \quad (69)$$

for the case of aperture 1 open only, aperture 2 open only, and both apertures open, respectively. The phase difference between the signals at each aperture can be determined using Eq. 69:

$$\varphi = \cos^{-1} \left[ \frac{2(S_{1+2} - S_1 - S_2)}{\sqrt{S_1 S_2}} \right] \quad (70)$$

For these initial experiments it is assumed that the phase fluctuations vary slowly with respect to the chopping rate of the apertures and that Eq. 70 can be used to indicate the degree of correlation between portions of the incident wavefront at various separation distances.

In addition to the returned signals, a portion of the transmitted  $\text{CO}_2$  laser beam is sampled and detected, by the bolometer detector shown in Fig. 24, for use as a reference signal and for observations of transmitter power stability.

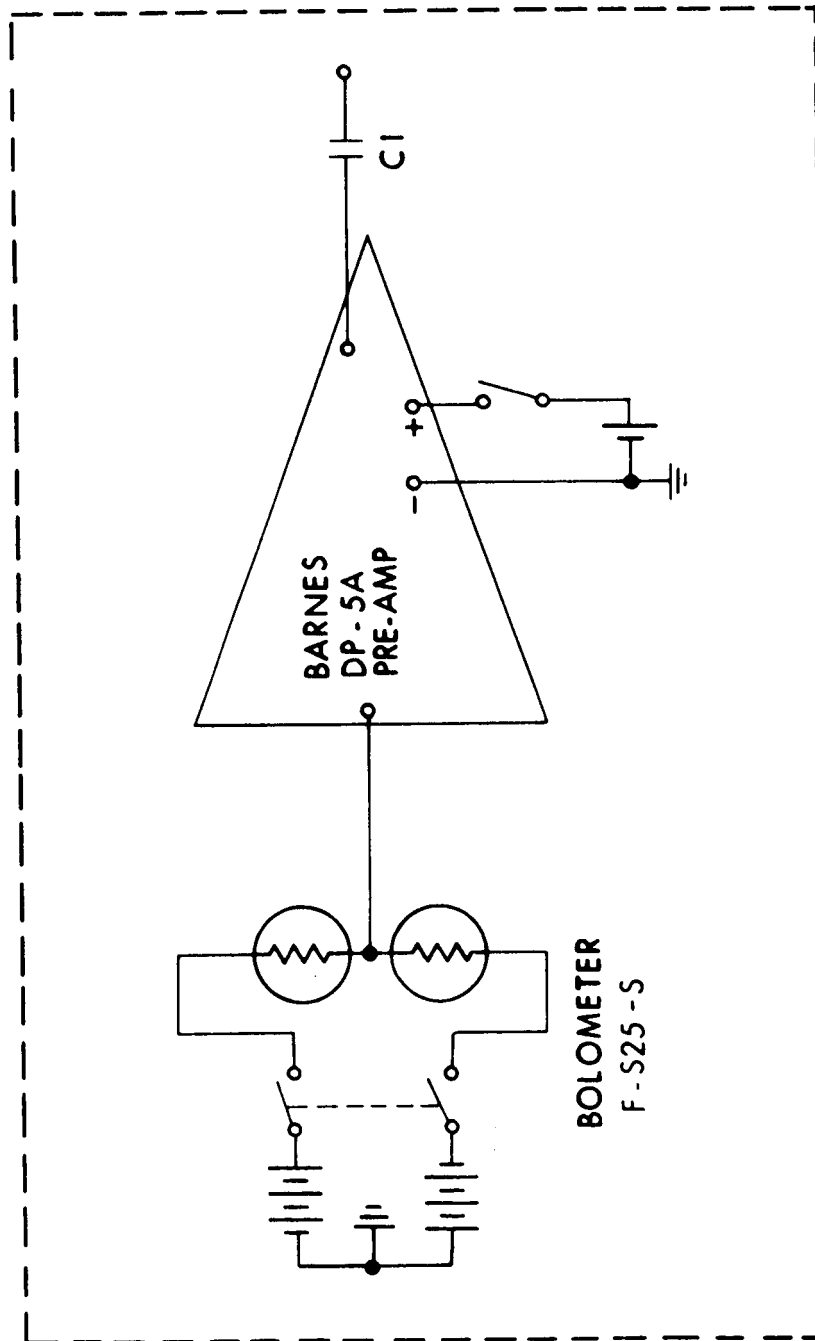


Figure 24. CO<sub>2</sub> Laser Reference Signal Detector

In addition to the primary optical equipment, the optical path is also instrumented with a telescope plus camera at the lab site and two high-contrast resolution targets at the hill site, where the corner reflectors are located. The target consists of the 10 sets of standard resolving power test target elements oriented horizontally on one target and vertically on the other, with angular spacings of from 5 to 40 microradians. Atmospheric visibility and seeing conditions determine the minimum resolvable spatial frequency that can be observed. The targets are sheltered from the sunlight and artificial lighting is supplied to remove the effects of ambient lighting from the measurements.

### 3.3 METEOROLOGICAL INSTRUMENTATION

Meteorological instruments are employed at the transmitter-receiver site and at the remote hill site. These instruments monitor the pertinent meteorological parameters for characterizing and recording the steady-state and transient nature of the atmosphere. In addition, these measured data are required for calculating the optical and turbulent properties of the atmosphere and for correlating the optical effects with prevailing meteorological and environmental conditions.

Typical values of atmospheric structure constants at the elevations of the optical path and points indicate that  $C_n$  should be fairly constant along the path, especially since the optical path is well above the terrain in between the terminal points.

Figure 19 is a photograph of the meteorological sensor mast at the transmitter-receiver location. A similar station exists at the remote site. Both stations are positioned at locations which most critically characterize atmospheric propagation effects: at the transmitter, the secondary transmitter-repeater (i.e., the corner reflector), and the

receiver. The optical path height between these locations is well above the terrain where the air is relatively well mixed and stable. Four temperature sensors, located at heights of 2.5, 3, 4, and 5 meters on the left side of the mast, provide measurements of average temperature and temperature fluctuation intensity and power spectrum. Two hot-wire anemometers, positioned at 3 and 5 meters on the right side of the mast, respond to wind velocity fluctuations up to 1 kHz. Two electro-humidity sensors are positioned at 2.5 and 4 meters and monitor relative humidity. One mechanical anemometer and a wind direction vane are located on top of the mast, and another is located atop the three-story building, above the transmitter-receiver location.

Figure 25 is a photograph of the temperature sensor, shield, and bridge. The semiconductor sensors and bridges have matched calibrated sensitivities of  $6.6 \text{ mV}/^{\circ}\text{F}$ , and they respond to step temperature changes in 2 milliseconds. The sensor covers serve both as radiation and wind shields. The schematic of the bridge is shown in Fig. 26.

Figure 27 is a photograph of one hot-wire anemometer system (West Coast Research Corporation Model 910). The meter reading (not linear, as shown) gives the average wind velocity; the system sensitivity calibration is about 10 divisions per ft/sec up to wind speeds of 4 ft/sec and 0.62 divisions per ft/sec to 20 ft/sec. An output jack at the rear of the instrument provides an ac signal proportional to wind velocity fluctuation intensities up to 1 kHz. Figure 28 is the system schematic. The remote meteorological station employs two air meters (Hastings-Raydist Model RB-1), which have logarithmic meter response to 30 mph, as shown in Fig. 29.

The electro-humidity sensors and bridge are shown in Fig. 30, and the schematic in Fig. 31. This system has maximum sensitivity at high relative humidities, where humidity might be significant in the

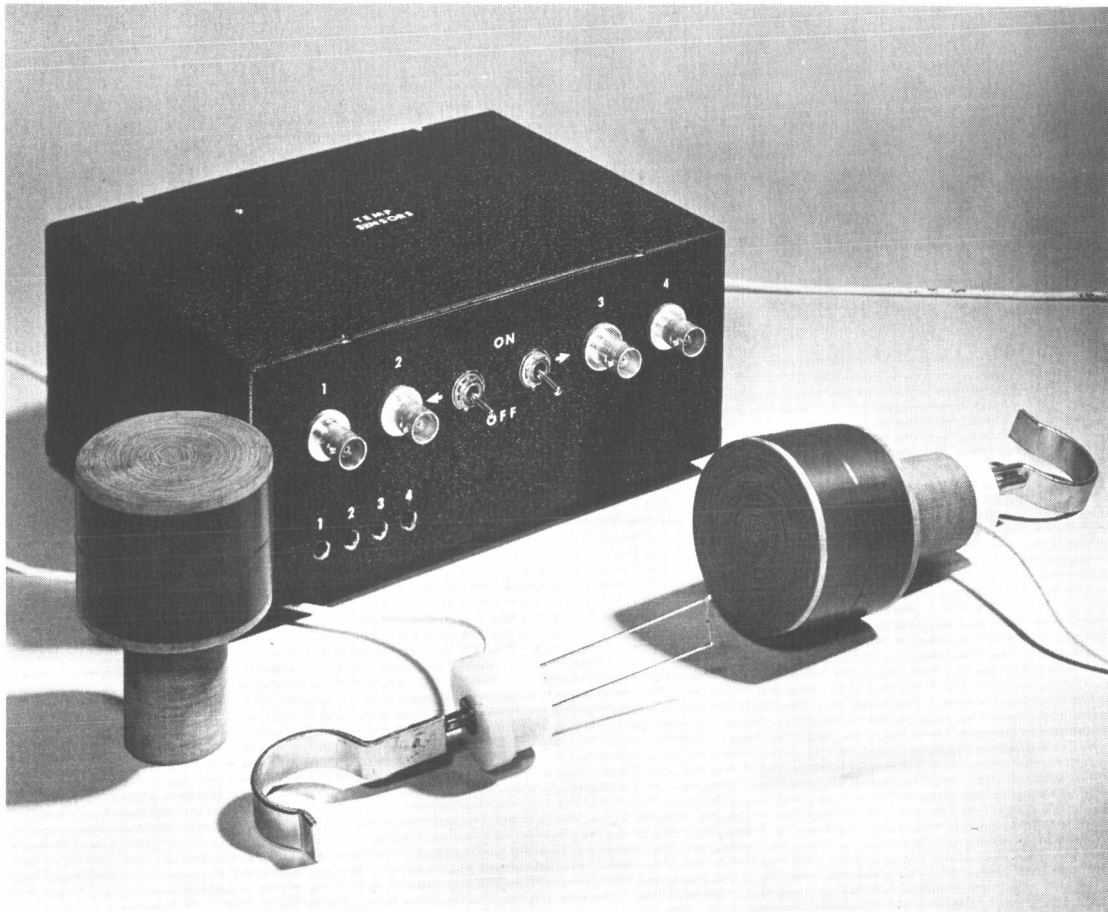


Figure 25. Temperature Sensor, Radiation and Wind Shield, and Bridge

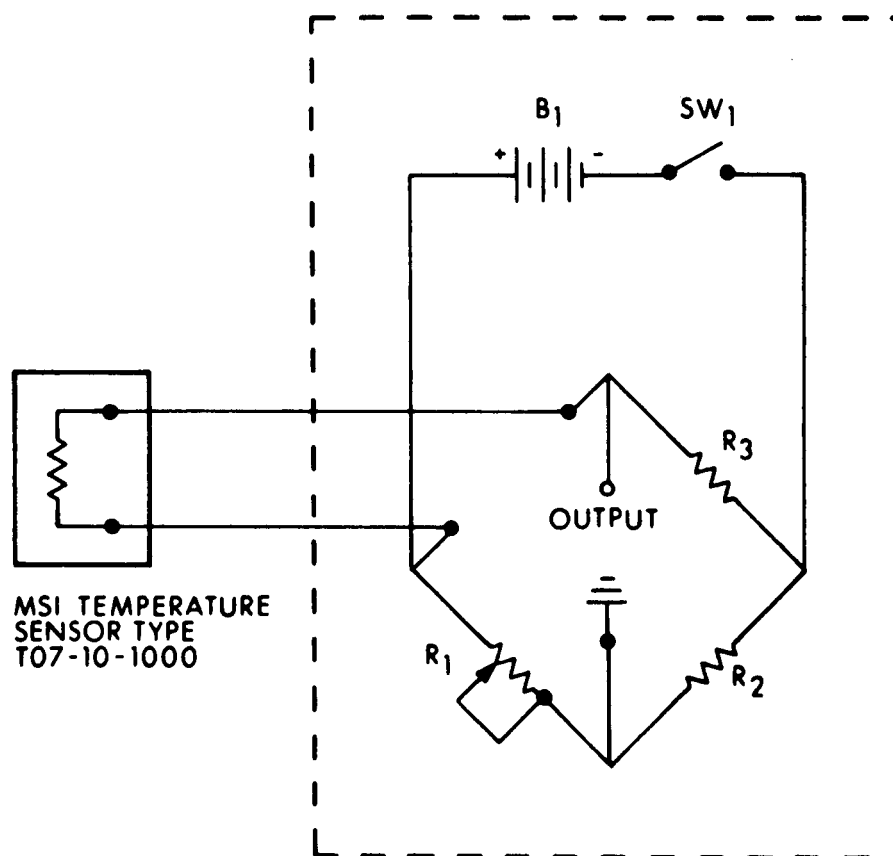


Figure 26. Temperature Sensor Bridge Schematic





Figure 27. Hot-Wire Anemometer System (WCRC Type) Sensor, Bridge, and Meter

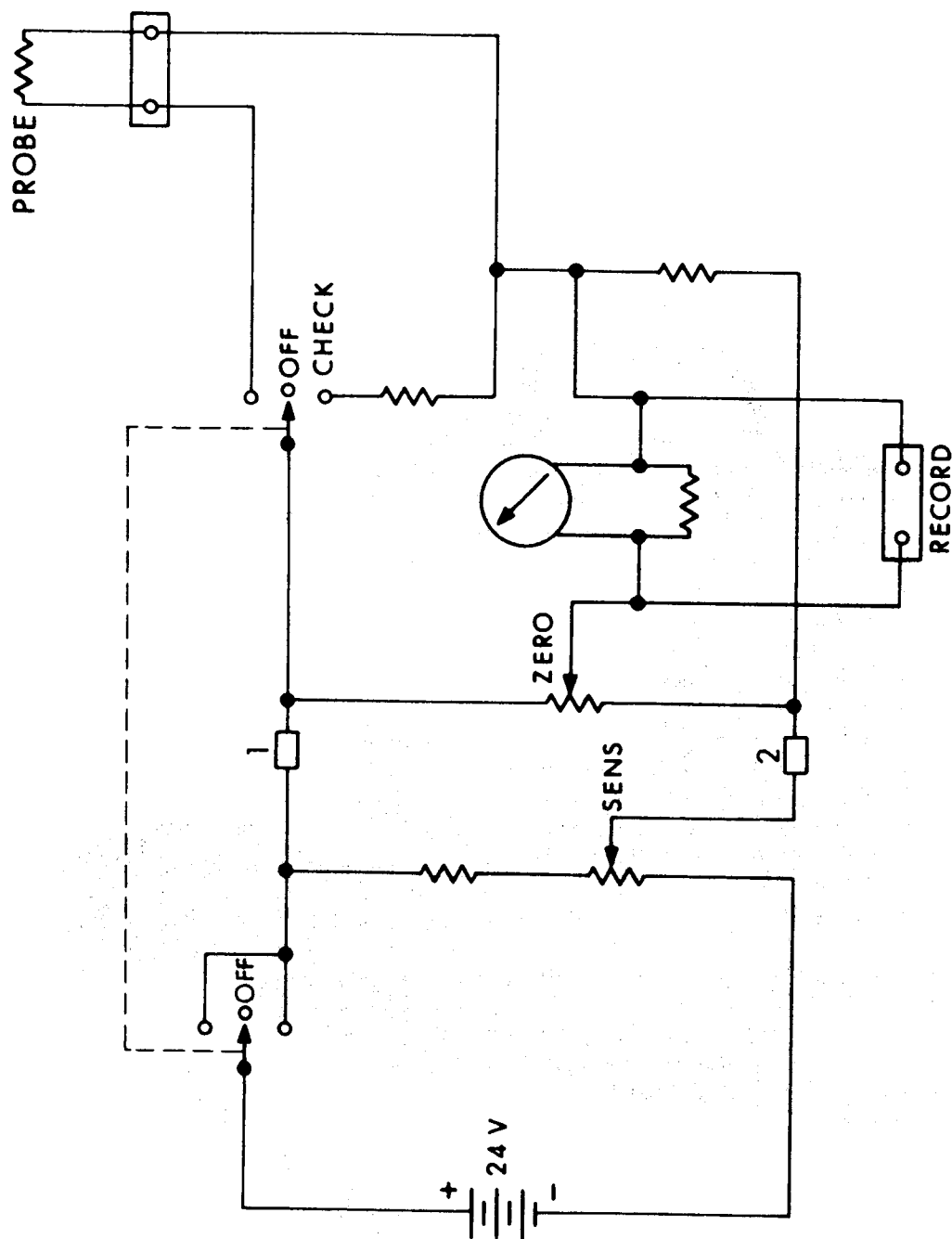


Figure 28. Hot-Wire Wind Velocity System (WCRC) Schematic



Figure 29. Hot-Wire Anemometer System (Hastings-Raydist Type)



Figure 30. Electro-Humidity Sensors and Bridge

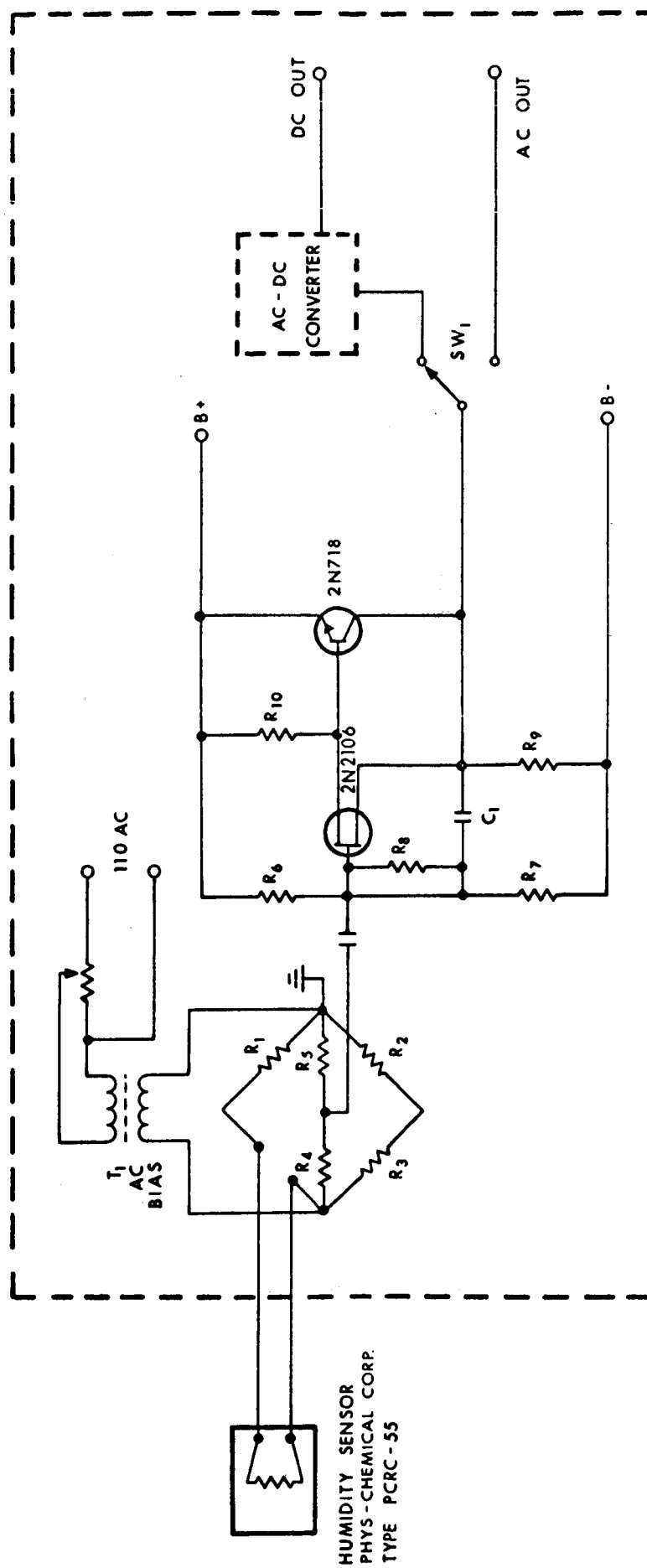


Figure 31. Humidity Sensor Electronics Schematic

propagation of  $10.6\mu$  radiation; typical sensitivity is 100 mV per percent change in relative humidity. These sensors have a response time of about 30 seconds for a 63% change in relative humidity.

Additional instruments include a wet-bulb hygrometer and an aneroid barometer. These instruments are housed in an instrument hut near the base of the sensor mast, together with the sensor bridges and meters and a graphic recorder, as shown in Fig. 20. Not shown in this photograph is a light meter for monitoring solar irradiance at the earth's surface.

Implementation of the data and signals from these meteorological instruments has been discussed in Section 2 and previous reports. An important feature of the experimental apparatus is the inclusion of multichannel graphic and magnetic recording instrumentation. Optical and meteorological sensor signals can be recorded simultaneously and subsequently analyzed and compared.

#### 3.4 DATA RECORDING INSTRUMENTATION

Multichannel sensor signals are graphically displayed on two dual-beam oscilloscopes (8 channel total) and on an oscillographic recorder (6 channel). These permanent graphic and photographic records greatly facilitate data reduction and visual correlation. In addition, the sensor signals are simultaneously recorded on an FM magnetic tape recorder (14 channel), which provides great flexibility during the data analysis for obtaining signal power spectra and auto- and cross-correlation functions. The combination of both graphical and magnetic recording significantly reduces the labor and time involved during data reduction; graphical records can be scanned for particular events and then magnetic records processed and analyzed.

### 3.5 EXPERIMENT DISCUSSION

The major portion of this program has been to develop experimental facilities, equipment, and techniques with which to investigate laser propagation over long paths in the lower atmosphere and to correlate the optical effects with meteorological conditions. Several significant experiments have been suggested (in Table III); however, the experiments were limited to two measurements, based upon practical considerations.

Experiments began during the fourth quarter of this study. During this time only preliminary and limited data were obtainable, owing to detector problems and, later, to unfavorable weather and "haze" conditions. These preliminary results are discussed briefly in the next section. Plans are to continue the experiments and report the data and conclusions in subsequent reports and papers.

PRECEDING PAGE BLANK NOT FILMED.

#### SECTION 4

#### EXPERIMENTAL RESULTS

Some typical experimental data are presented in this section. The data are so limited and insufficient that extensive data analysis and discussion are not warranted at this time.

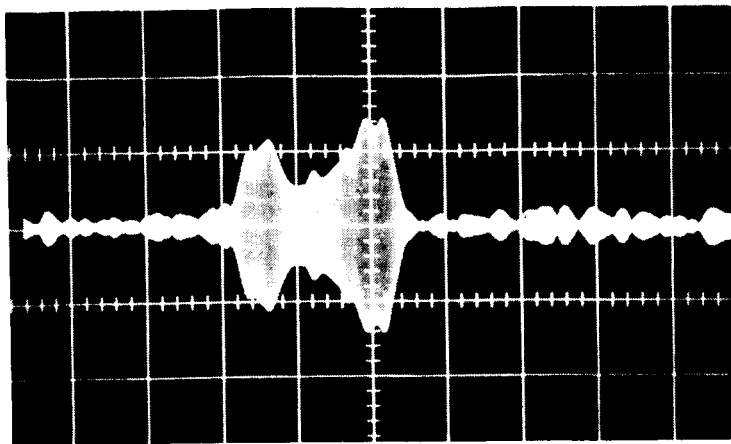
Figure 32 shows oscillographic recordings of the intensity fluctuations of the CO<sub>2</sub> laser beam after traversing a 6-mile folded optical path. In this case, a slow speed chopper was placed in front of a single corner cube; the chopping speed was 6 rpm with an observation window of 2 seconds. The second chopper was used initially to provide discrimination between the retroreflected signal and background or backscattered radiation. The times of observation for these signals ranged from 11:01 AM to 3:40 PM. The meteorological conditions are summarized in Table V.

TABLE V  
METEOROLOGICAL DATA SUMMARY

Time	Temperature (°F)	Pressure (in.)	Relative Humidity (%)	Wind Velocity			Gustiness (%)
				Max (mph)	Min (mph)	Avg (mph)	
11:45 AM	72	29.24	54	—	—	—	—
2:00 PM	75	29.24	54	6.5	1.5	5.5	73
3:45 PM	72	29.23	53	5.5	3.0	3.5	43



1V/D

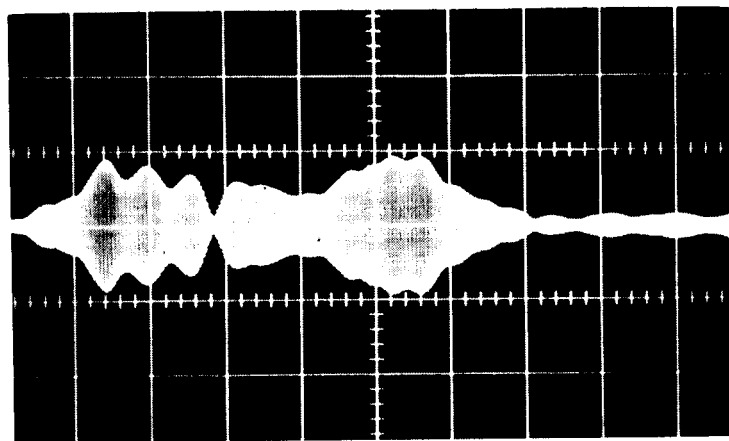


$f_m \sim 10$  cps

0.5 sec/D

a.  $m = 48\%$

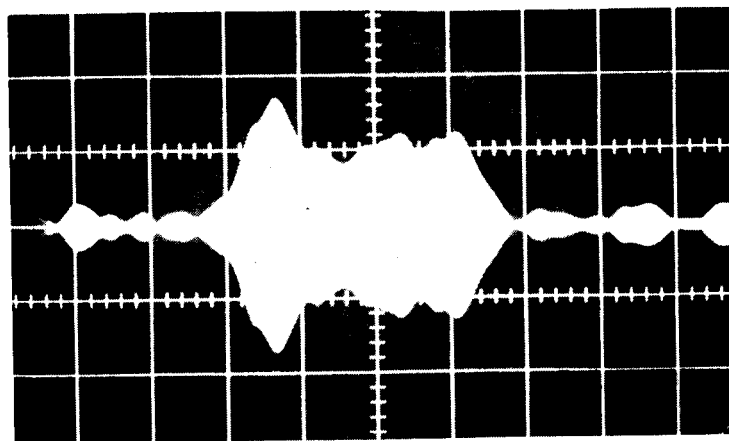
1V/D



0.2 sec/D

b.  $m = 47\%$

1V/D

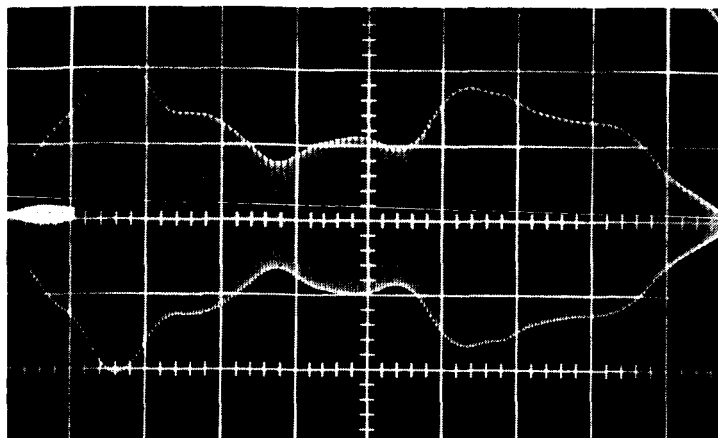


0.5 sec/D

c.  $m = 41\%$

Figure 32. Effects of Atmosphere on CO<sub>2</sub> Laser Intensity

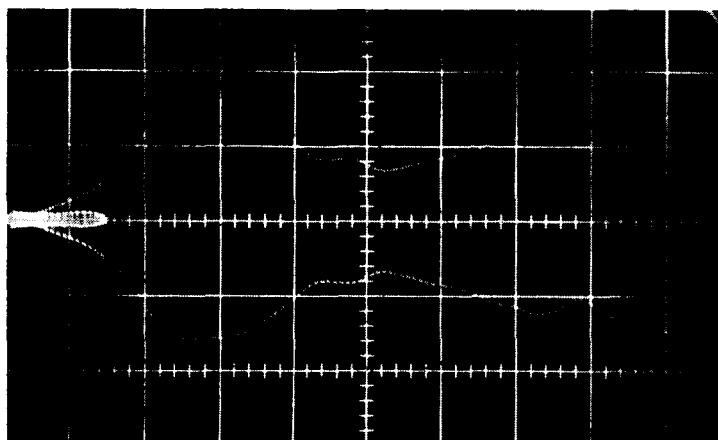
IV/D



0.2 sec/D

d.  $m = 50\%$

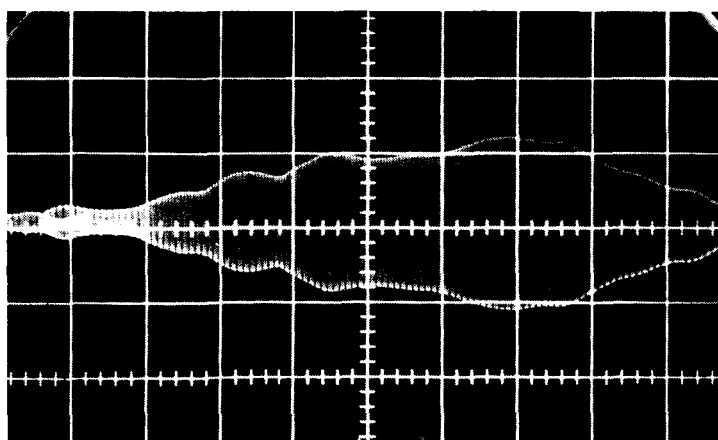
IV/D



0.2 sec/D

e.  $m = 42\%$

IV/D



0.2 sec/D

f.  $m = 44\%$

Figure 32. Effects of Atmosphere on CO<sub>2</sub> Laser Intensity (contd)

The percent modulation, given by

$$m = \frac{V_{\max} - V_{\min}}{2V_{\text{avg}}} \times 100$$

for the data shown in Fig. 32 is summarized in Table VI.

TABLE VI  
CO<sub>2</sub> LASER BEAM MODULATION SUMMARY

Time	V <sub>max</sub>	V <sub>min</sub>	~ V <sub>avg</sub>	m (%)
11:01	1.43	0.57	0.9	48
11:02	1.35	0.40	0.9	42
11:05	2.5	1.4	1.8	30
11:10	0.95	0.2	0.8	47
11:25	1.6	0.7	1.2	38
12:00	1.7	0.8	1.1	41
12:02	1.7	0.6	1.2	46
12:04	1.7	0.5	1.0	60
12:05	1.1	0.3	0.6	66
1:48	2.2	0.8	1.4	50
3:20	1.6	0.7	1.1	42
3:40	1.2	0.2	0.8	44*

\* 6 inch telescope

The oscillographic traces in Fig. 33 show typical intensity fluctuations of the He-Ne laser beam due to the random atmosphere. The top trace is the signal plus noise. The lower trace of Fig. 33a shows the noise alone. The lower trace of Fig. 33b shows the variation in the temperature during the observation time.

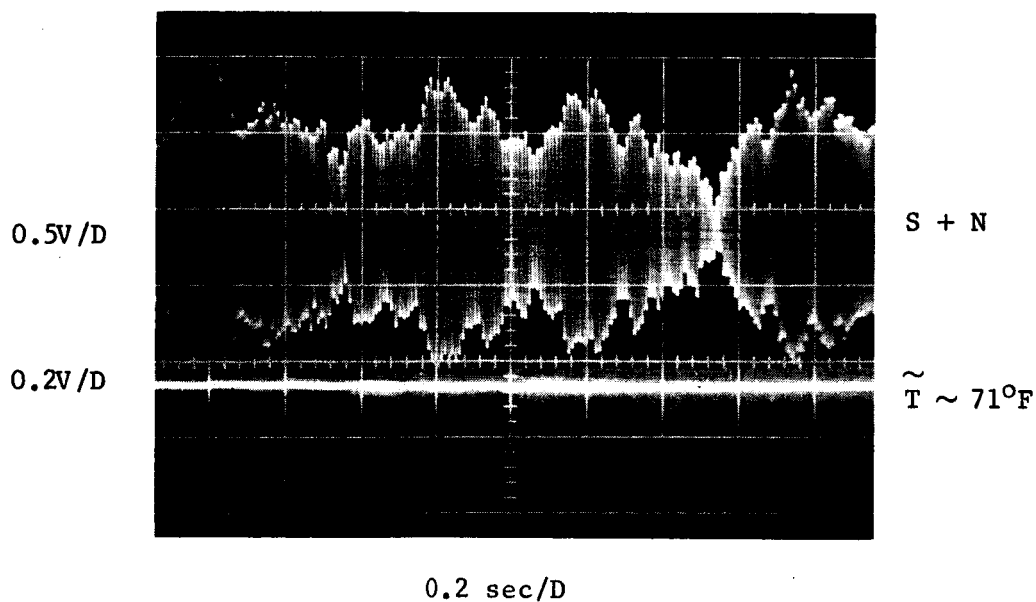
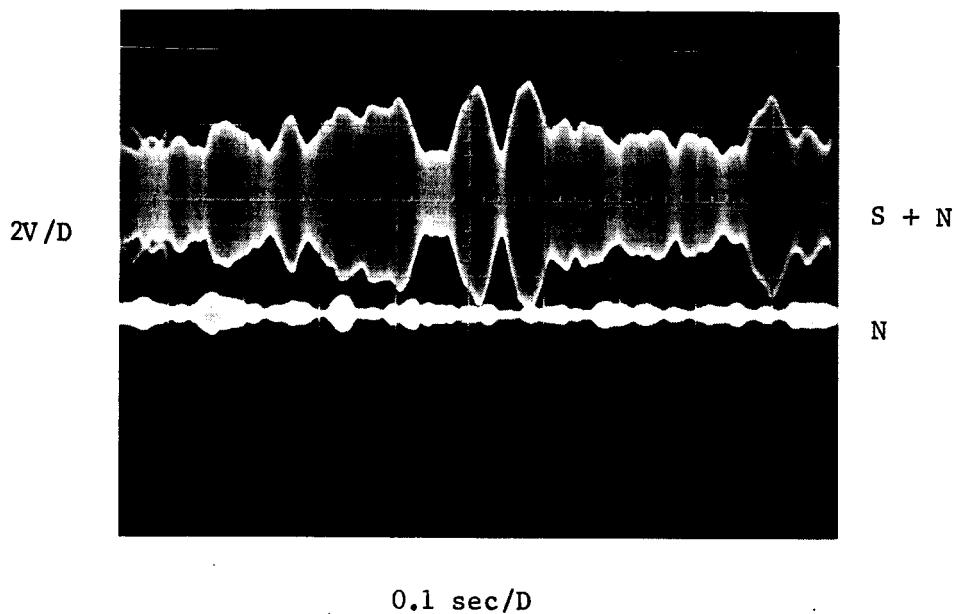


Figure 33. Effects of Atmosphere on He-Ne-Laser Intensity



## SECTION 5

### CONCLUSIONS AND RECOMMENDATIONS

The present theories of optical frequency interaction with the atmosphere have been reviewed and summarized. The bibliography included as the references and as Appendix A is nearly exhaustive on this subject. A number of significant experiments have been identified and are summarized in table form (Table III). Instrumentation has been procured and assembled to perform selected experiments and to correlate optical propagation parameters with meteorological parameters. This instrumentation included facilities at both a master station at the EOS Pasadena plant and a remote station located 5 km away in the nearby San Gabriel Mountains. Corner cube retroreflectors along with modest meteorological instrumentation constituted the remote station. Laser transmitters, at  $10.6\mu$  and  $0.6328\mu$ , and receivers along with more elaborate meteorological instruments constituted the master station.

Experimental results were not achieved until late in the fourth quarter and are not sufficient for drawing general conclusions. Received signals at both wavelengths clearly demonstrate atmospheric turbulence induced amplitude fluctuations and indicate that with a modest improvement in the signal-to-noise ratio, significant data can be extracted relating to interaction with the atmosphere.

Continued effort in this field should employ an improved signal-to-noise ratio and should concentrate on temporal and spatial coherence degradation. Improvements in the signal-to-noise ratio can be achieved by tighter beam pattern control on the transmitted beam. This may include modifications to achieve a more fundamental laser mode pattern

and may also include some form of collimating optics. The S/N can also be improved by relocating the remote station to a closer location. Since turbulence theory indicates significant interaction over a path length of a few hundred meters, this latter approach to better S/N is the most easily achieved and is to be recommended.

A continuation of the effort initiated by this program is essential to an understanding of laser radiation through the atmosphere. Particular emphasis must be given to coherence degradation since the information carried by an optical beam is directly dependent upon its coherence properties. In addition, the effects and limits of turbulence induced fluctuations are almost completely unknown, whereas effects and limitations imposed by hazes and particulate matter differ little from similar effects for noncoherent radiation and are fairly well established. Typical means and standard deviations of various coherent optical propagation degradation parameters are essential to planning for optical communication through the atmosphere. Such areas as site location, information capacity, and possible adaptive techniques to counter turbulence effects are highly dependent upon the continuation of such studies as reported herein.

Except for the obvious impracticality of point-by-point meteorological instrumentation along the transmission path, the meteorological instrumentation assembled during this program is complete with the exception of two parameters. No instrumentation has been procured for the measurement of microtemperature fluctuations nor for the measurement of the volumetric rate of dissipation of turbulence energy. The significance of these two parameters is such that their measurement must be included in future programs.

## REFERENCES

1. E. Brookner, M. Kolker, and R. M. Wilmotte, "Deep-Space Optical Communications," IEEE Spectrum, 4, 75, (1967)
2. G. Cato, L. Carrier, K. von Essen, Laser Systems Study, Part III: Effects of Clouds, Report 4440-Final III, Electro-Optical Systems, Inc., Pasadena, California, Dec 1965, (AD 479 487)
3. R. Kauth and J. Penquite, The Probability of Clear Lines of Sight Through a Cloudy Atmosphere, Report No. 6054-14-T, University of Michigan, Ann Arbor, Michigan, Sep 1966, (AD 800 118)
4. I. Lund, "Methods for Estimating the Probability of Clear Lines-of-Sight, or Sunshine, Through the Atmosphere," Journal of Applied Meteorology, 5, 625, (1966)
5. H. van de Huest, Light Scattering by Small Particles, John Wiley and Sons, New York, 1964
6. D. Deirmendjian, "Scattering and Polarization Properties of Water Clouds and Hazes in the Visible and Infrared," Applied Optics, 3, 187, (1964)
7. R. Dell-Imagine, "A Study of Multiple Scattering of Optical Radiation with Applications to Laser Communication," in Advances in Communication Systems (Vol. 2), A. V. Balakrishnan, Ed., Academic Press, New York, 1966
8. D. Portman, et al, Visual Resolution and Optical Scintillation Over Snow, Ice, and Frozen Ground; Part I, Research Report III, U.S. Army Material Command, Cold Regions Research and Engineering Laboratory, Hanover, New Hampshire, Apr 1964
9. R. Munick, "Meteorological Variables Affecting Turbulent Propagation Characteristics," Proceedings of Conference on Atmospheric Limitations to Optical Propagation, Boulder, Colorado, 1965
10. Handbook of Geophysics, The Macmillan Company, New York, N.Y., 1961, Ch. 13: "Electromagnetic Wave Propagation in the Lower Atmosphere."
11. H. Carlon, "The Apparent Dependence of Terrestrial Scintillation Intensity Upon Atmospheric Humidity," Applied Optics 4, 1089, (1965)
12. W. Conway, et al, "A Gradient Microwave Radiometer Flight Test Program," Proceedings of Second Symposium on Remote Sensing of Environment, University of Michigan, Ann Arbor, Michigan, Oct 1962, p. 145, (AD 299 841)



13. O. Sutton, Micrometeorology; A Study of Physical Processes in the Lowest Layers of the Earth's Atmosphere, McGraw-Hill, New York, 1953
14. V. Tatarski, Wave Propagation in a Turbulent Medium, McGraw-Hill, New York, 1961, Ch. 2
15. J. Lumley and H. Panofsky, The Structure of Atmospheric Turbulence, Interscience Publishers, New York, 1964, Ch. 3
16. L. Chernov, Wave Propagation in a Random Medium, McGraw-Hill, New York, 1960
17. R. Hufnagel and N. Stanley, "Modulation Transfer Function Associated with Image Transmission Through Turbulent Media," JOSA 54, 52, (1964)
18. P. Beckmann, "Signal Degeneration in Laser Beams Propagated Through a Turbulent Medium," Radio Science, J. of Research, NBS, 69D, 629 (1965)
19. H. Hodara, "Laser Wave Propagation Through the Atmosphere," Proceedings IEEE, 54, 368 (1966)
20. V. Tatarski, loc. cit., p. 9
21. V. Tatarski, loc. cit., p. 46 and p. 58
22. D. Fried, "Optical Heterodyne Detection of an Atmospherically Distorted Signal Wave Front," Proc. IEEE, 55, 57 (1967)
23. V. Tatarski, loc. cit., Parts III and IV
24. J. Davis, "Consideration of Atmospheric Turbulence in Laser System Design," Applied Optics 5, 139 (1966)

APPENDIX A

BIBLIOGRAPHY

on

ATMOSPHERIC EFFECTS ON OPTICAL COMMUNICATIONS

by

Lee W. Carrier

Optical Systems Division  
Electro-Optical Systems, Inc.  
Pasadena, California

July 1966

Prepared in part for NASA Electronic Research Center under Contract NAS12-130

## ATMOSPHERIC EFFECTS ON LASER BEAM CHARACTERISTICS

1. P. Beckmann, "Signal Degeneration in Laser Beams Propagated Through a Turbulent Atmosphere," Radio Science, J. of Res. NBS, 69D, 629 (1965)
2. A. L. Buck, "Laser Propagation in the Atmosphere," Proc. Conf. Atmospheric Limitations to Optical Propagation, Boulder, Colorado, 1965
3. A. Buck, "Effects of the Atmosphere on Laser Beam Propagation," Applied Optics, 6, 703 (1967)
4. J. Cornacchio and K. Farnham, "On the Measurement of the Complex Spatial Coherence of a He-Ne Laser Beam," Il Nuovo Cimento 42B, 108, (1966)
5. D. Dobbins and A. LaGrone, "Interaction of High Intensity Laser Beam with the Atmosphere," Presented at 18th Ann. Southwestern IEEE Conf., Dallas, Texas (April 1966)
6. C. Eaglesfield, "Statistics of Laser Radiation," Proc IEEE 54, 66 (1966)
7. F. E. Goodwin, "Laser Propagation in the Terrestrial Atmosphere," Proc. 1st Laser Conf., San Diego, Sept 1963
8. A. Hodara, "Laser Wave Propagation Through the Atmosphere," Proc. IEEE, 54, 368 (1966)
9. P. L. Kelley, "Self-Focusing of Optical Beams," Phys. Rev. Let. 15, 1005 (1965)
10. C. Knop, "The Dispersion Properties of Air as a Possible Limitation on the Maximum Useable Bandwidths of Coherent Optical Communication Systems," Proc. IEEE 52, 319 (1964)
11. B. Lewis, "Test for Detecting Self-Trapping in Optical Beams," Proc. IEEE 53, 1731 (1965)
12. B. Lewis, "Coefficient for Self-Trapping of Optical Beams," Proc. IEEE 54, 688 (1966)
13. H. C. McDowell and G. J. Stiles, "The Effect of Atmospheric Turbulence on Laser Beam Distribution," Proc. 1st Laser Conf., San Diego, Sept 1963
14. G. Meyers, D. Fried, and M. Keister, "Experimental Measurements of the Character of Intensity Fluctuations of a Laser Beam Propagating in the Atmosphere," Paper TB17, Presented at 1965 Annual Mtg., Optical Soc. of America, Philadelphia, Oct 1965
15. S. Miller and L. Tillotson, "Optical Transmission Research," Proc. IEEE, 54, 1300 (1966)
16. K. Mujamoto, "Propagation of Laser Light," JOSA, 54, 989 (1964)

17. H. W. Straub, Effects of Air Turbulence Upon Propagation of Light,  
Diamond Ordnance Fuze Laboratories, Washington 22 D. C., DDC  
AD 286049
18. J. Whitten, G. Prehmus, and K. Tomiyasu, "Q-Switched Laser Beam  
Propagation over a Ten-Mile Path", Proc. IEEE 53, 736 (1965)
19. R. Wilson and A. Penzias, "Effect of Precipitation on Transmission  
Through the Atmosphere at 10 Microns," Nature, 1081 (1966)

## ABSORPTION

1. D. E. Burch, et al, Infrared Absorption by Carbon Dioxide, Water Vapor, and Minor Atmospheric Constituents, Report No. AFCRL-62-698, Air Force Cambridge Research Laboratories, Hanscom Field, Mass., July 1962
2. T. S. Chu and D. C. Hogg, "The Attenuation of 3.392  $\mu$  He-Ne Laser Radiation by Methane in the Atmosphere," Bell System Tech. J., Feb. 1966, p. 301
3. J. A. Curcio, et al, "An Atlas of the Absorption Spectrum of the Lower Atmosphere from 5400 Å to 8520 Å," Applied Optics 3, 1401 (1964)
4. A. E. Douglas and K. P. Huber, "The Absorption Spectrum of NO<sub>2</sub> in the 3700-4600 Å Region," Canadian J. of Phys. 43, 74 (1965)
5. R. Eldridge, "Water Vapor Absorption of Visible and Near Infrared Radiation," Applied Optics, 6, 709 (1967)
6. B. M. Herman and D. N. Yarger, "The Effect of Absorption on a Rayleigh Atmosphere," J. of Atmos. Sci. 22, 644 (1965)
7. L. L. List and G. E. Oppel, Transmission Through Extreme Model Atmospheres, Report No. LMSC-A701650, Lockheed Missiles and Space Co., Sunnyvale, Calif., Sept. 1964
8. R. Long, Absorption of Laser Radiation in the Atmosphere, Report No. 1579-3, Antenna Laboratory, Dept. of Elect. Engineering, Ohio State University, Columbus, Ohio, May 1963 (AD410571)
9. J. H. Meyer and R. E. Newell, Preliminary Study of the Effect of Ozone on Atmospheric Transmission in the Range 0.25 Micron to 0.60 Micron, MIT Report No. AFESD-TDR-63-44, Lexington, Mass. (AD 402 842)
10. G. Plass, "The Absorption of Laser Radiation Along Atmospheric Slant Paths", Appl. Optics 5, 149 (1966)
11. F. R. Stauffer and T. E. Walsh, "Transmittance of Water Vapor -- 14 to 20 Microns," JOSA 56, 401 (1966)

## LASER LIGHT SCATTERING EFFECTS

1. L. Carrier, Laser Systems Study (Supplement), Electro-Optical Systems, Inc. Pasadena, Rept. No. 4440-Final, April 1965
2. B. Clemesha, G. Kent, and R. Wright, A Study of the Feasibility of Measuring Atmospheric Densities by Using a Laser Searchlight Technique, Scientific Rept. AF-AFOSR-616-64, Univ. of West Indies, Kingston, Jamaica, May 1965
3. B. Clemesha, G. Kent, and R. Wright, "Laser Probing the Atmosphere," Nature 209, 184 (1966)
4. R. Collis, "Lidar Detection of CAT," Astronautics and Aeronautics, Dec. 1964
5. R. Collis, "Lidar Observation of Cloud," Science 149, 978 (1965)
6. A Consortini, et al, "Influence of Atmospheric Scattering on the Line-Width of a Laser Beam," Alta Frequenza, 33, 714 (1964)
7. J. Curcio, et al, "Some Recent Experiments on the Transmission of Light Signals Over the Horizon," Paper FB12, Presented at 1964 Spring Mtg. of Opt. Soc. of America, Washington, D.C. April 1964
8. R. A. Dell-Imagine, "A Study of Multiple Scattering of Optical Radiation With Applications to Laser Communication," Paper presented at International Symposium Antennas and Propagation, Washington D.C., August-Sept. 1965
9. G. Fiocco and L. Smullin, "Detection of Scattering Layers in the Upper Atmosphere (60-140 km) by Optical Radar," Nature 199, 1275 (1963)
10. G. Fiocco and G. Grams, "Observations of the Aerosol Layer at 20 KM by Optical Radar," J. Atm. Science, 21, 323 (1964)
11. G. Fiocco and G. Colombo, "Optical Radar Results and Meteoric Fragmentation," J. Geophys. Res., 69, 1795 (1964)
12. G. Fiocco, "Optical Radar Results and Ionospheric Sporadic E." J. Geophys. Res. 70, 2213 (1965)
13. R. Fox, "Optical Radar Detection of Scattering Layers in the Atmosphere," Master Thesis, Dept. of Meteorology, Univ. of Wisconsin, 1964, DDC AD 441036
14. H. W. Halsey and G. L. Snyder, The Use of a Laser as an Atmospheric Probe, Rept. No. 64SD276, Missile and Space Division, General Electric, King of Prussia, Pa., 1964
15. W. Henneberger, "Scattering of Intense Light" Phys. Rev. 140, A1864 (1965)

16. S. Kainer, "Laser Beam 'Security'," Proc IEEE, 53, 1752 (1965)
17. M. Ligda, "Meteorological Observations With Lidar," Proc. of 11th Weather Radar Conf. NBS, Boulder, Colorado, Sept. 1964
18. O. Lillesaeter, Attenuation of a Parallel Beam of Light, Particularly by Snow, U. S. Gov. Res. Rept. AD 615 383
19. P. McCormick et al, "Backscattering From the Upper Atmosphere (75 KM-160KM) Detected by Optical Radar," Nature 209, 798 (1966)
20. R. Munick, "Turbulent Backscatter of Light," JOSA 55, 893 (1965)
21. E. P. Palmer, "Absolute Scattering Functions and Transmission Values For Interpreting Laser Light Scattering in the Mesosphere," J. Geophysical Res., 69, 2369 (1964)
22. R. Schotland and A. Nathan, "The Use of Lasers For the Remote Determinations of Atmospheric Temperature" Proc. 2nd Symposium on Remote Sensing of Environment, U. of Michigan, Feb. 1963

# OPTICAL SCINTILLATION

1. P. Beckman, "Signal Degeneration in Laser Beams Propagated through a Turbulent Atmosphere" Radio Science, J. of Res. NBS, 69D, 629 (1965)
2. H. Carlon, "The Apparent Dependence of Terrestrial Scintillation Intensity Upon Atmospheric Humidity" Appl. Optics 4, 1089 (1965)
3. S. Chandrasekhar, "A Statistical Basis of the Theory of Stellar Scintillation," Roy. Ast. Soc. Monthly Notices, 112, 475 (1952)
4. C. Coulman and D. Hall, "Optical Effects of Thermal Structure in the Lower Atmosphere," Applied Optics, 6, 497 (1967)
5. M. Ellison, "The Effects of Scintillations on Telescopic Images" Proc. of a Symposium on Astronomical Optics and Related Subjects, Z Kopal, ed. (Interscience, N.Y., 1956)
6. E. Megaw, "Scattering of Electromagnetic Waves by Atmospheric Turbulence," Nature 166, 1100 (1950)
7. J. Meyer-Arendt and C. B. Emmanuel, "Optical Scintillation: A Survey of the Literature" Tech. Note 225, Nat. Bur. Std, Boulder, Colo. April 5, 1965 (Contains 24 pages of references)
8. M. Minnaert, The Nature of Light and Colour in the Open Air, Dover Publ. Inc., New York, N.Y., 1954
9. S. J. Portman, et al, "Some Optical Properties of Turbulence in Stratified Flow Near the Ground," J. Geophys. Res. 67, 3223, (1962)
10. M. Wimbush, Optical Astronomical Seeing; A Review, Scientific Rept. No. 1, Hawaii Inst. of Geophysics, University of Hawaii, Honolulu, Hawaii, May 1961



## OPTICAL SEEING

1. R. Becker, "Effects of Atmospheric Turbulence on Optical Instrumentation," IRE Trans. On Mil, Elect. 5 (4), 352 (Oct 1961)
2. B. Bullock, G. Smith, and R. Borofka, "Atmospheric Boil Measurements" Proc. IRIS 5 (2), 41 (1960)
3. C. Coulman, "Optical Image Quality in a Turbulent Atmosphere" JOSA 55 806 (1965)
4. C. Coulman, "Dependence of Image Quality on Horizontal Range in a Turbulent Atmosphere," JOSA, 56, 1232 (1966)
5. E. Djurle and A. Bäck, "Some Measurements of the Effect of Air Turbulence on Photographic Images," JOSA, 51, 1029 (1961)
6. S. Duntley, A. Boileau, and R. Preisendorfer, "Image Transmission by the Troposphere I," JOSA, 47, 499 (1957)
7. S. Duntley, et al, "Reduction of Contrast by Atmospheric Boil" JOSA 53, 351 (1963)
8. D. Fried, "Optical Resolution Through a Randomly Inhomogeneous Medium for Very Long and Very Short Exposures," JOSA, 56 1372 (1966)
9. D. Fried, "Limiting Resolution Looking Down Through the Atmosphere," JOSA, 56, 1380 (1966)
10. A. Meinel, "Astronomical Seeing and Observatory Site Selection" in Telescopes G. Kuiper and B. Middlehurst, ed. Univ. of Chicago Press 1960, pp. 154-175
11. D. Portman et al, Visual Resolution and Optical Scintillation Over Snow, Ice, and Frozen Ground, Part I, Research Rept. 111, U.S. Army Material Command, Cold Regions Research and Engineering Laboratory, Hanover, New Hampshire, April 1964
12. L. A. Riggs et al, "Photographic Measurements of Atmospheric Boil," JOSA, 37 415, (1947)
13. C. Rogers, "Variation of Atmospheric 'Seeing' Blur With Object-To-Observer Distance," JOSA 55, 1151 (1965)
14. J. Stock and G. Keller, "Astronomical Seeing" in Telescopes, G. Kuiper and B. Middlehurst, eds. Univ. of Chicago Press, 1960, pp 138-153
15. R. N. Wolfe, C. A. Morrison, and H. R. Condit, "Experimental Technique for Studying Atmospheric Turbulence, JOSA 49, 829 (1959)

## TURBULENCE MODELS AND STUDIES

1. Development of a Model Turbulent Atmosphere, Perkin-Elmer Corp. Report No. 7211 - App. D.
2. G. Batchelor, "The Theory of Homogeneous Turbulence", Cambridge Univ. Press, 1953
3. P. Beckman, "Signal Degeneration in Laser Beams Propagated Through a Turbulent Atmosphere" Radio Science, J of Res. NBS 69D, 629 (1965)
4. K. Bourquin and F. Shigemoto, "A Laboratory Investigation of Turbulence Detection Using a Laser," NASA Conf. on Aircraft Operating Problems, Washington D.C. 1965
5. W. Brinks, "A Guide for Turbulent Atmosphere Propagation Experiments," Report No. TM-66-16, Harry Diamond Laboratories, Washington, D.C., October 1966 (AD 645 734)
6. W. Brown, "Validity of the Rytov Approximation in Optical Propagation Calculations," JOSA, 56, 1045 (1966)
7. A. Burns and C. Rider, Power Spectral Measurements of Clear Air Turbulence Associated with Jet Streams, Tech. Rept. No. 65210, Royal Aircraft Establishment, Sept. 1965, DDC AD. 476548
8. L. Chernov, Wave Propagation in a Random Medium, McGraw-Hill, N.Y., 1960
9. R. Clark "An Investigation of Certain Short Period Atmospheric Micro-Oscillations" J. Met. 10, 179 (1953)
10. A. Consortini, "Influence of the Atmospheric Turbulence on the Space Coherence of a Laser Beam, "Alta Frequency 178, 790 (1963)
11. H. Dryden, "A Review of the Statistical Theory of Turbulence," Quarterly Appl. Math 1, 7, (1943)
12. R. Fleagle, "The Optical Measurement of Lapse Rate" Bull. Amer. Met. Soc. 31, 51 (1950)
13. P. Franken, J. Jenney, and D. Rank, "Airborne Investigations of Clear-Air Turbulence with Laser Radars," Presented at 1966 Annual Sym. on Electron and Laser Beam Technology, Ann Arbor, (April 1966)
14. D. L. Fried and J. D. Cloud, "Optical Propagation in the Atmosphere at Low Altitudes: Theoretical Evaluation and Experimental Determination of the Phase Structure Function," Proc. Conf. Atmospheric Limitations to Optical Propagation, Boulder, 1965, p. 341
15. H. Hodara, "Laser Wave Propagation Through the Atmosphere," Proc. IEEE, 54 368, 1966
16. R. Hufnagel and N. Stanley "Modulation Transfer Function Associated With Image Transmission Through Turbulent Media" JOSA 54, 52 (1946)

17. F. L. Ludwig Atmospheric Effects on IR-Optical Observations of Re-Entering Objects, Tech Rept. No. 7, Stanford Research Inst. Oct 1962
18. R. J. Munick, "Meteorological Variables Affecting Turbulent Propagation Characteristics" Proc. Conf. Atmospheric Limitations To Optical Propagation, Boulder, 1965, p. 341
19. C. Priestley, Turbulent Transfer in the Lower Atmosphere, Univ. of Chicago Press, Chicago, 1959
20. E. Reisman and P. Sutton, "Feasibility Model for a Laboratory Simulator of Optical Turbulence" JOSA 56, 49 (1966)
21. O. Sutton, Micrometeorology; A Study of Physical Processes in the Lowest Layers of the Earth's Atmosphere, McGraw-Hill, N.Y., 1953
22. V. Tatarski, Wave Propagation in a Turbulent Medium, McGraw-Hill, N.Y., 1961

COHERENCE DEGRADATION EXPERIMENTS AND EFFECTS

1. Anon, "Coherent Optical Propagation Study," Report RADC-TR-65-313, Rome Air Development Center, N.Y., Nov 1965
2. D. Chase, "Coherence Function For Waves in Random Media," JOSA 55, 1559 (1965)
3. D. Fried and J. Cloud, "Optical Propagation in the Atmosphere at Low Altitudes: Theoretical Evaluation and Experimental Determination of the Phase Structure Function," Proc. Conf. Atmospheric Limitations to Optical Propagation, Boulder, Colo., 1965, p. 242
4. I. Goldstein, P. Miles, and A. Chabot, "Heterodyne Measurements of Light Propagation through Atmospheric Turbulence" Proc. IEEE 53, 1172 (1965)
5. I. Goldstein, A. Chabot, and P. Miles, "Heterodyne Measurements of Light Propagation through Atmospheric Turbulence," Proc. Conf. Atmospheric Limitations to Optical Propagation, Boulder 1965
6. J. M. Grant and H. Y. Ageno, "Measurement of the Degree of Coherence for Laser Light Traversing Fogs" ITT Federal Lab Report dated 9 Oct. 1964
7. H. Henry, Definition of Optical Atmospheric Effects on Laser Propagation, Vol III, Report NASA-CR-67382, Aug. 1965
8. R. Herrick, "Long-Distance Interferometry Through the Turbulent Atmosphere," Paper FC16, Presented at 1965 Annual Mtg. Optical Society of America, Philadelphia, Pa., Oct. 1965
9. R. F. Lucy, "The Effect of a Turbulent Atmosphere on a Coherent Laser System," NEREM Record, 1964, p. 172
10. P. L. Smith "Interpretation of the Fluctuations in Optical Radar Echoes from The Atmosphere" Proc. Conf. Atmospheric Limitations to Optical Propagation, Boulder, Colorado, 1965
11. H. Straub, "Coherence in Long-Range Laser Beams" Appl. Optics 4, 875 (1965)

## ATMOSPHERIC NOISE POWER SPECTRUM MEASUREMENTS

1. G. E. Axtelle, "Optical Propagation Studies," Proc. Conf. Atmospheric Limitation to Optical Propagation, Boulder, Colorado, 1965
2. R. Blackman and J. Tukey, The Measurement of Power Spectra, Dover, New York, 1959
3. A. L. Buck, "Laser Propagation in the Atmosphere" Proc. Conf. Atmospheric Limitation to Optical Propagation, Boulder, Colorado, 1965, p. 27
4. T. Chu, "On the Wavelength Dependence of the Spectrum of Laser Beams Traversing the Atmosphere," Applied Optics, 6, 163 (1967)
5. J. A. Collinson, "Modulation of Laser Beams by Atmospheric Turbulence," Proc. Conf. Atmospheric Limitation to Optical Propagation, Boulder, Colorado, 1965, p. 57
6. B. N. Edwards and R. R. Steen, "Effects of Atmospheric Turbulence on the Transmission of Visible and Near Infrared Radiation," Appl. Optics 4, 311 (1965)
7. W. R. Hinchman and A. L. Buck, "Fluctuations in a Laser Beam over 9- and 90- Mile Paths, Proc. IEEE, 52, 305 (1964)
8. D. C. Hogg, "On the Spectrum of Optical Waves Propagated through the Atmosphere," Bell System Tech. J. 42, 2967 (1963)
9. D. Hohn, "Effects of Atmospheric Turbulence on the Transmission of a Laser Beam at 6328 Å. I - Distribution of Intensity," Applied Optics, 5, 1427 (1966)
10. D. Hohn, "Effects of Atmospheric Turbulence on the Transmission of a Laser Beam at 6328 Å. II - Frequency Spectra," Applied Optics, 5, 1433 (1966)
11. J. F. Spalding and K. Tomiyasu, "Laser Beam Propagation in the Atmosphere," 1st Laser Conf., San Diego, 1963
12. M. Subramanian and J. A. Collinson, "Modulation of Laser Beams by Atmospheric Turbulence," Bell Systems Tech. J. 64, 543 (1965)

POLARIZATION FLUCTUATION

1. D. L. Fried and G. E. Mevers, "Atmospheric Optical Effects - Polarization Fluctuation," JOSA 55, 740 (1965)

OPTICAL COMMUNICATIONS, SYSTEMS, AND TECHNIQUES

1. Coherent Optical Propagation Study, Report RADC-TR-65-313, Rome Air Development Center, N.Y., Nov. 1965
2. Optical Space Communication Systems Study, Vol III, NASA Rept. N64-13133, Missile and Space Division, General Electric Company, Phil. Pa., Feb 1964
3. Experimental Laser Space Communications Program Task I: Problem Definition, Vol. I, Report N64-32083, October 1964
4. Optical Space Communications Systems Study Vol II: System Topics, Part One, NASA Report N64-18132, Feb. 1964
5. Optical Space Communications Systems Study Vol III: Systems Topics, Part Two, NASA Report N64-18133, Feb. 1964
6. Optical Space Communications Systems Study, Final Systems Study Vol IV NASA Report N64-18442, March 1964
7. A. Bahr "The Effect of Polarization Selectivity on Optical Mixing in Photoelectric Surfaces," Proc. IEEE, 53, 513 (1965)
8. L. Bloom and C. Buhrer "Reception of Single-Sideband Suppressed-Carrier Signals by Optical Mixing" Proc. IEEE 51, 610 (1963)
9. L. Bolgiano and L. Jelsma, "Communication Channel Model of a Photoelectric Detector" Proc. IEEE 52, 218 (1964)
10. K. Brinkman et al, Deep Space Optical Communications Systems Study, Rept. No. SSD3473R, Hughes Aircraft Company, Culver City, Calif., Aug. 1963
11. D. Chase, "Power Loss in Propagation Through a Turbulent Medium for An Optical-Heterodyne System with Angle Tracking," JOSA, 56, 33 (1966)
12. E. Chatterton, "Semiconductor Laser Communications Through Multiple-Scatter Paths," Proc. IEEE 53, 2114 (1965)
13. E. Chatterton, "Optical Communications Employing Infrared Emitting Diodes and FM Techniques" Proc. IEEE 51, 612 (1963)
14. T. F. Curran and M. Ross, "Optimum Detection Thresholds in Optical Communications" Proc. IEEE 53, 1770 (1965)
15. J. I. Davis, "Consideration of Atmospheric Turbulence in Laser Systems Design," Proc. Conf. Atmospheric Limitations to Optical Propagation, Boulder, Colo., 1965
16. J. I. Davis, "Consideration of Atmospheric Turbulence in Laser Systems Design," Appl. Optics 5, 139 (1966)

17. C. Doyle and M. White, "Dual Polarization FM Laser Communications" Proc. IEEE 53, 1353 (1965)
18. C. Eaglesfield, "Noise Factors at Optical Frequencies" Proc. IEEE (London) 111, 1241 (1964)
19. V. Fowler and L. Bloom, "Optical Time Multiplex - A Method for Extremely Wide Band Optical Communication," Paper 71, Presented at Int. Symp. on Laser Physics and Applications" Univ. of Bern, Bern Switzerland, (Oct. 1964)
20. D. L. Fried, "The Effect of Wave Front Distortion on the Performance of an Ideal Optical Heterodyne Receiver and an Ideal Camera," Proc. Conf. Atmospheric Limitations to Optical Propagation, 1965
21. D. L. Fried, "The Effect of Wave Front Distortion on the Performance of an Ideal Optical Heterodyne Receiver and an Ideal Camera," Proc. Conference on Atmospheric Limitations to Optical Propagation, 1965, p. 192
22. D. Fried, "Optical Heterodyne Detection of an Atmospherically Distorted Signal Wave Front," Proc. IEEE 55, 57 (1967)
23. D. Fried, J. Cloud and M. Sternberg, Experimental Laser Space Communications Program Task I: Problem Definition, Vol II, NASA Report N64-32756 (Oct 1964)
24. S. Gardner, "Some Effects of Atmospheric Turbulence on Optical Heterodyne Communications, 1964 IEEE International Conventional Record
25. S. Gardner, "Some Effects of Atmospheric Turbulence on Optical Heterodyne Communications," Proc. 1st Conf. on Laser Technology, San Diego, Sept. 1963
26. J. W. Goodman, "Some Effects of Target-Induced Scintillation on Optical Radar Performance," Proc. IEEE 53, 1688 (1965)
27. J. P. Gordon, "Quantum Effects in Communications Systems" Proc. IRE, 50 1898 (1962)
28. H. Hans and C. Townes, "Comments on 'Noise in Photoelectric Mixing'", Proc. IRE 50, 1544 (1962) (Comments by B. M. Oliver)
29. G. Heidbreder, "Aperture-Gain Loss Due to Atmospheric Turbulence," JOSA 56, 1634 (1966)
30. G. Hok, et al, Study of Problem Areas in Optical Communications, Report AFAL-TR-66-27, Air Force Avionics Laboratory, Wright-Patterson AFB, Ohio, April 1966 (AD 484 719)
31. M. Ito, "Transmitter for Coherent Light Communication System" Paper 34.1, presented at the International Convention, IEEE, New York, N.Y. (March 1964)



32. K. Johnson and D. Eden, "Solid-State Modulation and Demodulation of Light with Information from Five Television Channels Simultaneously," Proc. IEEE 53, 402 (1965)
33. S. Karp, "Spectrum Properties of Pulse Modulated Lasers" Proc. IEEE 52, 1264 (1964)
34. J. Kerr, "The FM Laser and Optical Communication Systems" Appl. Optics 5, 671 (1966)
35. M. King and S. Kaizer, "Some Parameters of a Laser-Type Beyond-the-Horizon Communication Link" Proc. IEEE 53, 137 (1965)
36. J. Lechleider, "Summary of Some Results in Optimum Linear Communications Systems," Proc. IEEE 54, 321 (1966)
37. J. Minkowski, G. Gundersdorf, and T. Gabriele, Study of Problem Areas in Optical Communications, Report AFAL-TR-66-214, Air Force Avionics Laboratory, Wright-Patterson AFB, Ohio, August 1966 (AD 805 607)
38. B. M. Oliver, "Signal-to-Noise Ratios in Photoelectric Mixing" Proc. IRE 49, 1960 (1961)
39. P. Rabinowitz, "Homodyne Detection of Phase Modulated Light" Proc. IRE 50, 2365 (1962)
40. P. Rabinowitz, J. LaTourrette, and G. Gould, "AFC Optical Heterodyne Detector," Proc. IEEE 51, 857 (1963)
41. W. S. Read, and D. L. Fried, "Optical Heterodyning with Noncritical Angular Alignment," Proc. IEEE 51, 1787 (1963)
42. W. S. Read and R. G. Turner, "Tracking Heterodyne Detection," Appl. Optics 4 1570 (1965)
43. B. Reiffen and H. Sherman "An Optimum Demodulator for Poisson Processes: Photon Source Detectors" Proc. IEEE 51, 1316 (1963)
44. M. Ross, "Quantum Effects and Noise in Optical Communications" Proc. IEEE 51, 602 (1963)
45. M. Ross, "Search Via Laser Receivers for Interstellar Communications," Proc. IEEE 53, 1780 (1965)
46. S. Saito and T. Kimura, "Demodulation of Phase-Modulated Optical Maser Beam by Autocorrelation Technique" Proc. IEEE, 52, 1048 (1964)
47. A. Siegman and B. McMurtry, "Lossless Beam Combination for Optical Heterodyning," Proc. IEEE, 52, 94 (1964)
48. H. S. Snyder and J. R. Platt, "Principles of Optical Communication Systems, General Properties of Non-Image Forming Projectors and Receivers," JOSA 38, 269, 1948
49. H. Steinberg, "Signal Detection With A Laser Amplifier" Proc. IEEE 52, 28, (1964)

50. H. Steinberg, "The Use of a Laser Amplifier in a Laser Communication System," Proc. IEEE 51, 943 (1963)
51. R. Targ, "Optical Heterodyne Detection of Microwave-Modulated Light" Proc. IEEE 52, 303, (1964)
52. L. Vallese and M. King, "A Frequency-Modulated Laser Communication Link," Proc. 8th Natl. Conv. on Mil. Elect. (Sept. 1964), p. 50
53. T. Waite and R. Gudmundsen, "A Balanced Mixer for Optical Heterodyning: The ANN Detector," Proc. IEEE 54, 297, (1966)
54. T. Waite, "A Balanced Mixer for Optical Heterodyning: The Magic T Optical Mixer," Proc. IEEE 54, 334 (1966)

#### ADDITIONAL TOPICS

1. R. Tomlinson, "Atmospheric Breakdown Limitations to Optical Maser Propagation," Nat. Bur. of Stds. of Research, Radio Science 69D, 1431 (1965)
2. Phenomena in the Atmosphere - Optical Phenomena, AID Report 60-54, Air Information Division, Sept. 1960 (AD 245 012)
3. C. Boudreau and M. Stone, Scattering and Attenuation by Precipitation Particles, 26th Reference Bibliography, Lincoln Laboratory, Lexington, Mass., August 1965 (AD 628 200)
4. Y. Kounder, Optics of the Earth's Atmosphere and Turbid Media, ATD Report P-65-66, Library of Congress, October 1965 (AD 622 849)

APPENDIX B

APPLIED OPTICS PAPER

by

Lee W. Carrier, Glenn A. Cato, and Kenneth J. Von Essen

OT3-002 (Rev. A)



# The Backscattering and Extinction of Visible and Infrared Radiation by Selected Major Cloud Models

L. W. Carrier, G. A. Cato, and K. J. von Essen

Volume backscattering functions and optical extinction coefficients are computed for eight suggested major cloud models using the Mie theory for optical wavelengths of 0.488  $\mu$ , 0.694  $\mu$ , 1.06  $\mu$ , 4.0  $\mu$ , and 10.6  $\mu$ . Results show that there is no clear advantage of one wavelength over another for improving cloud transmission; however, backscattering is significantly reduced at the longer wavelengths. Variations in the optical properties of clouds are also discussed and calculations summarized to indicate the effects of cloud thickness, inhomogeneity, and geographical location on the backscatter function and extinction coefficient.

## I. Introduction

The optical radiation scattering properties of the atmosphere are subjects of significant importance to the meteorologist, the optical systems designer, the laser atmospheric probe experimenter, and are of increasing importance to the laser safety monitor and others. Optical radiation is reflected, refracted, and diffracted by air molecules, natural aerosols, and particulate matter in the atmosphere. As a consequence, signal radiant energy diminishes, and back-scattered noise radiant energy increases at an optical receiver; in the last case, when the optical receiver is the human eye there may be a potential human hazard. There are increasing numbers of active optical laser and nonlaser systems in operation in the atmosphere; the successful performance of many of these systems requires operation under any atmospheric condition, including operation in clouds. To effect a reliable system design, accurate knowledge of the scattering properties of clouds is necessary.

There are at present an insufficient number of articles on the transmission and backscattering properties of clouds for those portions of the optical spectrum of current interest, i.e., at visible, near-ir, and the 4- $\mu$  and 10- $\mu$  atmospheric windows and for a wide range of cloud types and cloud conditions. Deirmendjian<sup>1</sup> has determined the theoretical scattering properties of cumulus clouds and hazes for these key portions of the

optical spectrum, and Bauer<sup>2</sup> has calculated the scattering properties of five different cloud particle size distributions for 2.5- $\mu$  to 6- $\mu$  radiation. Others have used various approximation methods to determine cloud optical properties. The purpose of this paper is to extend previous works by presenting the theoretical scattering parameters for eight cloud models and for 0.488- $\mu$ , 0.694- $\mu$ , 1.06- $\mu$ , 4.0- $\mu$ , and 10.6- $\mu$  radiation. These wavelengths have been selected because they correspond to the monochromatic wavelengths of operationally significant lasers, excluding 4.0  $\mu$ .

The approach will be to present representative cloud drop size distributions and concentrations for major cloud types, assuming spherical water droplets only, and to calculate the optical extinction coefficients and volume backscattering functions for each cloud model using the exact Mie theory. The exact theory is used because the accuracy and wavelength sensitivity of the approximation methods are insufficient for reliable determination of the scattering properties of the drop sizes and optical wavelengths considered. Of course, the accuracy of the exact calculation depends upon the accuracy of the cloud model and the effects of multiple scattering. The effects of variations in cloud models on the optical properties will also be considered briefly.

## II. Representative Physical Properties of Major Cloud Types

The optical properties of clouds depend largely on the number and size distribution, or drop size spectrum, of water drops that make up the cloud, and these drop spectra can vary significantly in nature. The problem of establishing a truly representative cloud model is not an easy task. The cloud models for the eight major cloud types that are reported in this paper were constructed after an extensive survey of the literature as

The authors are with Electro-Optical Systems, Inc., a subsidiary of Xerox Corporation, Pasadena, California 91107.

Received 9 May 1966.

This work was performed in part under contracts from U.S. Naval Ordnance Laboratory, Corona, California, and NASA Electronics Research Center, Cambridge, Massachusetts.

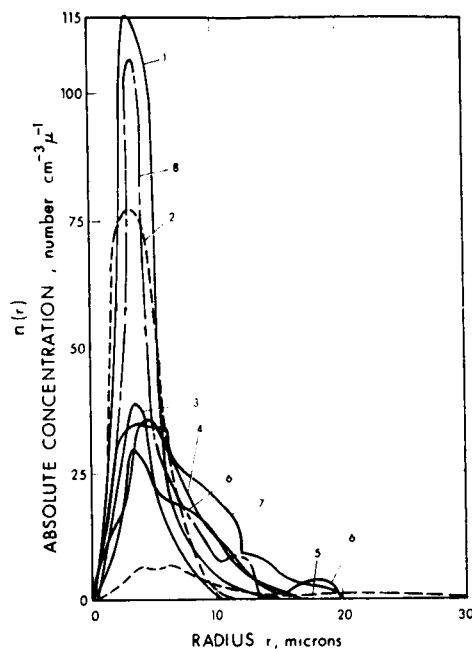


Fig. 1. Model cloud drop spectra (1) stratus I, (2) stratocumulus, (3) Fair-weather cumulus, (4) stratus II, (5) cumulonimbus, (6) cumulus congestus, (7) nimbostratus, and (8) altostratus.

well as consultations with meteorologists throughout the country.\* Some possible variations from the cloud models are also presented. These variations are not meant to exhaust all possible deviations from the cloud models, but to indicate relative effects of cloud thickness, inhomogeneity, altitude, and geographical location on the cloud optical properties. Cirrus and other clouds consisting of ice particles are not considered in this paper.

Model drop spectra for each of the major cloud types are shown in Fig. 1. The number of droplets per unit volume which have radii between  $r$  and  $r + dr$  are shown versus drop radius,  $r$ . Table I summarizes the important physical properties of each cloud type.

The stratus I model is based on observations by Neiburger and Chien off the coast of California.<sup>1</sup> The altostratus and stratocumulus models are taken from a series of measurements made by Diem<sup>2</sup>; altitudes of the cloud bases varied from 1520 m to 2750 m, tops ranged from 1825 m to 3970 m in altitude, and typical cloud thicknesses were 1825 m.<sup>6</sup> The nimbostratus model is that reported by Weickmann and aufm Kampe.<sup>7</sup> The fair weather cumulus cloud model is similar to the Standard Weather Code "Low Cloud, Type 2", defined as a cumulus cloud having little vertical development and flattened in appearance; over the oceans these clouds are often called trade wind cumulus. The stratus II model, after Diem,<sup>2</sup> is repre-

sentative of a stratus deck over land. Considerable variation exists among stratus clouds at different locations, and the stratus I and II models represent extremes. The distribution for the cumulus congestus, a very common stormy weather cloud, was taken from a series of 150 samples of cumulus clouds which were reported by Durbin<sup>8,9</sup>; in severe storms, clouds have been found with a total concentration of only 12 drops/cm<sup>3</sup>, but with an average radius as large as 25  $\mu$ . The cumulonimbus, which is associated with thunderstorms, has a double mode at 4  $\mu$  and 6  $\mu$  with a significant number of large drops of radii up to 30  $\mu$ ; some researchers (such as Weickmann and aufm Kampe<sup>7</sup>) report a significant number of drops in cumulonimbus with radii as large as 100  $\mu$ , but these larger droplets would be encountered less frequently than the model with radii up to 30  $\mu$ .

The altocumulus cloud is another meteorologically important cloud, but no complete drop spectrum was found in the literature. Mull<sup>10</sup> reported that with a 3-cm radar the smallest sized drop that he detected in altocumulus was on the order of 6  $\mu$  to 8  $\mu$  and was independent of the concentration of drops within the cloud. This is a rather large drop size and is comparable to the mode radius for convective clouds like cumulus congestus and cumulonimbus. Gates and Shaw<sup>11</sup> performed calculations using some distributions reported by Weickmann and aufm Kampe<sup>7</sup> for nimbostratus and by Durbin<sup>9</sup> for fair-weather cumulus. They selected these two distributions to bracket the altocumulus clouds that they had encountered most frequently. Pending the selection of data specifically for altocumulus clouds, it is recommended that the droplet spectra and optical properties of nimbostratus and fair-weather cumulus be used for altocumulus. The actual values for altocumulus are expected to lie somewhere between these limits.

Natural clouds are inhomogeneous and the drop spectra can be expected to vary, depending upon the

Table I. Model Cloud Drop Size and Concentration

Cloud type	$N^a$ (No./ cm <sup>3</sup> )	$r_{mode}$ ( $\mu$ )	$r_{min}$ ( $\mu$ )	$r_{max}$ ( $\mu$ )	$\Delta r$ ( $\mu$ )
Stratus I	464	3.5	0	16.0	3.0
Altostratus	450	4.5	0	13.0	4.5
Stratocumulus	350	3.5	0	11.2	4.4
Nimbostratus	330	3.5	0	19.8	9.5
Fair-weather cumulus	300	3.5	0.5	10.0	3.0
Stratus II	260	4.5	0	20.0	5.7
Cumulus congestus	207	3.5	0	16.2	6.7
Cumulonimbus	72	5.0	0	30.0	7.0

$N^a$  = total concentration.

$r_{mode}$  = mode radius = radius corresponding to the maximum number of droplets.

$r_{min}$  = minimum radius.

$r_{max}$  = maximum radius.

$\Delta r$  = bandwidth of the drop-size distribution at half-value points.

$\mu$  = microns.

\* One of the authors (GAC) has been a professional meteorologist; for lists of data sources the interested reader is referred to Ref. 3.

cloud thickness, altitude above the cloud base, and vertical development. Furthermore, the drop spectrum of a given type of cloud varies with geographical location. As a result, optical properties of the clouds can be expected to vary commensurate with these variations. These variations and the optical models are discussed briefly in the next section.

### III. Theoretical Optical Scattering Properties of Clouds

Optical properties of the model clouds can be determined from the Mie theory of scattering, which accounts for diffraction, refraction, reflection, and absorption processes that take place at each scattering center. The Mie theory is an exact theory for a plane, perfectly coherent, monochromatic wave which impinges upon a homogeneous and isotropic spherical particle of any known size and index of refraction. Refer to van de Hulst<sup>12</sup> for details of the theory as only the pertinent expressions are given here.

It is assumed that the scattering particles are in sufficiently dilute suspension so that dependent- and multiple-scattering effects can be neglected, and that linear superposition of the scattered waves is appropriate. The effects of air molecules, aerosols, haze, and water vapor on optical waves are also ignored; to determine the optical properties of these atmospheric constituents, the reader is referred to Elterman,<sup>13</sup> Fenn,<sup>14</sup> Jullrich,<sup>15</sup> Deirmendjian,<sup>1</sup> and Stewart and Hopfield,<sup>16</sup> respectively. In most cases, the scattering components associated with these atmospheric constituents are significantly less than those for clouds.

Two optical properties of clouds that are of interest to the optical systems analyst are the extinction coefficient due to scattering, denoted as  $b$ , and the volume backscattering function, denoted as  $\beta(\pi)$ . Optical scattering extinction,  $b$ , has its usual significance in governing the exponential rate of decrease in light intensity, due to scattering, per path length,  $l$ , i.e.,

$$I = I_0 \exp(-bl). \quad (1)$$

The magnitude of  $b$  depends upon the wavelength of the light and the size, number, and complex index of refraction of the suspended particles. The magnitude of  $b$  is determined from the particle size distributions from Fig. 1 and the Mie theory using the relation

$$b = \sum_{r_{\min}}^{r_{\max}} n(r) \delta r \pi^2 K_{\text{ext}}(x, m) \text{ m}^{-1}. \quad (2)$$

where  $n(r)$  is the number of particles per unit volume per  $\delta r$  radius interval,  $x$  is particle size parameter  $2\pi r/\lambda$ ,  $m$  is complex index of refraction,  $K_{\text{ext}}$  is total extinction cross section  $= (4/x^2) \text{Re}\{S(0)\}$ , and  $\text{Re}\{S(0)\}$  is the real part of the Mie amplitude function evaluated at  $\theta = 0^\circ$ . Equation (2) must be used with caution for the case of large particles since it is tacitly assumed that all scattered light, including that diffracted at small forward angles, is removed from the beam when it is observed or detected. In order for this to be so, the distance to the detector must be large

and the angle subtended by the detector must be sufficiently small. Suitable conditions are discussed by Green and Lane,<sup>17</sup> for example.

The second important optical property associated with the scattering by cloud droplets is the magnitude of the optical radiation that is reflected back in the direction of the source (i.e., scattering angle  $\theta = \pi$ ). In terms of the Mie parameters, the backscattered radiance produced by a monochromatic, polarized beam of light incident upon a distribution of scatterers is given by

$$J(\pi) = \frac{\lambda^2}{4\pi^2} HV \sum_{r_{\min}}^{r_{\max}} n(r) \delta r i_1(\pi, x, m) (W - \text{sr}^{-1}), \quad (3)$$

where  $\lambda$  is the wavelength of light,  $H$  is the incident-beam irradiance,  $V$  is the scattering volume under observation, and  $i_1(\pi, x, m)$  is the Mie intensity function of a scattered component whose electric vector is perpendicular to the plane of observation. Another way of writing Eq. (3) is

$$J(\pi) = \beta(\pi) HV, \quad (4)$$

where  $\beta(\pi)$  is the angular volume scattering function for  $\theta = \pi$ , i.e., backscattering function in  $\text{m}^{-1}\text{sr}^{-1}$ . Combining Eqs. (3) and (4) and rearranging terms, we have

$$\beta(\pi) = \frac{\lambda^2}{4\pi^2} \sum_{r_{\min}}^{r_{\max}} n(r) \delta r i_1(\pi, x, m). \quad (5)$$

Equation (5) expresses the magnitude of the backscattered radiance per unit incident irradiance per unit scattering volume and is a complicated function of the size parameter, index of refraction, and scattering angle. A similar expression can be written by substituting  $i_2$  for  $i_1$ , where  $i_2$  is the Mie intensity function of a scattered component whose electric vector is parallel to the plane of observation. When  $\theta = \pi$ , then  $i_1 = i_2$ .

Numerous tables of Mie scattering functions exist; however, they were found inadequate for the large range of drop sizes found in clouds and for the refractive indices of interest. Calculation of the Mie intensity functions,  $i_1$  and  $i_2$ , and the total scattering cross sections,  $K_{\text{ext}}$ , can be accomplished through an iterative evaluation of the complex Mie series. For numerical evaluation, the number of iterative terms must be large enough for the desired convergence of the infinite series in order to achieve reasonable computational accuracy. For large values of  $x$ , the number of iterations becomes exceedingly large, necessitating the use of high-speed digital computers.

Mie scattering functions and extinction cross sections were computed with the CDC 3100 computer in FORTRAN language using Deirmendjian's computational scheme and recursion criterion.<sup>18</sup> Values of  $i_1$ ,  $i_2$ , and  $K_{\text{ext}}$  were obtained for a real index of refraction of  $m = 1.33$ , and for various drop size parameters up to  $x = 250$ ; these calculations were compared with other tables of Mie functions<sup>19-21</sup> wherever comparable, and were found to agree to at least three significant figures for  $x$  to 250. Therefore, it is assumed that



Table II. Summary of the Backscattering Functions and Extinction Coefficients of the Major Cloud Types

Scattering Function $\beta(\pi)$ ( $\text{m}^{-1}\text{sr}^{-1}$ )					
Cloud type	Wavelength				
	0.488 $\mu$	0.694 $\mu$	1.06 $\mu$	4.0 $\mu$	10.6 $\mu$
Nimbostratus	$7.16 \times 10^{-3}$	$6.03 \times 10^{-3}$	$6.45 \times 10^{-3}$	$3.96 \times 10^{-3}$	$1.54 \times 10^{-4}$
Altostratus	$6.77 \times 10^{-3}$	$4.52 \times 10^{-3}$	$4.99 \times 10^{-3}$	$3.20 \times 10^{-3}$	$1.25 \times 10^{-4}$
Stratus II	$6.04 \times 10^{-3}$	$4.76 \times 10^{-3}$	$4.62 \times 10^{-3}$	$2.87 \times 10^{-3}$	$1.31 \times 10^{-4}$
Cumulus congestus	$3.97 \times 10^{-3}$	$3.01 \times 10^{-3}$	$3.66 \times 10^{-3}$	$2.43 \times 10^{-3}$	$7.88 \times 10^{-5}$
Stratus I	$3.13 \times 10^{-3}$	$2.88 \times 10^{-3}$	$3.08 \times 10^{-3}$	$1.47 \times 10^{-3}$	$7.42 \times 10^{-5}$
Cumulonimbus	$2.40 \times 10^{-3}$	$2.21 \times 10^{-3}$	$2.19 \times 10^{-3}$	$9.13 \times 10^{-4}$	$1.16 \times 10^{-4}$
Stratocumulus	$2.44 \times 10^{-3}$	$1.91 \times 10^{-3}$	$2.08 \times 10^{-3}$	$8.91 \times 10^{-4}$	$5.95 \times 10^{-5}$
Fair Wx cumulus	$1.18 \times 10^{-3}$	$8.68 \times 10^{-4}$	$1.00 \times 10^{-3}$	$4.17 \times 10^{-4}$	$2.31 \times 10^{-5}$

Optical Extinction $b$ ( $\text{m}^{-1}$ )					
Cloud type	Wavelength				
	0.488 $\mu$	0.694 $\mu$	1.06 $\mu$	4.0 $\mu$	10.6 $\mu$
Nimbostratus	$1.28 \times 10^{-1}$	$1.30 \times 10^{-1}$	$1.32 \times 10^{-1}$	$1.47 \times 10^{-1}$	$1.36 \times 10^{-1}$
Altostratus	$1.08 \times 10^{-1}$	$1.09 \times 10^{-1}$	$1.12 \times 10^{-1}$	$1.30 \times 10^{-1}$	$8.39 \times 10^{-2}$
Stratus II	$1.00 \times 10^{-1}$	$1.01 \times 10^{-1}$	$1.03 \times 10^{-1}$	$1.14 \times 10^{-1}$	$1.04 \times 10^{-1}$
Cumulus congestus	$6.92 \times 10^{-2}$	$6.98 \times 10^{-2}$	$7.13 \times 10^{-2}$	$8.10 \times 10^{-2}$	$6.76 \times 10^{-2}$
Stratus I	$6.69 \times 10^{-2}$	$6.79 \times 10^{-2}$	$6.97 \times 10^{-2}$	$9.01 \times 10^{-2}$	$4.28 \times 10^{-2}$
Cumulonimbus	$4.35 \times 10^{-2}$	$4.38 \times 10^{-2}$	$4.44 \times 10^{-2}$	$4.82 \times 10^{-2}$	$5.09 \times 10^{-2}$
Stratocumulus	$4.53 \times 10^{-2}$	$4.60 \times 10^{-2}$	$4.71 \times 10^{-2}$	$5.96 \times 10^{-2}$	$2.48 \times 10^{-2}$
Fair Wx cumulus	$2.10 \times 10^{-2}$	$2.13 \times 10^{-2}$	$2.19 \times 10^{-2}$	$2.76 \times 10^{-2}$	$1.17 \times 10^{-2}$

calculations of  $i_1$ ,  $i_2$ , and  $K_{\text{ext}}$  are accurate to at least three significant figures for the large values of  $x$  encountered for each cloud type.

Histograms were made of each cloud droplet spectral curve shown in Fig. 1, using increments,  $\delta r$ , of 0.25  $\mu$  for radii. Particle concentrations for each droplet radius, given by  $N_k = n(r_k)\delta r_k$ , were punched on cards for subsequent entry into the computer. Computer calculations of the backscattering functions and optical extinction coefficient from Eqs. (2) and (3) were made for each cloud model using  $m = 1.33$  for wavelengths 0.488  $\mu$ , 0.694  $\mu$ , and 1.06  $\mu$ , using  $m = 1.353 - i0.006$  for  $\lambda = 4.0 \mu$ , and using  $m = 1.212 - i0.06$  for 10.6- $\mu$  radiation.<sup>1</sup> The calculations of optical properties of major cloud models are summarized in Table II. Comparison of the optical properties in Table II with the physical properties of the clouds in Table I reveals that the cloud parameters which strongly affect the cloud optical parameters are large particle drop concentration, mode radius, maximum drop size, and bandwidth of the drop size spectra. The interrelationships do not follow a simple form. Note, however, that relatively small concentrations of large particles can mask the effects of large concentrations of small particles.

It is also apparent from Table II that the optical transmission of each cloud type is relatively insensitive to wavelength, owing to the predominance of large particle or geometrical scattering and the absorption of the longer wavelength radiation.

Backscatter, on the other hand, is wavelength dependent. In some cases there are nearly two orders of magnitude reduction in the backscattering of 10.6- $\mu$  radiation compared with 1.06- $\mu$  radiation, and an even

greater reduction with respect to 0.488- $\mu$  radiation. Since optical backscatter is angle dependent, it is also of interest to note how  $\beta(\pi)$  varies for angles other than 180°. These data are applicable to the situation in which the unpolarized illuminator and the receiver of an active optical system are located some distance apart and are not colinear. For other angles,  $i_1$  is not equal to  $i_2$  and the ratio of the polarized components  $\beta_1/\beta_2$  differs from unity. Calculations of optical backscatter,  $\beta(\theta) = \beta_1(\theta) + \beta_2(\theta)$ , and the ratio  $\beta_1/\beta_2$  were made using the stratocumulus and stratus II cloud types, for example, for incident light of wavelength 1.06  $\mu$ . These data are shown in Fig. 2; it is noted that the effect of backscatter can be reduced by a factor of about three by placing a receiver at a 25° viewing angle relative to the transmitted beam. The plot of  $\beta_1/\beta_2$  indicates the difference in backscatter that would be observed if unpolarized light were transmitted and crossed polarizer-analyzer pairs were used to monitor the backscattered components. For these clouds and wavelengths, only a maximum value of 3.4 could be expected at a relative viewing angle of 30°, consequently, cross-polarization techniques for discriminating against backscatter are marginal at 1.06  $\mu$ . Some improvement could be expected for the case of 10.6  $\mu$ , which effectively changes the scattering from geometrical to Rayleigh scattering.

The cloud models depicted in Fig. 1 represent typical conditions. It is now instructive to see the effects of variations in physical properties on the cloud optical properties. In actual practice the droplet spectra of clouds vary with thickness, altitude above the base, and geographical location; specific examples have been

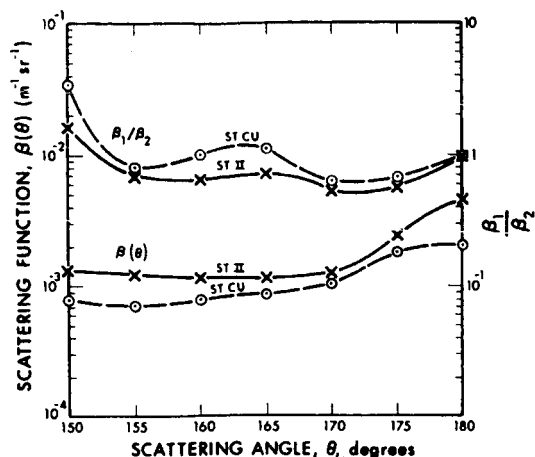


Fig. 2. Angular dependence of the backscatter functions associated with the stratocumulus (St Cu) and the stratus II (St II) cloud models ( $\lambda = 1.06 \mu$ ).

selected which reveal wide variations in droplet spectra. The following discussion of these variations and their related optical effects is based on a wavelength of  $1.06 \mu$ .

Cumulus clouds are particularly inhomogeneous. Some possible variations in optical properties at the points within a cumulus cloud are indicated in Table III, as a consequence of varying concentrations and numbers of large particles. The middle droplet spectrum has a great many small drops, but it is narrow, resulting in a larger value of  $\beta$  and a smaller value of  $b$  than the other parts of the cloud. At the point of

maximum concentration, the backscatter is not particularly large, but the extinction coefficient is comparatively larger than the second position presumably due to a combination of a large total concentration and a large maximum radius. As indicated by these data, inhomogeneity can result in variations in optical backscatter and extinction by a factor of about six, or possibly even higher.

The effects of the broadening of the spectrum and the reduction in the total drop concentration that occurs in thicker clouds are shown in Table IV. The thicker the cloud deck, the greater is the backscattering function. Increased cloud thickness also causes some increase in the extinction coefficient. The thicker stratus cloud of Table IV contains larger drops than the other two, and the calculated effects of neglecting drops over  $25\text{-}\mu$  radius and under  $10\text{-}\mu$  radius are also shown in the table. These results clearly show the greater optical effects of large particles compared with the smaller particles. Neglecting particles with radii greater than  $25 \mu$ , i.e., a 10% reduction in total concentration, results in a decrease in  $\beta(\pi)$  by a factor of about two. On the other hand, neglecting particles below  $10 \mu$  (over 70% of particle concentration) does not affect the optical parameters by more than 10%.

The altitude of the scattering volume above the cloud base also affects the cloud optical properties, and two differing examples are cited. In the first case of the Hawaiian trade-wind cumulus, as shown in Table V, the backscatter function is greatest at the lowest altitude (where the total concentration is greatest and there

Table III. Effect of Inhomogeneity<sup>a</sup> ( $\lambda = 1.06 \mu$ )

Cloud type sample height (m)	$\beta(\pi)$ ( $\text{m}^{-1}\text{sr}^{-1}$ )	$b$ ( $\text{m}^{-1}$ )	$N$ ( $\text{cm}^{-3}$ )	$r_{\text{mode}}$ ( $\mu$ )	$r_{\text{min}}$ ( $\mu$ )	$r_{\text{max}}$ ( $\mu$ )	$\Delta r$ ( $\mu$ )
Cumulus							
1. 1035	$1.36 \times 10^{-3}$	$2.78 \times 10^{-2}$	64	4.5	0	12.8	6.4
2. 1035	$8.37 \times 10^{-3}$	$1.67 \times 10^{-2}$	145	1.5	0	10.8	2.8
3. 1035 <sup>b</sup>	$4.38 \times 10^{-3}$	$9.13 \times 10^{-2}$	173	4.5	0	16.0	5.4

<sup>a</sup> Calculations based on droplet spectrum reported by Durbin<sup>9</sup> in September 1951.

<sup>b</sup> Somewhat similar physical properties to cumulus congestus, where  $\beta(\pi) = 3.66 \times 10^{-3} \text{m}^{-1}\text{sr}^{-1}$  and  $b = 7.13 \times 10^{-2} \text{m}^{-1}$ .

Table IV. Effect of Cloud Thickness ( $\lambda = 1.06 \mu$ )

Cloud type and thickness (m)	$\beta(\pi)$ ( $\text{m}^{-1}\text{sr}^{-1}$ )	$b$ ( $\text{m}^{-1}$ )	$N$ ( $\text{cm}^{-3}$ )	$r_{\text{mode}}$ ( $\mu$ )	$r_{\text{min}}$ ( $\mu$ )	$r_{\text{max}}$ ( $\mu$ )	$\Delta r$ ( $\mu$ )
Stratus <sup>a</sup>							
1. 213-305	$1.98 \times 10^{-3}$	$4.22 \times 10^{-2}$	133	4.5	0	27.5	4.4
2. 610	$2.43 \times 10^{-3}$	$4.93 \times 10^{-2}$	63	4.8	1.2	42.2	4.6
3. 1975-2130	$3.34 \times 10^{-3}$	$6.04 \times 10^{-2}$	40	5.0	0	60.8	8.0
Note 1	$1.35 \times 10^{-3}$	$2.83 \times 10^{-2}$	36	---	0	25.0	---
Note 2	$3.01 \times 10^{-3}$	$5.38 \times 10^{-2}$	12	---	10	60.8	---
Cumulus <sup>b</sup>							
1. 230-765	$2.80 \times 10^{-3}$	$6.00 \times 10^{-2}$	211	4.0	0	19.8	4.0
2. 1175-2130	$6.23 \times 10^{-3}$	$1.27 \times 10^{-1}$	206	4.0	0	30.2	7.2

<sup>a</sup> Stratus cloud physical properties after Singleton and Smith.<sup>22</sup>

<sup>b</sup> Cumulus cloud physical properties after Khrgran.<sup>23</sup>

Note 1: Stratus size distribution (1975-2130 m) cutoff at  $25 \mu$ .

Note 2: Stratus size distribution (1975-2130 m) cutoff at low end.

**Table V. Effect of Altitude Above Cloud Base<sup>a</sup> ( $\lambda = 1.06 \mu$ )**

Trade-Wind Cumulus off the East Coast of Hawaii (Base = 670 m Top = 2900 m)							
Sample height (m)	$\beta(\pi)$ ( $\text{m}^{-1}\text{sr}^{-1}$ )	$b$ ( $\text{m}^{-1}$ )	$N$ ( $\text{cm}^{-3}$ )	$r_{\text{mode}}$ ( $\mu$ )	$r_{\text{min}}$ ( $\mu$ )	$r_{\text{max}}$ ( $\mu$ )	$\Delta r$ ( $\mu$ )
1. 990	$1.94 \times 10^{-2}$	$3.77 \times 10^{-1}$	74	10	0	25	8.5
2. 1300	$1.48 \times 10^{-2}$	$2.92 \times 10^{-1}$	51	15	0	23.2	8.5
3. 1600	$1.43 \times 10^{-2}$	$2.99 \times 10^{-1}$	27	17.5	0	32.2	12.5
4. 1900	$1.37 \times 10^{-2}$	$2.77 \times 10^{-1}$	30	10.0	0	34.8	16.0

Continental Cumulus over the Blue Mountains Northwest of Sydney, Australia (Base = 2200 m Top = 3660 m)							
Sample height (m)	$\beta(\pi)$ ( $\text{m}^{-1}\text{sr}^{-1}$ )	$b$ ( $\text{m}^{-1}$ )	$N$ ( $\text{cm}^{-3}$ )	$r_{\text{mode}}$ ( $\mu$ )	$r_{\text{min}}$ ( $\mu$ )	$r_{\text{max}}$ ( $\mu$ )	$\Delta r$ ( $\mu$ )
1. 2500	$7.15 \times 10^{-3}$	$1.78 \times 10^{-1}$	490	5.5	0	12.2	3.0
2. 2775	$6.84 \times 10^{-3}$	$1.48 \times 10^{-1}$	270	7.0	0	11.5	3.5
3. 3000	$8.68 \times 10^{-3}$	$1.64 \times 10^{-1}$	250	7.5	0	11.5	2.0
4. 3420	$1.34 \times 10^{-2}$	$2.47 \times 10^{-1}$	350	7.5	0	13.0	2.0

<sup>a</sup> Cloud physical properties after Squires.<sup>24</sup>

**Table VI. Geographical Location<sup>a</sup> ( $\lambda = 1.06 \mu$ )**

Cloud type and location	$\beta(\pi)$ ( $\text{m}^{-1}\text{sr}^{-1}$ )	$b$ ( $\text{m}^{-1}$ )	$N$ ( $\text{cm}^{-3}$ )	$r_{\text{mode}}$ ( $\mu$ )	$r_{\text{min}}$ ( $\mu$ )	$r_{\text{max}}$ ( $\mu$ )	$\Delta r$ ( $\mu$ )
Cumulus and Cumulonimbus							
1. Pacific Coast of USA	$5.94 \times 10^{-3}$	$1.20 \times 10^{-1}$	90	9	0	17.2	7.6
2. Other parts of USA	$8.71 \times 10^{-3}$	$1.74 \times 10^{-1}$	160	7.5	0	16.0	6.3
Stratus and Stratocumulus							
1. Pacific Coast of USA	$4.88 \times 10^{-3}$	$1.00 \times 10^{-1}$	100	5	1.2	16.5	6
2. Other parts of USA	$8.70 \times 10^{-3}$	$1.89 \times 10^{-1}$	320	5.5	0	15.5	4.7
Alto cumulus and Altostratus							
1. Pacific Coast of USA	$1.99 \times 10^{-3}$	$3.90 \times 10^{-2}$	35	7.5	0.8	16.0	6.2
2. Other parts of USA	$3.47 \times 10^{-3}$	$6.90 \times 10^{-2}$	75	6.0	0	17.0	7

<sup>a</sup> Cloud physical properties after Lewis.<sup>25</sup>

is a preponderance of small drop sizes). Although  $\beta(\pi)$  is greatest here, there actually is not a great deal of variation in  $\beta$  from one altitude to the next. The same could be said for  $b$ . This constancy is particularly striking when compared to the effects of inhomogeneity and thickness on  $\beta$  and  $b$ , shown in Tables III and IV, respectively.

In the second case of the continental cumulus cloud with large vertical development, as shown in Table V, the maximum values of  $\beta$  and  $b$  occur near the top of the cloud (where the total concentration has an intermediate value, but where there is a preponderance of larger droplets). The scattering function increases by about a factor of two, and optical extinction increases by about 50% over the altitude range of this cloud.

With respect to geographical location, clouds formed inland generally contain a larger total number of water drops. As indicated in Table VI, the other droplet

characteristics vary from one cloud type to another. All of the optical properties display a strong dependence on geography. The angular volume scattering function  $\beta(\pi)$  is greater by about 75% for the inland clouds, and the extinction coefficient,  $b$ , is about 60% larger.

In summary, the variability of cloud optical properties is shown in Fig. 3, based on the data from Tables II-VI. The top two curves show the range of calculated values of optical extinction from the fair-weather cumulus cloud model, at the low values, to the nimbostratus cloud model, at the upper values. A similar pair of curves is shown for the backscattering function. The vertical bars at  $\lambda = 1.06 \mu$  summarize a possible range of variations of  $\beta$  and  $b$  for cumulus type clouds.

#### IV. Some Concluding Remarks

Representative cloud models have been proposed for the eight commonly encountered water clouds, and their

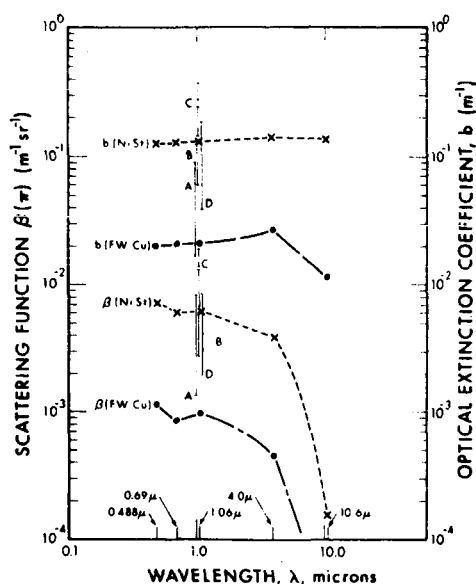


Fig. 3. Variability of cloud optical properties.  $\beta$  and  $b$  are plotted for fair-weather cumulus and nimbostratus. A, B, C, D refer to variations in optical properties of cumulus clouds due to inhomogeneity, thickness, altitude, and geographical location, respectively.

respective optical properties have been determined using the exact Mie theory. Since the Mie theory is exact, the calculated optical properties are accurate only for the cloud models used. From Fig. 3, and other supporting data, the magnitude of the optical extinction for each of the cloud models is fairly constant at the selected wavelengths over the range  $0.488\text{--}10.6\ \mu$ ; however, significant reductions in backscattering functions occur at  $10.6\ \mu$  compared with the visible wavelengths. Rather wide variations in optical properties can occur for clouds with drop spectra that differ from the cloud models. Almost an order of magnitude difference in  $\beta$  in  $b$  is calculated for cloud inhomogeneity and geographical location; the effects of cloud thickness and altitude on the cloud optical properties, although appreciable, are not as significant for the cases examined.

The probability of occurrence of each of the cloud types at various places around the world is also of interest to the optical systems analyst, although not discussed here; the interested reader is referred to previous work by the authors, for example, where frequency of occurrence of cloudy skies by amount and type are reported for the Northern Hemisphere.<sup>3</sup>

The largest source of uncertainty in the application of the optical property calculations is the neglect of multiple scattering effects. According to van de Hulst, a simple test for whether or not multiple scattering is probable is based upon the magnitude of the optical depth of the scattering medium, i.e.,  $\tau = bL$ . The probability that multiple scattering effects may modify the effective volume backscattering function and extinction coefficient increases for  $\tau > 0.1$ . It is apparent from Table II that multiple scattering effects are highly probable for each of the cloud models and

should ultimately be considered for the case of large transmitter beamwidths and for optical receivers with wide fields of view.

Direct comparison of the optical effects reported here with other theoretical calculations is difficult since other authors use differing cloud models. Deirmendjian's cloud distribution ( $N = 100\text{ cm}^{-3}$ ,  $r_{\text{mode}} = 4.0\ \mu$ ), for example, corresponds roughly with our fair-weather cumulus model ( $N = 300\text{ cm}^{-3}$ ,  $r_{\text{mode}} = 3.5\ \mu$ ) except for concentration. Comparison of his  $\beta_{\text{ext}}$  with our  $b$  at  $\lambda = 0.45\ \mu$ ,  $1.61\ \mu$ ,  $3.90\ \mu$ , and  $10.0\ \mu$  shows agreement to within a factor of about three when the difference in concentrations is considered.

Direct comparison of theoretical with experimental determination of the optical properties of clouds is even more difficult. Recent measurements of optical backscatter from stratocumulus and cumulus clouds have been made by Curtis.<sup>26</sup> Comparison of the measured values of  $\beta$  with those calculated from the cloud models shows the theoretical values to be about an order of magnitude greater than those measured. The differences are most probably due to the differences in cloud properties and multiple-scattering effects.

This comparison of our theoretical results with other theoretical and experimental results is included only to show the reasonableness of our computer calculations.

The significance of this paper is believed to be that data are published on the optical properties of each of the important cloud types for several wavelengths at which laser transmitters are, or soon will be, available. These data are based on a computer analysis, for which light scattering tables either do not exist or the labor involved in the calculations using present tables is exceedingly large, and provide a basis for accurately determining the performance and reliability of active optical systems which operate in clouds that are similar to the model clouds described here.

The authors particularly thank D. Deirmendjian of the Rand Corporation for his suggestion and comments during the initial development of our computer program. Also, we appreciate and acknowledge the splendid cooperation and work of Tagore Feldsburg for his computer programming and analysis and the meaningful discussions held with Leonard Nugent and George Clark of Electro-Optical Systems, Inc.

## References

1. D. Deirmendjian, *Appl. Opt.* **3**, 187 (1964).
2. E. Bauer, *Appl. Opt.* **3**, 197 (1964).
3. G. Cato, L. Carrier, and K. von Essen, Rept. 4440-Final III, Electro-Optical Systems, Inc., Pasadena, Calif. (December 1965), AD 479487.
4. M. Neiburger and C. W. Chien, *Am. Geophys. Union Mono.* No. 5 (1960).
5. M. Diem, *Meteorologische Rundschau* **9** and **10**, pp. 261-273 (March/April 1948).
6. F. Robinson, EMI Electronics, Ltd., Rept. DMP 1665/1 (December 1963), AD 438400.
7. H. Weickmann and H. aufm Kampe, *J. Meteorol.* **10**, 204 (1953).
8. W. Durbin, *Tellus* **7**, 202 (1959).
9. W. Durbin, "Droplet Sampling in Cumulus Clouds", *Air*

- Ministry Meteorol. Res. Comm. Publ. 991 (1956) AD147512.
10. S. Mull, Indian J. Meteorol. Geophys. **12**, 243 (1961).
11. D. Gates and C. Shaw, J. Opt. Soc. Am. **50**, 876 (1960).
12. H. van de Hulst, *Light Scattering by Small Particles* (John Wiley and Sons, Inc., New York, 1964), Ch. 9.
13. L. Elterman, Rept. AFCRL-63-675, USAF Cambridge Res. Labs., Bedford, Mass. (1963).
14. R. Fenn, USAERDL Tech. Rept. 2411, Fort Monmouth, New Jersey (1963).
15. K. Bullrich, in *Advances in Geophysics*, H. Landsberg and J. van Meighem, Eds. (Academic Press Inc., New York, 1964), Vol. 10.
16. H. S. Stewart and R. F. Hopfield, in *Applied Optics and Optical Engineering, Volume I, Light: Its Generation and Modification*, R. Kingslake, Ed. (Academic Press Inc., New York, 1965), Ch. 4.
17. H. L. Green and W. R. Lane, *Particulate Clouds: Dusts, Smokes, and Mists* (D. Van Nostrand Company, Princeton, N.J., 1957), Ch. 4.
18. D. Deirmendjian and R. Clasen, Rept. R-393-PR, Rand Corp., Santa Monica, Calif. (1951).
19. R. Penndorf, AFCRL Rept. RAD-TR-61-32, USAF Cambridge Res. Labs., Bedford, Mass. (1961).
20. R. Gumprecht and C. Sliepcevich, *Tables of Light-Scattering Functions for Spherical Particles* (Engineering Research Institute, University of Michigan, Ann Arbor, 1951).
21. S. Twomey and H. Howell, Appl. Opt. **4**, 503 (1965).
22. F. Singleton and D. Smith, Roy. Meteorol. Soc. J. **96**, 454 (1960).
23. A. Khrgran, Ed., *Cloud Physics*, 1961; available as: Office of Technical Services Transl. OTS-63-11141.
24. P. Squires, Tellus **10**, 256 (1958).
25. T. Malone, Ed., *Compendium of Meteorology*, (American Meteorological Society, Boston, 1951).
26. E. Curtis, NAVWEPS, Rept. 8817, NOL, Corona, Calif. (1965) (Confidential).